EVALUATION OF FRP PRESTRESSED PANELS/SLABS FOR I-225 / PARKER ROAD PROJECT

by

Reuben Zylstra
P. Benson Shing
Yunping Xi

Department of Civil, Environmental
& Architectural Engineering
University of Colorado
Boulder, CO 80309-0428

Sponsored by
U.S. Department of Transportation
Federal Highway Administration

December 2001

Report No. CDOT-DTD-R-2001-14
Colorado Department of Transportation
Research Branch
4201 E. Arkansas Ave.
Denver, CO 80222

EXECUTIVE SUMMARY

Under the Innovative Bridge Research and Construction (IBRC) program of the Federal Highway Administration (FHWA), the Colorado Department of Transportation (CDOT) has introduced fiber reinforced polymeric (FRP) reinforcement in a current bridge project at I-225/Parker Road. In this project, precast prestressed concrete panels are used as stay-in-place forms for a bridge deck. Some of these panels are prestressed with carbon fiber reinforced polymeric (CFRP) tendons and the rest with regular seven-wire steel strands. The primary objective of this project is to demonstrate the feasibility of using CFRP tendons in place of seven-wire steel strand for prestressed concrete panels. Furthermore, the applicability of current AASHTO provisions to CFRP prestressed panels is investigated and additional design requirements for FRP reinforcement are identified from research results in the literature. This study includes the review of existing literature on FRP reinforcement, evaluation of the bond strength of the FRP bars used in the bridge project by pullout tests, and the testing of three prestressed panels and two composite slabs to failure.

Pullout tests conducted in this study showed that Leadline CFRP prestressing tendons and C-BAR glass fiber reinforced polymeric (GFRP) reinforcing bars had higher bond strengths than seven-wire steel strand and regular steel reinforcing bars, respectively.

Load tests were first performed on two panels, one prestressed and reinforced with FRP and the other prestressed and reinforced with steel. Both panels were

designed to barely satisfy the AASHTO specifications. An additional panel that was prestressed and reinforced with FRP and brought from the I-225/Parker Road project was tested as well. This panel was conservatively designed with a significant reserve capacity compared to the first two. Load tests were also performed on steel and FRP prestressed panels that had a 125 mm (5 in.) composite topping slab. All test results show the feasibility of using CFRP tendons for prestressing and GFRP bars for temperature and distribution reinforcement in precast bridge panel construction. The GFRP reinforcement was selected according to the recommendation for temperature reinforcement in the ACI 440H draft report.

Load distribution data were taken during the composite slab tests to validate the adequacy of the Equivalent Width Strip method used in AASHTO LRFD Specifications. The method was found to be conservative for both steel and FRP reinforced composite slabs.

However, results show that the steel reinforced slab better distributed the loading in the transverse direction than the FRP reinforced slab. This suggests that the recommendation for temperature reinforcement in the ACI 440H draft report may not be adequate for distribution reinforcement.

ACKNOWLEDGMENTS

This study was sponsored by the Federal Highway Administration (FHWA) and conducted in conjunction with the Colorado Department of Transportation (CDOT) as part of FHWA's Innovative Bridge Research and Construction Program. The project was monitored by Matthew Greer of the Colorado Division of FHWA, and administered by Ahmad Ardani of the Research Branch of CDOT.

The technical input provided by Michael McMullen, who is the lead engineer of CDOT in this project, is gratefully acknowledged. The writers would like to thank Matthew Greer of FHWA, Michael McMullen and Mark Leonard of Staff Bridge of CDOT, Ahmad Ardani and Richard Griffin of the Research Branch of CDOT, who were instrumental in making this project a success.

The writers appreciate the invaluable assistance of William Phaup, James Lewis, and John Hamilton, undergraduate students at the University of Colorado, in carrying out the experimental work.

Opinions expressed in this report are, however, those of the writers and do not necessarily represent those of CDOT or FHWA.

TABLE OF CONTENTS

1. INTRODUCTION

1.1 Background

Use of fiber reinforced polymers (FRP) for prestressing and reinforcing concrete structures as an alternative to steel has received increasing attention in the last decade. The benefits of using FRP tendons and bars are that they are non-corrosive, lightweight, non-conductive, magnetically neutral, and extremely strong in tension. The corrosion resistance of FRP reinforcement is highly beneficial to bridges, whose service life is often limited by the corrosion of the reinforcement. Thus, the use of FRP may lead to a substantial increase of the lifespan of bridges.

Currently, high prices, lack of standard design specifications, and constructibility issues limit the use of FRP in prestressed and reinforced concrete structures. Most applications are limited to situations where the use of FRP is essential. Such applications include structural flooring to support sensitive magnetic equipment and structures subject to a corrosive marine environment. However, in recent years, many state transportation departments in partnership with the Federal Highway Administration (FHWA) are introducing these new materials to bridge structures with the intention of gaining design and construction experience and long-term performance data on FRP. Several bridges using FRP prestressed bars and reinforcement were constructed in Canada. In 1993, a bridge was built in Calgary using FRP prestressing tendons (Rizkalla and Tadros, 1994). Another bridge containing FRP prestressing tendons was built in Headingsley, Manitoba in 1997.

The ACI 440H Committee has prepared a draft of code modifications for concrete structures prestressed and reinforced with FRP. This document can be perceived as the first attempt in the United States to introduce code provisions for the use of FRP materials in concrete structures.

Under the Innovative Bridge Research and Construction (IBRC) program of the FHWA, the Colorado Department of Transportation (CDOT) has introduced FRP reinforcement in a current bridge project at I-225/Parker Road. The bridge construction, underway at the time of this report, is shown in Figure 1.1. In this project, precast prestressed concrete panels are used as stay-in-place forms for a bridge deck. Some of these panels are prestressed with carbon fiber reinforced polymer (CFRP) tendons and the rest with regular seven-wire steel strands. Furthermore, deformed glass fiber reinforced polymer (GFRP) bars are used as temperature reinforcement in the former panels. GFRP bars are also used in the railings of a temporary bridge in this project. The primary objective of this project is to demonstrate the feasibility of using CFRP tendons in place of seven-wire steel strand for prestressed concrete panels. The precast panels are supported on two cast-in-place, post-tensioned concrete box girders. The panels are designed to carry construction loads. A topping slab will be added to the panels to form a composite bridge deck to carry the traffic. The panel design is extremely conservative. This ensures the safety of the bridge with the use of the new materials that have not been well studied. In spite of this, because of the lack of standard design provisions for FRP reinforced concrete structures, studies must be conducted to validate the load

carrying capacity of the deck panels and to examine the long-term performance of the bridge deck containing FRP reinforcement. Furthermore, the applicability of current AASHTO provisions to CFRP prestressed panels must be investigated and additional design requirements for FRP reinforcement must be identified from research results in the literature. These studies have been conducted at the University of Colorado at Boulder as part of the IBRC project. The studies include the load tests of simply supported deck panels in Phase I and the evaluation of the long-term performance of such decks by testing a 30-ft. long and 16-ft. wide, 2/3-scale three-girder deck under fatigue loads in Phase II. Furthermore, a rational design methodology that can lead to a significant reduction of reinforcement in bridge decks has been developed. The use of this new design method can partly offset the high cost of FRP reinforcement.

1.2 Scope

This report summarizes the work of the Phase I study, which includes the review of existing literature on FRP reinforcement, evaluation of the bond strength of the FRP bars used in the bridge project, and the testing of three panels and two composite slabs to failure. The panels and slabs were simply supported. The panels were 90 mm (3.5 in.) thick and were constructed with steel and CFRP prestressing tendons to compare their performances. One of the panels that had FRP prestressing bars was brought from the bridge site for evaluation. This panel was conservatively designed. The remaining two panels were designed to barely satisfy the minimum requirements of AASHTO with additional considerations for the FRP reinforcement. The

composite slabs had a 125 mm (5 in.) topping cast on top of the 90 mm (3.5 in.) panels. One had an FRP prestressed panel and the other had a steel prestressed panel. For the two composite slabs that were tested, the effective widths of the slabs subjected to the wheel load of a design truck were evaluated from the test results and compared to the recommendation in the AASHTO LRFD Standard Specifications (1998).

1.3 Organization of the Report

The contents of this report have been organized in the following fashion. Chapter 2 focuses on the bond strength of FRP and steel bars with concrete. This chapter presents a literature review of current research on pullout tests and development lengths for FRP and steel reinforcement, the pullout tests conducted in this study, and results obtained.

In Chapter 3, the design of the test panels is presented in detail. A brief overview of the allowable stress design method and a thorough discussion of the calculation of the nominal moment capacities of steel/FRP prestressed panels and composite slabs with different reinforcement levels are presented. A discussion of material properties and the factors affecting FRP performance is also presented.

In Chapter 4, the construction of the test panels and composite slabs are described, and the test setup developed to evaluate the panels and composite slabs is presented.

In Chapter 5, results of the panel and slab tests are presented. The test results are analyzed and compared to the design strengths. The performance of the panels prestressed with CFRP bars and steel strands are compared. The load distribution in the composite slabs under a wheel load is examined with the strain gage data and compared to the AASHTO LRFD Specifications.

A summary of this study and the conclusions drawn from it are presented in Chapter 6.

Figure 1.1 I-225/Parker Road Bridge Construction

2. BOND STRENGTH AND PULLOUT TESTS

2.1 General

In the I-225/Parker Road project, both FRP and steel prestressing/reinforcing bars are used for the precast panels. The steel products used by the contractor are standards of the concrete industry, namely, seven-wire strand and epoxy-coated bars. However, due to the limited use of FRP products in construction, only a few FRP product alternatives exist on the market. In spite of this, there are a limited number of options when looking at both FRP prestressing tendons and FRP reinforcing bars. For FRP prestressing tendons, the contractor chose Leadline carbon fiber reinforced polymer (CFRP) tendons. These bars have been studied by other researchers (Dolan et al., 2000; Lu et al., 2000; Mahmoud et al., 1996) and have proven to be a viable product. In addition, the manufacturer of Leadline has developed an anchor chuck that can be used to grip their FRP bars for ease in the prestressing process. For glass FRP reinforcing rods, the contractors chose C-BAR GFRP bars. Like Leadline, these bars have also been studied extensively by researchers (Rizkalla, 1991; Karlsson, 1997; Conrad et al., 2000). These bars have surface deformations very similar to that of regular steel bars.

In order to take full advantage of the high tensile strength of FRP bars, it is essential to quantify the bond strength between FRP bars and concrete. The differences in material properties and geometry between FRP and steel bars make it difficult to apply the established development length equations in the ACI code (ACI

Committee 318, 1999) to FRP bars. The ACI 440H draft document (2000) contains recommendations for FRP use in reinforced concrete and provides development length equations for mild reinforcement only. Current research has shown that the development length equation used for steel prestressing strand largely overestimates the development length required for FRP (Lu et al., 2000). Development length is normally not a factor in concrete bridge design as bridge girders and structural beams tend to provide sufficient embedment lengths. However, in applications such as precast bridge deck panels, development length can be the governing factor. Thus, for this situation and others similar to it, a good understanding of development length is imperative.

In view of the importance of development length in bridge panel design, pullout tests are necessary to quantify the bond strengths of the FRP products used in this project, in particular, with respect to those of regular steel products. This chapter will present pullout test results for the materials chosen by the contractor to be used in panel construction. These materials are: CFRP prestressing tendons (Leadline), seven-wire steel strand, GFRP reinforcement (C-BAR), and standard reinforcing steel. Using the pullout results, the bond strengths of the materials can be compared and an understanding of the failure mechanisms that govern pullout will be attained. All four bar samples are shown in Figure 2.1. It must be mentioned that for the pullout tests, only black steel bars are used for comparison with GFRP bars, even though epoxy-coated bars are used in actual construction.

2.2 Development Length

In prestressed concrete, transfer length is the distance required to transmit the effective prestressing force from the prestressing tendon to the concrete. When a member is loaded to its ultimate flexural strength, an additional bond length beyond the transfer length is required to develop the tendon stress at the nominal flexural strength. This additional bond length is called flexural bond length. Development length (l_d) is considered as the sum of the transfer length and the flexural bond length. The ACI 318-99 equation for the development length of a prestressed steel tendon is given by equation 2.1 for use with US customary units where l_d is in inches. The variables include various states of tendon stress, f_{pe} (effective prestress) and f_{ps} (stress in strand at nominal flexural strength) given in ksi, as well as the nominal bar diameter d_b, given in inches.

$$l_d = \frac{1}{3} f_{pe} d_b + (f_{ps} - f_{pe}) d_b \qquad (2.1)$$

In addition to the equation for prestressing strand, ACI 318-99 (1999) has a development length equation for standard steel reinforcement shown in equation 2.2.

$$l_d = \frac{3}{40} \frac{f_y}{\sqrt{f_c'}} d_b \cdot \frac{\alpha\beta\gamma\lambda}{\frac{c + K_{tr}}{d_b}} \qquad (2.2)$$

where α = bar location factor

β = coating factor

γ = bar size factor

λ = lightweight aggregate concrete factor

c = spacing or cover dimension (in.)

K_{tr} = transverse reinforcement index

f_y = yield stress of reinforcement (psi)

f'_c = concrete compressive strength at 28 days (psi)

According to the ACI 440H draft document, development length for FRP reinforcement is given by the larger of equations 2.3a and 2.3b. Each of these equations is an empirical equation that uses US customary units where l_d is in inches.

$$l_d = \frac{A_{f,bar} f_u}{17\sqrt{f'_c}} \qquad (2.3a)$$

$$l_d = \frac{f_u d_b}{2700} \qquad (2.3b)$$

where $A_{f,bar}$ = cross sectional area of the reinforcing bar (in^2)

f_u = ultimate strength of the reinforcing bar (psi)

2.3 Pullout Tests

The use of pullout tests to investigate bond strength is fairly common in research today. They are simple to conduct and have proven to be a reliable indicator of bond

quality. However, it must be noted that the conditions in pullout tests do not reflect the actual conditions that govern bond in both reinforced concrete and prestressed concrete structures. According to Mahmoud (1999), the bond strengths developed in a pullout test generally are larger than those developed in a prestressed beam test. This can be attributed to two factors. First, in a standard pullout test, a rod is pulled out of a cured concrete specimen. In order to accomplish this, the concrete is subjected to compression while the rod is subjected to tension. This is different than what occurs in a prestressed beam test where both the concrete and the reinforcement are in tension. In the case of the prestressed beam test, the concrete in tension has a higher probability of being cracked, resulting in lower bond strengths. Second, in pullout tests, the contact between the loading plate and the concrete specimen will induce radial friction confinement on the rod near the loaded end. This confinement will add further resistance to pullout, increasing the bond strength.

An additional factor is noted for prestressing strand that may increase the bond strength in a prestressed beam test, thus counteracting the trends described in the previous paragraph. When a strand is prestressed, the diameter decreases. When the prestressing force is released, the diameter of the strand increases at the unstressed end, increasing the friction against the concrete surface that surrounds it. This is termed the Hoyer effect. For prestressing tendons, the tendons are normally not pretensioned in pullout specimens. Hence, the Hoyer effect is not present reducing the bond strength for the pullout specimens.

In spite of the aforementioned factors, most researchers have found that pullout tests provide an effective comparison tool for bond strength. By correlating pullout and beam tests, pullout tests performed at a later time can be used to verify the adequacy of the development length equation for the particular material.

2.4 Literature Review

2.4.1 Brearley and Johnston – Prestressing Strand

Brearley and Johnston (1990) completed a study to determine the effects of a grit-impregnated epoxy coating on the bond of prestressing strand. Fifty-two direct tension pullout tests were performed on specimens made of concrete and prestressing strand. The strand was 1863 MPa (270 ksi), seven-wire, low relaxation strand made by Florida Wire and Cable Company. The concrete mix was designed to have a minimum 28-day strength of 34.5 MPa (5000 psi). The test program considered variations in strand size and surface conditions. Of particular interest for the research presented in this report is the bond exhibited by the uncoated, 9.5 mm (3/8 in.) diameter strand.

The concrete specimens used were 203 mm (8 in.) by 203 mm by 305 mm (12 in.) prisms with the unprestressed strand embedded concentrically along the entire 305 mm axis. Five tests were performed at 28 days on 9.5 mm (3/8 in.) diameter uncoated strands. A center-hole hydraulic ram, operated with a manual pump, was used to pull the strand out of the concrete prism. The strand was concentrically run

through the hydraulic ram assembly and anchored with a prestressing chuck. Washers and steel loading plates were used to minimize the stresses in the concrete near the strand. Slip measurement was measured at the loaded end and the free end of the strand with a dial gage. Results showed that the average ultimate bond strength for the five specimens tested was 3.8 MPa (0.55 ksi) with values ranging from 2.9 to 4.9 MPa (0.42 to 0.71 ksi).

The authors later concluded that the pullout bond strengths did reflect the bond performance in beam tests that were performed in follow-up experiments.

2.4.2 Cooke, Shing, and Frangopol – Prestressing Strand

Cooke et al. (1998) completed a research report for the Colorado Department of Transportation and the Federal Highway Administration on transfer and development length of steel strand in prestressed box girders. The concrete mix had a specified 28-day strength of 69 MPa (10 ksi). In addition to directly testing three box girders, nine pullout tests were performed. Using a pullout procedure developed by Mostafa (1977), 15 mm (0.6 in.) diameter prestressing strands were embedded 457 mm (18 in.) in concrete. The block dimension was 2438 mm (96 in.) long by 914 mm (36 in.) deep by 610 mm (24 in.) wide with 8 strands placed in each block, embedded in the direction of the 914 mm depth. The specimen contained substantial confining steel and also had sufficient spacing between each strand so that stresses from one test would not disturb the concrete in a later test. The high strength concrete was allowed to cure for 2 days before pullout tests started and the compressive strength was 39

MPa (5690 psi) on the day of the tests. A similar setup to that described in the preceding pullout test was used incorporating a center hole ram, hand pump, prestressing chuck, and steel block.

Load at first slip and the maximum load were recorded giving average values of 134 and 215 kN (30 and 48 kips), respectively. Using the given 457 mm (18 in.) embedment, bond strengths were 7.3 and 11.8 MPa (1.1 and 1.7 ksi) for the 134 and 215 kN loads, respectively.

The corresponding beam tests performed showed satisfactory results for the development length stipulated in ACI 318 (equation 2.1).

2.4.3 Mahmoud, Rizkalla, and Zaghloul – Leadline

In 1999, Mahmoud et al. conducted research on transfer and development lengths of CFRP prestressing tendons. A total of 52 pretensioned concrete beams and pretensioned prisms were tested in this study. The beam and prism specimens were pretensioned with 8 mm (0.315 in.) Leadline tendons, 10.5/12.5/15.2 mm (0.41/0.49/0.6 in.) carbon fiber composite cables (CFCC), and 12.7 mm (0.5 in.) steel strand. The prestressing levels varied from 58 to 80 percent of the guaranteed strength reported by the manufacturers. Furthermore, all specimens were fitted with strain gages which were fixed to the prestressed strands to monitor strains during release and loading. The prestressing tendons were debonded over 50 mm or 100 mm (2 or 4 in.) at each end of the beam to minimize stress disturbances as well as confinement within the support zone. Some of the beams were fitted with stirrups to

provide sufficient reinforcement to avoid premature shear failure. This was done to compare the effects of confinement versus no confinement.

The prisms varied in cross section based on the size of prestressing reinforcement used. The intent was to achieve approximately equal stresses in the concrete cross section after transfer for the different types of the prestressing reinforcement used in this study. Embedment lengths varied from 750 mm (29.5 in.) to 1900 mm (75 in.). The method of casting involved positioning a hollow jack and a hollow load cell between two prism molds. The prestressing tendon was then prestressed and the prisms were poured. Teflon sheets were placed between the jack and the concrete surface to permit transverse deformations of the concrete during testing. Displacement transducers (LVDTs) were positioned at the ends of the tendon and Demec points were glued to the concrete surface to help monitor concrete strains.

The beams were tested in flexure using a universal testing machine with 1000 kN (225 kip) capacity to apply a one-point or a two-point static load. The prism tests were carried out in two steps. Upon release of the jacking force, the stress from the tendon was transferred to the prisms. The strain gages attached to the prestressed strands and the Demec points were used to determine the transfer lengths at the two ends. After these measurements were made, a load was applied by the hollow jack while slip was measured with the LVDTs.

Based on results from the prism tests, the authors proposed the following equation for transfer length which is a function of the diameter of the tendon (d_b), the initial prestressing level (f_{pi}), and the concrete compressive strength at transfer (f'_{ci}).

$$L_t = \frac{1.89 f_{pi} d_b}{\alpha_t f'^{0.67}_{ci}} \qquad (2.4)$$

The coefficient α_t is determined from a regression analysis of the test data and the factor 1.89 is used for conversion from metric to US customary units. For Leadline, α_t is 1.9. The equation for flexural bond length was determined in the beam tests. In this equation, the flexural bond length is a function of the increase of stress from the effective prestress level (f_{pe}) to the ultimate tensile strength (f_{pu}), the tendon diameter (d_b), and the concrete strength at the time of the test (f'_c).

$$L_f = \frac{1.89\left(f_{pu} - f_{pe}\right) d_b}{\alpha_f f'^{0.67}_{c}} \qquad (2.5)$$

The coefficient α_f is determined from a regression analysis of the test data and the factor 1.89 is again used for conversion to English units. For Leadline, α_f is 1.0. The summation of equations 2.4 and 2.5 is the development length for Leadline in pretensioned applications.

2.4.4 Conrad, Bakis, Boothby and Nanni – Leadline / C-BAR

Conrad et al. (2000) completed a report for the Federal Highway Administration on recommendations for prestressing highway bridges with CFRP tendons. The

primary purpose in conducting pullout tests was to compare the effects of tendons conditioned in high alkaline solutions against those that were not. The specimen consisted of a 152 mm (6 in.) concrete cube with a tendon penetrating through the center. Concrete strength was 34 MPa (5000 psi) and pullout was performed by a hydraulic universal testing machine. With one moving head and one stationary head, the bar could be simply attached to the moving head while the concrete cube could be fixed beneath the stationary head. Three to four specimens were replicated for each different embedment length and material.

For Leadline tendons, 8 mm (0.31 in.) tendons with embedments based on bar diameters (d_b) of $5d_b$, $10d_b$, and $15d_b$ were used. Their results show that the average maximum bond stresses decreased from 20.7 to 19 MPa (3 to 2.8 ksi) as the embedment increased. Leadline tendons performed better than all other FRP tendons tested, even those with ribbed surfaces. Upon close visual inspection of the bonding surface between Leadline and concrete, it was noted that there was no visual damage to the concrete. The shearing of the spiral deformation on the Leadline surface caused the bond failure.

Twelve-millimeter diameter C-BAR reinforcing bars were used in a pullout setup identical to that defined for Leadline. The average bond strengths found for the $2.5d_b$ and $5d_b$ embedments were 18 and 16.6 MPa (2.6 and 2.4 ksi), respectively. All bars with $10d_b$ embedment failed by rupture in the FRP bar at the grip before maximum bond strength could be reached.

2.4.5 Lu, Boothby, Bakis and Nanni – Leadline

Following up the pullout tests conducted by Conrad et al. (2000), a series of beam tests were performed to enable the direct evaluation of development length. Results of this study show significant conservatism in using the ACI development length equation (equation 2.1) for FRP. Lu et al. (2000) recommend the following changes to the ACI formula. First, the rupture strength (f_u) of the FRP tendons should be used instead of the stress at the nominal flexural strength of the cross-section (f_{ps}) in the second half of the ACI formula. Second, the higher bond stress developed by FRP tendons should be taken into account. To account for this, the flexural bond length is reduced by 25 percent. The equation proposed is as follows:

$$l_d = \frac{1}{3} f_{pe} d_b + \frac{3}{4}(f_u - f_{pe}) d_b \qquad (2.6)$$

Lastly, the authors found that for different FRP materials, the development length trend agreed almost perfectly with the bond strength trend in the pullout tests.

2.4.6 Karlsson - C-BAR

Karlsson (1997) completed his Ph.D. thesis at the Chalmers University of Technology dealing with bond between C-BAR and concrete. The author looked at various parameters including concrete strength, bar diameter, embedment length, and concrete cover. The specimen size used was a 203 mm (8 in.) concrete cube with a

concentrically placed reinforcing bar. The pullout test setup is very similar to those presented previously. In order to provide an anchor to grip the specimen with, Karlsson chose to slide steel tubes over the C-BAR rods. Epoxy was used to fill in the gaps and to bond the rod to the steel tube. The steel tubes had inner and outer diameters of 20 and 22 mm (0.79 and 0.87 in.), respectively, and were 254 mm (10 in.) long. Then, grips used in normal tension testing machines were used to grip the steel tubes.

Of the data obtained by Karlsson, the results that are of interest here are those for the 13 mm (0.5 in.) diameter bar with concrete strength of 29 and 42.8 MPa (4200 and 6200 psi). Bond lengths of $3d_b$, $5d_b$, and $7d_b$ were used for the tests. The three tests using 29 MPa concrete were somewhat inconclusive as one bar failed in rupture, and in another test, the load was extremely low. The third test gave a bond strength of 18.6 MPa (2.7 ksi). For the 42.8 MPa concrete, the bond strength of the three specimens was very consistent and gave an average of 21.4 MPa (3.1 ksi).

The author drew many conclusions from the data, but most importantly found that C-BAR had higher bonding capacity than Swedish Ks400 steel bar of the same diameter with ribs. It also proved comparable to the Swedish Ks600 steel bar with ribs.

2.4.7 Rizkalla et al. – C-BAR

A research team from the University of Manitoba completed research for Marshall Industries Composites, Inc., the manufacturer of C-BAR (Rizkalla, 1997).

Testing focused on the material properties of C-BAR. Using pullout tests, varying embedment length and the presence of confinement were explored. The concrete specimens tested were inverted T-sections with a top width of 152 mm (6 in.) and a bottom width of 457 mm (18 in.). The specimens were constructed 1524 mm (60 in.) long so that six C-BAR rods could easily be placed in each. Both the base and the middle were reinforced with confining steel. A total of 26 C-BARs were tested including eight bars that were shallowly embedded in the unconfined concrete region at the top of the specimens. The research team utilized a simple technique to eliminate the radial friction confinement from the contact between the loading plate and the concrete surface at the top of the concrete near the bar. A loading frame was constructed so that it was supported by the base of the inverted T-section rather than the top of the concrete near the reinforcing bar. For anchorage, the same style steel pipe as used by Karlsson was filled with epoxy resin and gripped with a standard tension grip.

The average concrete compressive strength used was 44.2 MPa (6400psi). The eight unconfined C-BAR specimens had maximum bond stresses of 11 MPa (1.6 ksi) while the 18 confined C-BAR specimens had average maximum bond stresses of 21.4 MPa (3.1 ksi). The data for the bond strengths all came from rods with embedments of $2.5d_b$ and $5d_b$. All embedment lengths greater than this resulted in failure by C-BAR rupture. Further data obtained by the authors show that epoxy-coated steel had a larger ultimate bond strength than that of C-BAR, conflicting with conclusions drawn by Karlsson.

2.4.8 Eligehausen, Popov, and Bertero – Reinforcing Steel

Eligehausen et al. (1983) conducted numerous pullout tests on deformed steel bars in concrete in an attempt to better understand the bond stress-slip relationship between the two materials. The authors explored numerous parameters including: confinement, bar diameter, concrete strength, bar spacing, pullout rate, and cyclic loading. Special care was taken to make sure that the specimen design would be free of the effect of additional parameters. All of the 125 pullout specimens tested had embedment lengths of $5d_b$. With this bond length, the authors felt that the slip measured at the free end of the bar would represent the local slip in the middle of the embedment length with sufficient accuracy. At the same time, this length was long enough that it would reduce the scatter of results observed in tests using shorter embedment lengths. Specimen size varied based on the type of bar used. The dimensions of the rectangular test specimens were 305 mm (12 in.) by $15d_b$ by $7d_b$, with $15d_b$ being in the direction along which the steel bar was placed. Since the three bars studied were #6, #8, and #10, this lead to a variety of specimen sizes. Pullout was performed by a hydraulic universal testing machine.

Only two specimens were tested without confinement. The concrete compressive strength was approximately 30.7 MPa (4450 psi) and the bar size was #8 (25 mm diameter). In both cases, the specimens failed by splitting of the concrete along the longitudinal axis of the bar. The bond strength at failure was 6 MPa (870 psi). Upon closer examination, the concrete between the lugs (deformations on the steel surface)

was found intact and uncrushed. For confined specimens, the average bond strength was about 13 MPa (1.9 ksi).

2.5 Experimental Program

2.5.1 Material Properties

The FRP bars tested in the pullout tests were chosen by the precaster for the I-225/Parker Road project as was mentioned in Section 2.1. The steel strand and deformed bars are used for comparison purposes. Table 2.1outlines the material properties of the bars as reported by the manufacturers.

Table 2.1 Nominal properties of reinforcing materials
(1 ksi = 6.9 MPa)

	Material Properties		
Reinforcement Type	Yield Strength *ksi*	Ultimate Strength *ksi*	Modulus of Elasticity *ksi*
Leadline	NA	409	21320
C-BAR	NA	105	6000
Rebar	40	65	29000
7-wire prestressing strand	245	270	27000

LEADLINE

Leadline is a CFRP rod that is pultruded and epoxy-impregnated. It is manufactured by Mitsubishi Chemical Corporation of Japan. The intended use of Leadline is for prestressing. As shown in Figure 2.1, the rod has a shallow helical depression that extends along its entire length. The carbon fiber used in Leadline has

a tensile strength of approximately 4830 MPa (700 ksi). The composition of Leadline is 65 percent carbon fiber and 35 percent epoxy resulting in a theoretical tensile strength of 3140 MPa (455 ksi). However, the tensile strength is very much related to the grip used to apply the tensile force. Currently, the manufacturer has developed a grip that can provide a guaranteed tensile strength of 2820 MPa (409 ksi). The grip/anchor is shown in Figure 2.2. The modulus of elasticity of Leadline is 147 GPa (21320 ksi).

Additional tests were performed on Leadline by Cusson (2001) at the University of Colorado. Preliminary results from three 10 mm (0.39 in.) Leadline tendons show a mean tensile strength of 3059 MPa (444 ksi).

Ten millimeter (0.39 in.) Leadline tendons were used for the pullout tests.

C-BAR

C-BAR is a GFRP bar manufactured in a pultrusion process by Marshall Industries Composites, Inc. C-BAR is used as a replacement for mild reinforcing steel. The fiberglass used to manufacture C-BAR reinforcing rods has a maximum tensile strength between 2070 and 3450 MPa (300 and 500 ksi) depending on the grade used. The rods are composed of 70 percent fiberglass and 30 percent epoxy/other additives, thus giving a theoretical strength ranging from 1415 to 2415 MPa (210 to 350 ksi) (Karlsson, 1997). In the C-BAR used in the pullout tests for this research, the guaranteed tensile strength is 725 MPa (105 ksi). The modulus of elasticity is 41 GPa (6000 ksi). No commercial grips have been developed for this

type of bar. The common method used for tension tests is to slide a steel tube over the C-BAR and fill it with epoxy. After curing, large grips can be used to grasp the steel tubing directly. The surface deformation on the C-BAR is formed using a hybrid pultrusion/compression molding process. These raised deformations effectively develop mechanical interlock with the concrete increasing the bond strength significantly. Figure 2.1 shows these deformations.

Along with the tests performed on Leadline by Cusson at the University of Colorado as discussed previously, tests were also performed on C-BAR. Preliminary results from three 10 mm C-BAR reinforcing rods show a mean tensile strength of 819 MPa (119 ksi).

Thirteen millimeter (0.5 in.) C-BAR reinforcing bars were used for the pullout tests.

STEEL REBAR

The reinforcing steel used was uncoated #4 bar (13 mm in diameter). It has a nominal yield strength of 270 MPa (40 ksi) and was manufactured by Fiero Metals in California. The reinforcing steel met the requirements of ASTM A 615.

SEVEN-WIRE STEEL PRESTRESSING STRAND

The prestressing strand used in testing is standard 9.5 mm (3/8 in.) diameter seven-wire, low relaxation strand. The nominal yield strength is 1865 MPa (270 ksi)

and was manufactured by Florida Wire and Cable. The strand was manufactured to meet the requirements of ASTM A 416.

CONCRETE

The concrete mix design used in the pullout tests is given in Table 2.2. It is a special mix developed at the University of Colorado as part of the Innovative Bridge Research and Construction (IBRC) project with CDOT. It has low cement paste and high fly ash content to reduce temperature and shrinkage cracks and chloride permeability. In an attempt to comply with ASTM A 882 standard for pullout tests, 31 MPa (4500 psi) was chosen as the target concrete compressive strength. The water-cement ratio was 0.41. When considering the water-cement ratio for a mix design containing fly ash and silica fume, these two ingredients must be added to the weight of cement. The aggregate had a maximum size of 25 mm (1 in.) and was from a river bottom, making it rounded and smooth. A high range water reducer was used to improve workability.

Table 2.2 Concrete mix design

Major components	*kg/m^3*	*lbs/yd^3*
Cement	297	500
Water	151	254
Sand	806	1360
Gravel	946	1595
Fly ash	59	100
Silica fume	12	20
Additives	*ml/m^3*	*oz/yd^3*
High range water reducer	2200	57
Micro Air	260	17

Four batches were made. Each batch was 0.19 m^3 (0.25 yd^3). This was enough to fill five pullout specimens as well as three to four 152 mm (6 in.) by 305 mm (12 in.) cylinders for compression testing. The pullout specimens were made with 152 mm by 305 mm cylinder molds with a reinforcing bar or prestressing tendon placed concentrically in the cylinder. All but one compression test cylinder were tested at 28 days. The measured concrete strengths are shown in Table 2.3.

Table 2.3 Measured concrete strengths

Batch #	**Curing time** (*days*)	$\mathbf{f'_c}$ (*psi*)	**Average** (*psi*)
1	3	2518	
1	28	3873	3953**
1	28	4032	
2	28	4315	
2	28	4150	4231
2	28	4226	
3	28	4200	
3	28	4191	4147
3	28	4050	
4	28	4287	
4	28	4713	4502
4	28	4934	
4	28	4076	

**based on 28-day break strength

The average strengths listed in Table 2.3 were all within the desired range. In all cases, the compressive strengths were reasonably consistent.

2.5.1 Test Specimen

There are a variety of methods to conduct pullout tests. Some standards exist, but most of the time the specimen is altered in order to more effectively attain the results desired. In the case of this research, it was important to have a simple specimen that could be used with different reinforcing materials for consistency in comparison. The main consideration for the specimens was that development lengths chosen for each material type would result in a similar failure type. Concrete splitting, bar rupture, or anchor failure would lead to inconclusive results. Thus, special caution was used to make sure these would not happen.

The bar sizes that were tested were based on the bars used in the design of the CDOT bridge deck. But more importantly, the comparable materials (Leadline and prestressing steel; C-BAR and reinforcing steel) were to have approximately the same dimensions. Thus, 9.5 mm (3/8 in.) prestressing strand and 10 mm (0.39 in.) Leadline were chosen along with #4 (13 mm) reinforcing steel and 13 mm (0.5 in.) C-BAR.

Literature and testing standards in the prestressing industry were the basis for specimen design. ASTM A 981 and ASTM A 882 are the standard specifications for bond tests of uncoated prestressing strand and epoxy-coated prestressing strand, respectively. However, even though ASTM A 981 is the standard for uncoated strand, it suggests the use of cement grout and incorporates a steel tube to confine the grout around the tendon. This setup was determined not suitable for the data desired. ASTM A 882 recommends the use of a standard 152 mm (6 in.) by 305 mm (12 in.) concrete cylinder to conduct pullout tests. In addition to the fact that other

researchers have followed a similar setup, this specimen would provide an uncomplicated setup that would be simple to duplicate. Confining reinforcement was an option that was not recommended by this standard, but has been considered by other researchers. For the sake of simplicity, it was deemed unnecessary for this experiment.

The embedment length was carefully chosen so that concrete splitting failure would be unlikely while still allowing for sufficient development to attain consistent results. However, an initial consideration for FRP specimens is that although they have high tensile strength, they are difficult to grip without crushing the transversely isotropic fibers. Thus, depending on the grip used, it is essential that the strength of the bond is not stronger than the strength of the grip. In order to prevent crushing in the FRP bar, a method similar to that used by Rizkalla (1997) and Karlsson (1997) was used. They proposed the use of a 254 mm (10 in.) long steel tube slightly larger than the outside diameter of the bar/rod being tested. The space between the bar and the tube was to be filled with epoxy. In this research, the strength of the epoxy chosen was unknown, so 356 mm (14 in.) steel tubes were used to provide additional anchor strength. One tube with respective inner and outer diameters of approximately 19 and 27 mm (0.75 and 1.06 in.) was used for the C-BAR reinforcing bars. The tube used for the Leadline tendons had inner and outer diameters of 16 and 22 mm (0.63 and 0.87 in.), respectively. Thus, for both anchor tubes, there was about 3-4 mm (0.12-0.16 in.) of space between the centered FRP bar and the inside of the steel tube. In order to keep the tubes centered on the FRP bars, properly sized washers were

taped to the ends of the tubes. The epoxy used was West Systems 205 Fast Hardener. This anchor system provided adequate grip without crushing the fibers.

For C-BAR, literature has shown that embedments from $5d_b$ to $7d_b$ have given satisfactory results without prominent concrete splitting failure. Because the embedment for splitting failure is very close to $7d_b$, both lengths were used. For Leadline, the range used by Conrad (2000) provided satisfactory results so an embedment of $10d_b$ was chosen. In the case of the two steel specimens, standard prestressing chucks were used for anchoring, thus gripping was not essential in choosing a bond length. For prestressing tendons, ASTM A 882 recommends an embedment length of 191 mm (7.5 in.) for a 9.5 mm (3/8 in.) diameter bar. For reinforcing steel, a similar embedment to that of Eligehausen et al. (1983) was chosen. They used $5d_b$ for each bar and in the unconfined case, failure was governed by concrete splitting. Although splitting was undesirable, the bars they tested were #8 bars (25 mm diameter), which are significantly larger than the #4 bars (13 mm diameter) tested in this setup. It was felt that the smaller #4 bar would not cause concrete splitting. A small increase from $5d_b$ was deemed necessary to improve the consistency of the results so $6d_b$ was chosen.

In order to create the proper bond length, PVC pipe was cut into various lengths, 50 to 200 mm (2 to 8 in.), and placed around the bar similar to the methods of many other researchers. Where the PVC fit loosely around the bar, tape was wrapped to keep the bar centered. Non-adhesive sealer was used to seal the ends so concrete would not seep into the bond free zone during construction. Fifty to one hundred

millimeters (2 to 4 in.) of bond free length was introduced at the bottom of a specimen while 100 to 200 mm (4 to 8 in.) was introduced the top as shown in Figure 2.3.

2.5.2 Test Program

For this study, the primary parameter varied was the bar type. Table 2.4 gives a summary of the test program. Four to six tests were chosen for each bar type and embedment length. This was a reasonable number for the scope of the work and still allowed for statistical significance in the event that some tests had to be discarded. No automated data acquisition system was used to obtain continuous load-slip data. The test data taken would be load at 0.025 mm (0.001in.) slip, load at first slip, the value of the first slip, and the maximum load reached. The load at 0.025 mm slip is prescribed by ASTM 882 as a load value to compare with tabulated required minimum values.

Table 2.4 Pullout test program

Specimen number	Concrete batch	Material	Embedment *inches / (mm)*	Bar diameter *inches / (mm)*
1	1	Leadline ($10d_b$)	3.93 / (100)	0.394 / (10)
2	1	C-BAR ($5d_b$)	2.56 / (65)	0.512 / (13)
3	1	C-BAR ($7d_b$)	3.58 / (91)	0.512 / (13)
4	1	rebar ($6d_b$)	3.00 / (76)	0.5 / (12.7)
5	1	rebar ($6d_b$)	3.00 / (76)	0.5 / (12.7)
6	2	C-BAR ($7d_b$)	3.58 / (91)	0.51 / (13)
7	2	C-BAR ($5d_b$)	2.56 / (65)	0.51 / (13)
8	2	prestressing strand ($20d_b$)	7.50 / (191)	0.375 / (9.5)
9	2	prestressing strand ($20d_b$)	7.50 / (191)	0.375 / (9.5)
10	2	Leadline ($10d_b$)	3.93 / (100)	0.39 / (10)
11	3	Leadline ($10d_b$)	3.93 / (100)	0.39 / (10)
12	3	C-BAR ($7d_b$)	3.58 / (91)	0.51 / (13)
13	3	C-BAR ($5d_b$)	2.56 / (65)	0.51 / (13)
14	3	rebar ($6d_b$)	3.00 / (76)	0.5 / (12.7)
15	3	rebar ($6d_b$)	3.00 / (76)	0.5 / (12.7)
16	4	prestressing strand ($20d_b$)	7.50 / (191)	0.375 / (9.5)
17	4	prestressing strand ($20d_b$)	7.50 / (191)	0.375 / (9.5)
18	4	prestressing strand ($20d_b$)	7.50 / (191)	0.375 / (9.5)
19	4	Leadline ($10d_b$)	3.93 / (100)	0.39 / (10)
20	4	Leadline ($10d_b$)	3.93 / (100)	0.39 / (10)

Note: Mixes 1-2 and 3-4 were poured on separate days.

2.5.3 Fabrication and Curing of Test Specimens

All test bars were cleaned of any excess debris with a rag. The seven-wire steel strand was cleaned with a wire brush in the region of the embedment length in order to remove the excess rust that had formed on the surface. This was not necessary for the reinforcing steel as no rust was visible. A wood frame was constructed as shown in Figure 2.4. For stability, the wood frame was secured to a sturdy steel frame at both ends as shown in the figure. The purpose of the wood frame is two-fold. First, the two pieces that span above the cylinders keep the bars and tendons in a sturdy,

vertical position. This was done by fixing the bars to the wood at both locations with flexible wire. The second purpose for the frame was to fix the base of the plastic concrete molds in location. As is shown in Figure 2.4, the cylinders are secured in place. Not visible are the 38 mm (1.5 in.) wood spacers that fit between each cylinder, keeping it from moving. This precision was necessary as the bars must be as close to the center as possible to optimize the concrete cover available.

The concrete was poured carefully in order to keep the bottom of the bars from moving. This was particularly difficult with the flexible seven-wire steel strand. Because the bars were sturdily connected to the frame above, it was possible to tap the bars after pouring to make sure they were in their original position. No plunger vibrator was used for fear of disturbing the specimens. For this reason, as was discussed earlier, a special mix with water reducers was used to facilitate consolidation. The cylinders were filled slowly and tapped in order to insure consolidation. Upon completion, the specimens were covered with plastic covers and left for 2 days. Then the specimens were removed from their molds and stored in a fog room (100 percent humidity, 20 degrees Celsius).

Before testing, approximately 6 to 12 mm (0.25 in. to 0.5 in.) of concrete was removed from the base of the cylinder to expose the bottom of the bar being tested. This was done so that slip data could be measured from the base of the pullout rod/bar. Also, for the case of Leadline and seven-wire prestressing strand, the excess tape was drilled out using a hole saw in order to insure that the tape would not play a

role in the pullout results. Both of these procedures were performed with extreme caution so as not to disturb any of the specimens.

2.5.4 Experimental Setup and Testing Procedure

Two slightly different testing setups were utilized based on the anchors used. A large grip was needed to grip the steel tubes that acted as anchors for the FRP bars. A Baldwin Universal Testing Machine had tension grips that were able to effectively grab the large steel tubes. In order to use the universal testing machine (UTM), the pullout setup was suspended beneath the testing machine as is shown in Figure 2.5.

The reinforcing steel and seven-wire strand could be gripped with a prestressing chuck. A simple setup shown in Figure 2.6 was used by placing two I-beams next to each other and placing the specimen and hydraulic ram on top. This process is more efficient for repeated testing.

Figure 2.7 shows the dimensions and schematic of the FRP testing setup using the UTM. A 19 mm (0.75 in.) thick steel washer with a 38 mm (1.5 in.) hole in the center and a 3 mm (0.13 in.) thick rubber spacer was placed on top of the specimen to help eliminate any stress concentrations on the top of the concrete cylinder near the protruding bar. The ram was an Enerpac center-hole hydraulic ram (model RRH-306), controlled with a 68.9 MPa (10,000 psi) Enerpac hand pump (model P-84). A 32 mm (1.25 in.) thick steel plate with steel angles welded on each corner was used in the UTM setup to keep the jack from pushing directly against the grips above it. On the base of the concrete cylinder, a specially fabricated piece secured with two hose

clamps was used to firmly hold a dial gage to measure bar slip during pullout. Figure 2.8 shows a close-up of the setup. The dial gage had 0.025 mm (0.001 in.) increments and a range of movement of 18 mm (0.7 in.). In the UTM setup, the cylinder, ram, and steel plate were stacked and placed on the bottom (moving) head of the UTM. This setup was then raised into position so that the top head (stationary) could grip the steel tubes. Once this was done, the lower head was lowered and the dial gage was fixed to the cylinder.

In both setups, the ram was extended until there was a load applied against the prestressing chucks or the top head of the UTM. The load was applied at a slow rate; however, there was no way to accurately measure this rate as the load application was done by hand. The applied loadings were measured with a pressure gage on the hand pump which had increments of 0.345 MPa (50 psi). With a piston area of 4219 mm^2 (6.54 $in.^2$), this provides load increments of 1.5 kN (337 lbs.).

2.7 Results

2.7.1 General

In this section, the experimental results will be presented along with a discussion of the various failure modes observed. Results are organized by the types of bars tested so that direct comparisons can be made. Pullout forces (F) were converted to bond strengths (τ) using equation 2.7.

$$\tau = \frac{F}{\pi d_b l_e} \qquad (2.7)$$

where l_e = embedment length (see Table 2.4)

d_b = nominal bar diameter

The effect of concrete strength is not considered here. As stated in Section 2.3.6, the concrete strengths were uniform enough that they would not affect the results of the test. Furthermore, in looking at the bond strength data shown in Table 2.5 through Table 2.9, no clear trend exists with the small variation of concrete strength.

2.7.2 Test Results

The results for the pullout of Leadline are shown in Table 2.5. All tests were performed at 28 days unless otherwise noted. Each test gave consistent data except for Specimen #10. In each of the other cases, loading steadily increased up to a slip of 3.8 to 4.3 mm (0.15 to 0.17 in.). At this point, there was a sudden loss of load and the bar began pulling out of the concrete cylinder with minimal additional load applied. There was no additional load capacity after this. There were problems with the epoxy anchor on Specimen #1. It had to be re-epoxied and pulled out at a later date. The final cure time for Specimen #1 was 31 days. The results for this specimen do not differ from the others significantly enough to discard its data. The average bond strength found in this study was 10.9 MPa (1.58 ksi). However, Conrad et al. (2000) attained bond strengths of 20 MPa (2.9 ksi). No clear reasoning for this

difference is evident as the concrete strength and degree of confinement provided by the concrete cover appear very similar.

Table 2.5 Pullout results for 10mm Leadline; embedment = $10d_b$

(1 ksi = 6.9 MPa / 1 in. = 25.4 mm)

#	**Average f'_c** (psi)	**First slip** (inches)	**Bond strength** *0.001in. slip* (ksi)	**Average bond strength** *0.001in. slip* (ksi)	**Bond at first slip** (ksi)	**Average bond strength** *first slip* (ksi)	**Maximum bond strength** (ksi)	**Average maximum bond strength** (ksi)
1	3953	0.16	0.6270	0.6632	1.6880	1.5846	1.6880	1.5846
10	4231	0.002	0.6673		1.1978		1.1978	
11	4147	0.15	0.7344		1.8492		1.8492	
19	4502	0.17	0.6941		1.5000		1.5000	
20	4502	0.17	0.5934		1.6880		1.6880	

Table 2.6 shows the results of the pullout tests for 9.5 mm (3/8 in.), seven-wire steel strand. Again, the results appeared to be consistent. During the tests, the strand would initially exhibit negligible slip. This is shown by the low values of first slip and the high loads attained at a slip of 0.025 mm (0.001 in.). In the case of Specimens #8 and #9, the tendons reached maximum bond strength before a slip of 0.025 mm. However, after reaching the maximum bond strength, the tendons retained bond strengths of 478 to 606 MPa (0.75 to 0.95 ksi) up to slip of 40 to 50 mm (1.5 to 2 in.). This residual strength is thought to be due to the spiral winding of prestressing strand. Because the concrete mold around the tendon never sheared, the tendon was forced to twist out. This was validated upon release of the ram load as the tendon quickly unraveled. It is difficult to compare these values to those determined in the literature. Confinement, bar size, concrete strength, and surface condition of strands were

different from those used in this setup. However, the results found were between those found by Brearley et al. (1990) and Cooke et al. (1998).

Table 2.6 Pullout results for 3/8in. 7-wire steel strand; embedment = $20d_b$ (1 ksi = 6.9 MPa / 1 in. = 25.4 mm)

#	**Average f'_c** (psi)	**First slip** (inches)	**Bond strength** *0.001in. slip* (ksi)	**Average bond strength** *0.001in. slip* (ksi)	**Bond at first slip** (ksi)	**Average bond strength** *first slip* (ksi)	**Maximum bond strength** (ksi)	**Average maximum bond strength** (ksi)
8	4231	X	X	0.6908	1.1066	0.9163	1.1066	0.9904
9	4231	X	X		0.8290		0.8290	
16	4502	0.0095	0.4071		0.9067		1.0362	
17	4502	0.003	0.8882		0.9067		0.9622	
18	4502	0.0015	0.7772		0.8327		1.0177	

The C-BAR results for $5d_b$ and $7d_b$ will be explored independently of each other due largely to the fact that failure modes were significantly different. For the shorter embedment length of $5d_b$, Table 2.7 gives the results. Although only three tests were conducted, the results proved very consistent. Specimen #2 had the same anchor problem described for Specimen #1. Again, it was simply re-epoxied and tested at 31 days and the results did not show any significant changes. The mode of failure for C-BAR was difficult to quantify. Loading increased steadily until it reached its maximum value. At this point, there was a loud acoustic emission followed by an immediate decrease in load carrying capacity. However, upon inspection of each specimen, no visible cracks were found. Once loading was again initiated, the load increased up to a sub-maximum level before it dropped dramatically again at the cue of another acoustic emission. This process continued through a third time (for one of

the specimens) at which no further significant load was attained. Karlsson (1997) gives a thorough description of the failure modes pertaining to the bond failure of C-BAR. The failure routine described is thought to be a result of the shearing off of the ribs.

The rather large bond strengths attained here compare satisfactorily with studies done by Conrad et al. (2000) and Karlsson (1997). Compared to the results found by Rizkalla (1997), the large difference can be attributed to the lack of radial friction confinement in their test setup. In this test setup, the hydraulic jack was placed directly on the top surface of the specimen causing a certain amount of radial friction confinement. For C-BAR, because the ribs on the surface are raised so high, confinement can make a significant difference when considering overall bond capacity.

Table 2.7 Pullout results for 13mm C-BAR; embedment = $5d_b$

(1 ksi = 6.9 MPa / 1 in. = 25.4 mm)

#	**Average f'_c** (psi)	**First slip** (inches)	**Bond strength** *0.001in. slip* (ksi)	**Average bond strength** *0.001in. slip* (ksi)	**Bond at first slip** (ksi)	**Average bond strength** *first slip* (ksi)	**Maximum bond strength** (ksi)	**Average maximum bond strength** (ksi)
2	3953	0.03	1.0996	1.1420	3.2850	3.1526	3.2850	3.1526
7	4231	0.025	1.2029		2.8082		2.8082	
13	4147	0.03	1.1234		3.3645		3.3645	

For C-BAR with a longer embedment length of $7d_b$, Table 2.8 gives the results. Again, the results proved to be consistent. Each specimen acted similarly to what was exhibited by the $5d_b$ embedment case, except that complete splitting failure of the concrete cylinder occurred before the maximum bond strength could be reached.

Thus, the maximum bond strengths were governed by a mechanism that is different from that with an embedment length of $5d_b$. Figure 2.9 shows the splitting crack on the specimen. The tensile stress near the bonded region in the concrete created by the pullout action of the bar caused immediate splitting failure as shown in Figure 2.9. A small amount of load capacity was shown by the pullout specimen after the splitting failure, but this quickly dropped to zero.

Table 2.8 Pullout results for 13mm C-BAR; embedment = $7d_b$

(1 ksi = 6.9 MPa / 1 in. = 25.4 mm)

#	**Average f'_c** (psi)	**First slip** (inches)	**Bond strength** *0.001in. slip* (ksi)	**Average bond strength** *0.001in. slip* (ksi)	**Bond at first slip** (ksi)	**Average bond strength** *first slip* (ksi)	**Maximum bond strength** (ksi)	**Average maximum bond strength** (ksi)
3	3953	0.015	1.3020	1.2944	2.5451	2.6019	2.5451	2.6019
6	4231	0.025	1.2566		2.5168		2.5168	
12	4147	0.02	1.3247		2.7438		2.7438	

Table 2.9 shows the results for the pullout tests for #4 steel bars. The load steadily increased up to the first slip where the maximum load was reached. However, for Specimen #15, the slip remained constant at 0.76 mm (0.03 in.) for a short while as the load increased. Soon after, the specimen reached its maximum capacity and the residual bond strength was reduced to almost zero. The results here do not relate well with those found by Eligehausen et al. (1983). Even in their case where steel confinement was provided, the bond strength never consistently exceeded 13.8 MPa (2000 psi).

Table 2.9 Pullout results for #4 bar reinforcing steel; embedment = $6d_b$

(1 ksi = 6.9 MPa / 1 in. = 25.4 mm)

#	**Average f'_c** (psi)	**First slip** (inches)	**Bond strength** *0.001in. slip* (ksi)	**Average bond strength** *0.001in. slip* (ksi)	**Bond at first slip** (ksi)	**Average bond strength** *first slip* (ksi)	**Maximum bond strength** (ksi)	**Average maximum bond strength** (ksi)
4	3953	0.061	1.2837	1.3566	2.7063	2.9006	2.7063	2.9006
5	3953	0.049	1.5613		3.1226		3.1226	
14	4147	0.075	1.1935		2.8589		2.8589	
15	4147	0.035	1.3878		2.9144		2.9144	

2.7.3 Visual Inspection

After the data was taken and preliminary analysis was complete, each pullout specimen was split along its axis so that the tendon/bar and concrete interaction surface would be exposed. In all cases, specimens in each group had almost identical failure modes.

In the specimens with steel bars, the concrete was crushed along the bonding surface by the raised ribs. With an embedment length of $5d_b$, the C-BAR specimens had partial shearing of the windings. With an increased embedment length of $7d_b$, the C-BAR specimens still showed some shearing of the windings, but not as much as for the $5d_b$ embedment. When comparing the bond failure mechanisms for steel bars and C-BAR, it may seem counter-intuitive that the lower bond strength of the steel caused concrete crushing while the higher bond strength of the C-BAR caused shearing of the windings. This could be explained by the larger size of the C-BAR windings compared to the steel ribs. The larger area of the C-BAR windings reduced the bearing stress in the concrete, increasing the force needed for crushing.

In the seven-wire prestressing strand specimens, a perfect concrete spiral remained which formed around the strand during casting. During pullout, the strand twisted out without any shearing of the concrete. This was exactly as expected. In the Leadline specimen, the raised portion of the spiral deformation sheared off along the whole embedment length.

2.7.4 Discussion of Results

A direct comparison of Leadline and prestressing strand shows that Leadline consistently has higher bond strength. Five Leadline tests give an average bond strength of 10.9 MPa (1.58 ksi) while five steel strand tests give an average bond strength of 6.8 MPa (0.99 ksi). The bar chart in Figure 2.10 gives a comparison of the final bond test results.

Making the same comparison for C-BAR and reinforcing steel, it can be inferred that C-BAR has a higher bond strength than steel bars. In this case, the results are only separated by a small difference. Three C-BAR tests with an embedment length of $5d_b$ give an average bond of 21.7 MPa (3.15 ksi) while the #4 bars give an average bond strength of 20 MPa (2.9 ksi).

Results for C-BAR as shown in section 2.7.2 are similar to what others have obtained (Karlsson, 1997; Conrad, 2000). The tests performed by Eligehausen et al. (1983) were inconclusive because concrete splitting was the governing failure mechanism. Since the tests discussed here did not show any concrete splitting, a comparison cannot be made.

In order to further examine the results, the ultimate bond strength found in the pullout tests for C-BAR and reinforcing steel is related to the development length required. Nilson and Winter (1991) have presented this relation. If the tensile stress reached in the steel is designated as f_s, the average bond force per unit length (U) can be computed:

$$U = \frac{f_s A_b}{l} \qquad (2.8)$$

where A_b = area of the bar

If the unit bond force U is smaller than the ultimate value U_n which can be estimated from pullout tests, no bond failure will occur over the length l. Then, in order to make sure that a bar is anchored with sufficient bond to develop its maximum usable strength (yield stress, f_y), the required development length can be estimated by equation 2.9.

$$l_d = \frac{f_y A_b}{U_n} \qquad (2.9)$$

Table 2.10 compares the development lengths obtained by the ACI equation for steel and the equation for FRP bars in the ACI 440H draft document with the development lengths predicted by equation 2.9 using the average bond strengths obtained in this study. In using equation 2.9 for C-BAR, f_u was used in place of f_y. This is due to the

fact that FRP materials are brittle with no material nonlinearity. In the calculations, values for the variables defined in the ACI code (equation 2.2 in this chapter) are as follows: $\alpha = 1.0$, $\beta = 1.0$, $\gamma = 1.0$, $\lambda = 1.0$, and $(c + K_{tr})/d_b = 2.5$.

Table 2.10 Comparison of development lengths (1 in. = 25.4 mm)

Material	**ACI equation for steel** (equation 2.2)	**ACI 440H draft equation for FRP** (equation 2.3a/2.3b)	**Calculated development length** (equation 2.9)
C-BAR		20 in.	4.36 in.
Reinforcing Bar	15 in.		1.75 in.

The values in Table 2.10 show an extremely large safety margin in the design equations.

Figure 2.1 Materials used in testing (from left to right): reinforcing steel, C-BAR, prestressing strand, and Leadline

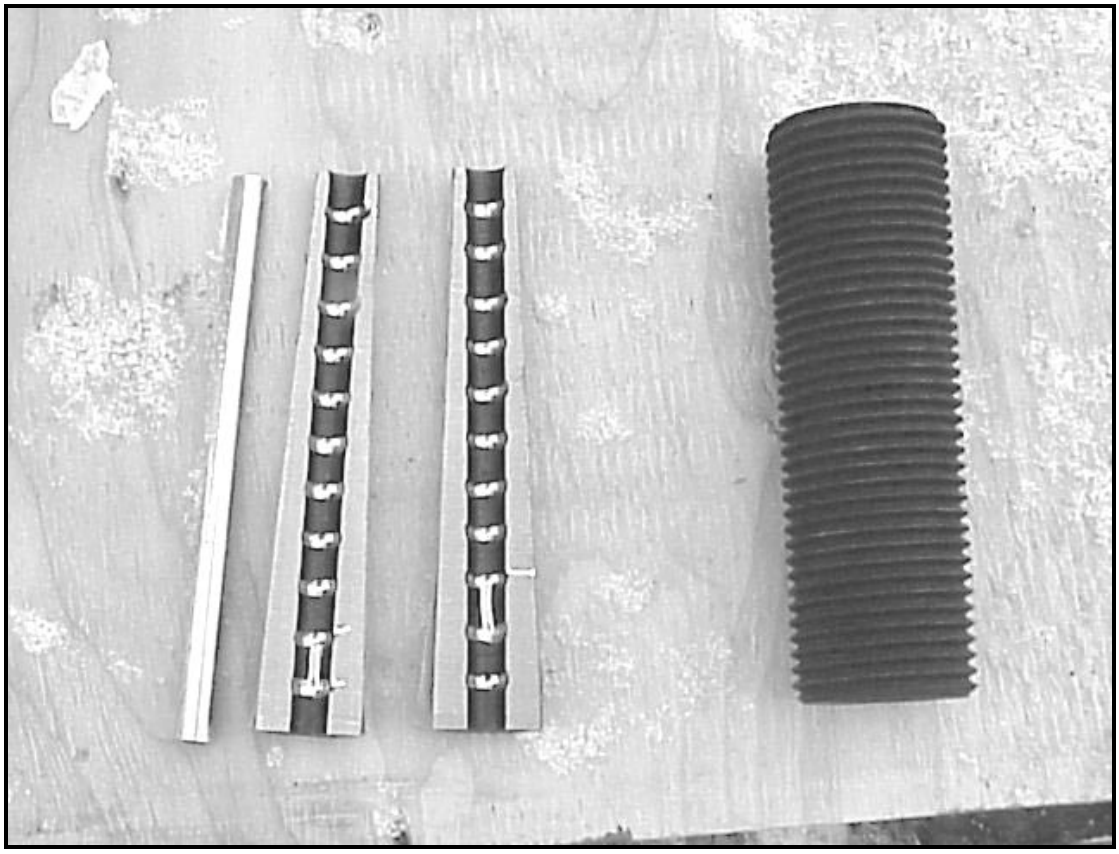

Figure 2.2 Leadline anchor pieces (left to right, aluminum sleeve, two grooved wedge pieces, steel socket)

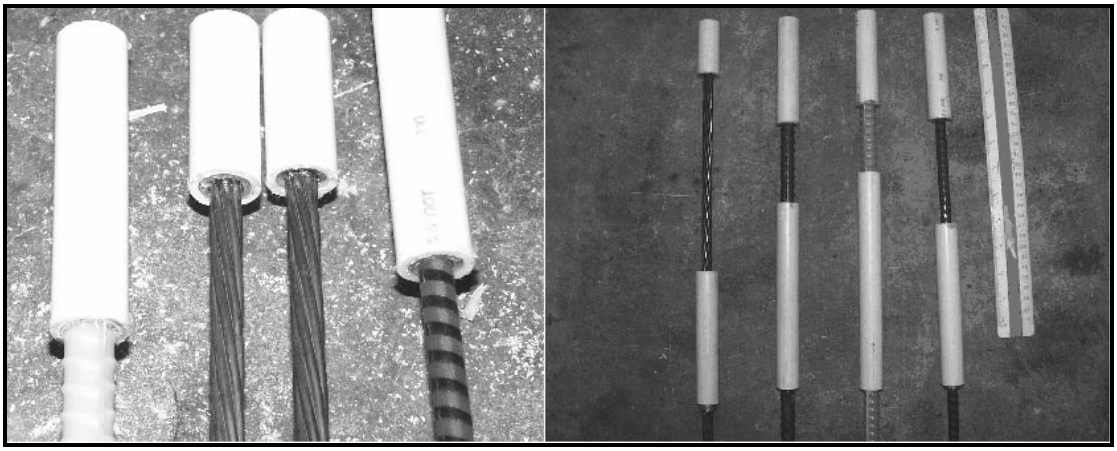

Figure 2.3 Debonded areas and embedment length

Figure 2.4 Specimen casting setup

Figure 2.5 FRP bar specimen setup using Universal Testing Machine

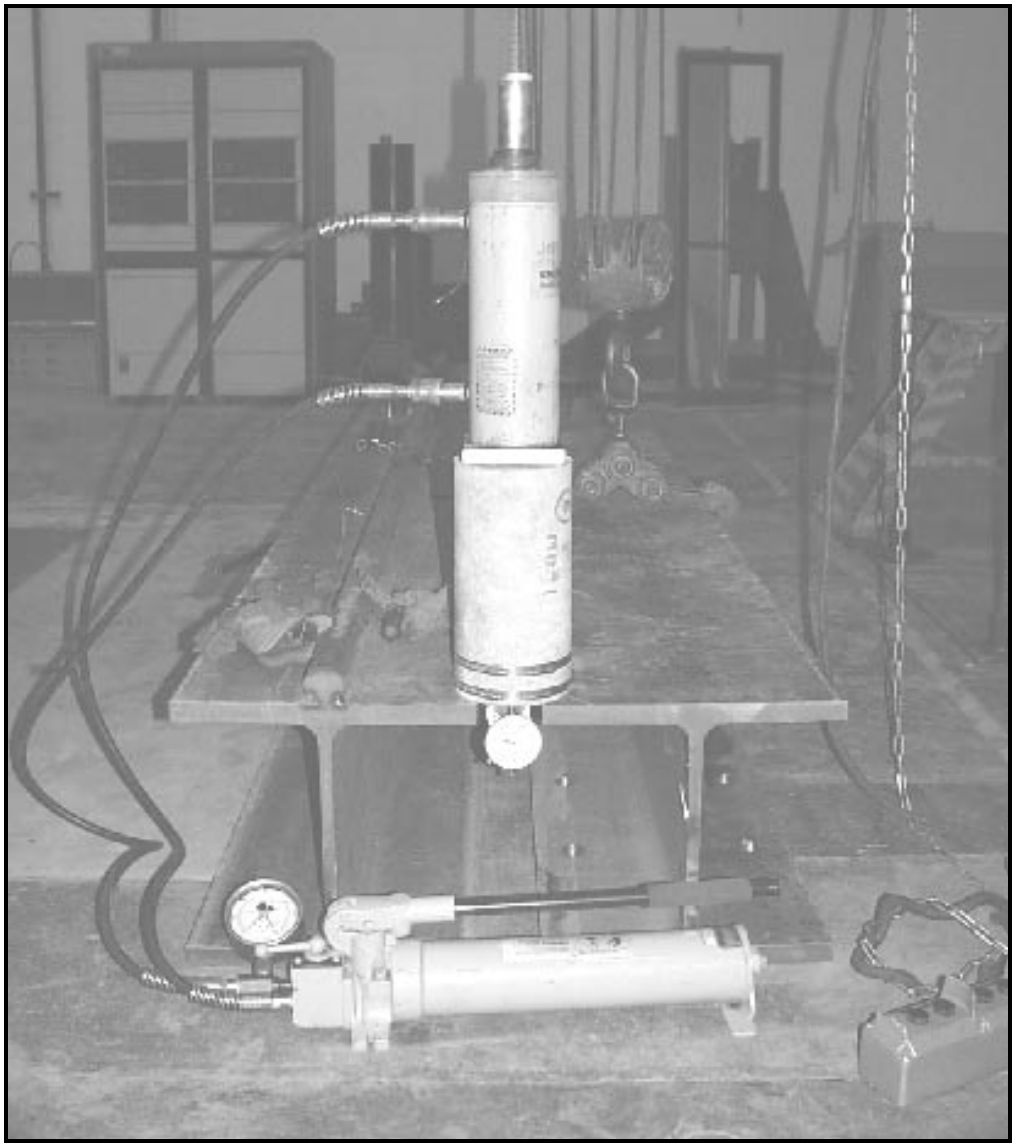

Figure 2.6 Steel bar specimen setup

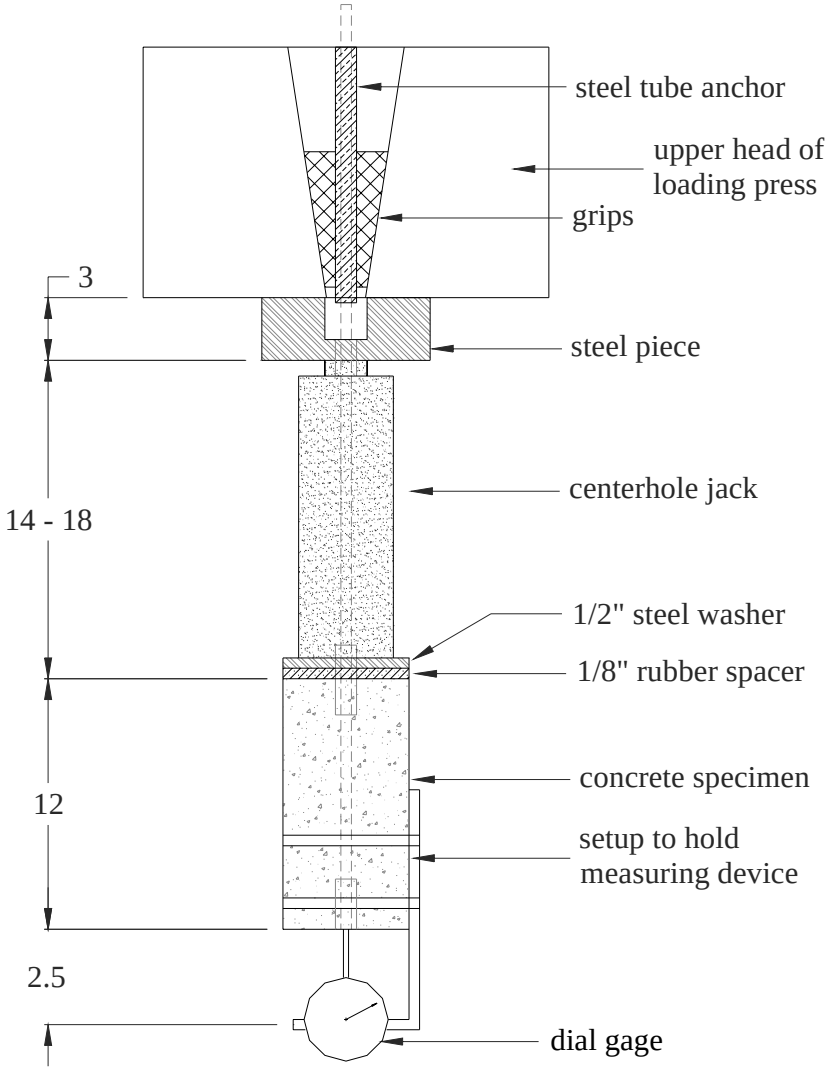

Figure 2.7 UTM pullout setup for FRP bar specimens (values in inches) (1 in. = 25.4 mm)

Figure 2.8 Dial gage at specimen base

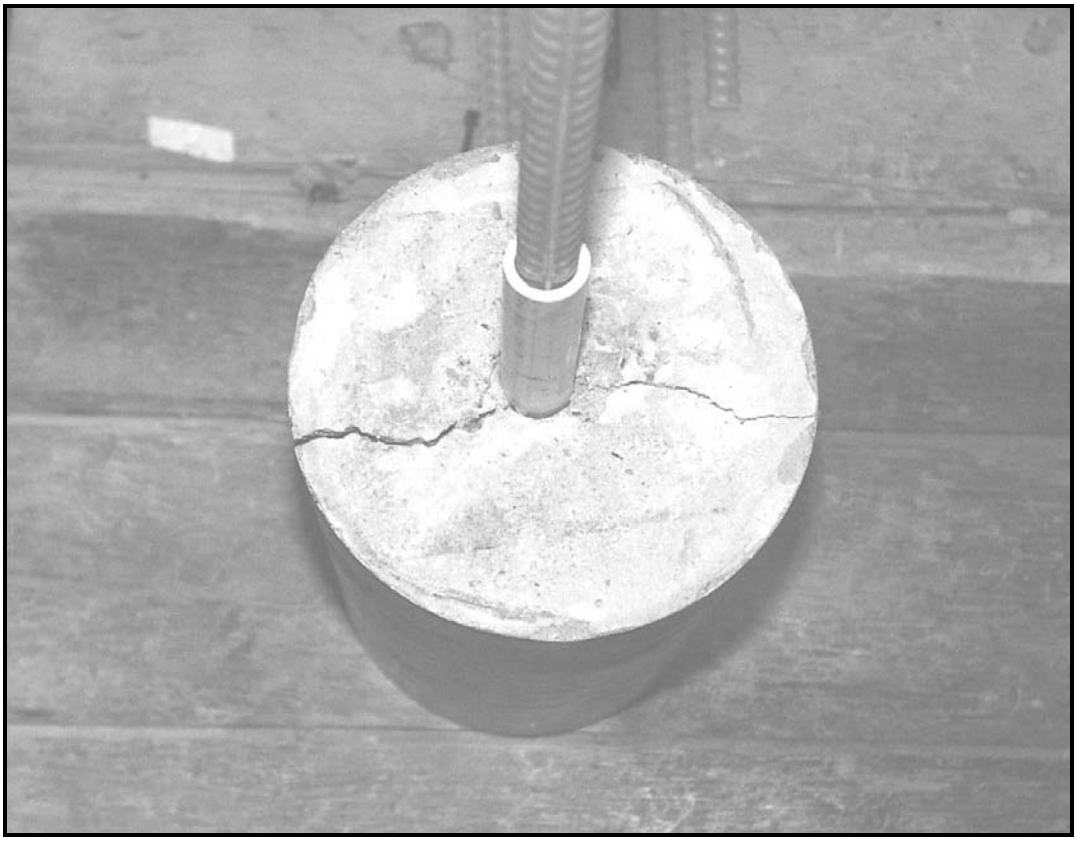

Figure 2.9 Concrete splitting during pullout

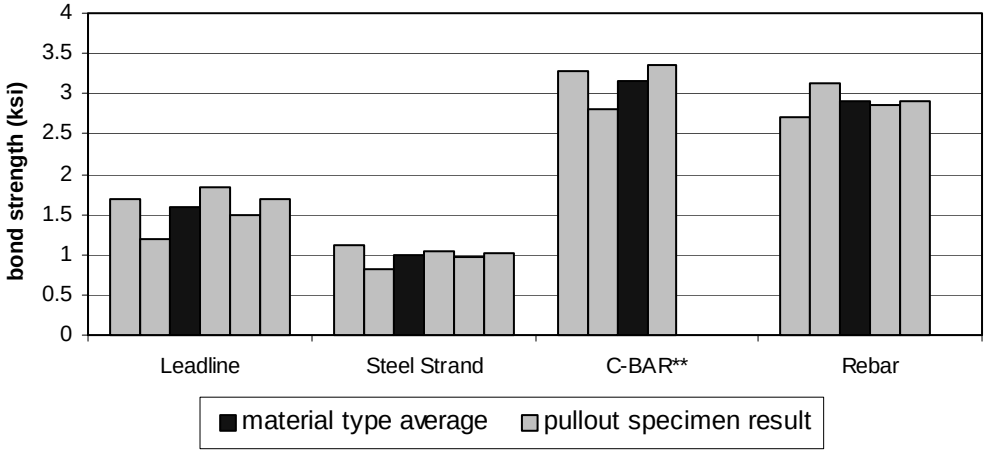

**$5d_b$ embedment length

Figure 2.10 Bond strengths for each specimen in pullout tests (1 ksi = 6.9Mpa)

3. DESIGN OF PRECAST PANEL WITH COMPOSITE TOPPING

3.1 General

The panels being investigated in this study are designed to rest on two post-tensioned cast-in-place box girders as shown in Figure 3.1. They are used as stay-in-place forms that are later strengthened with the casting of a 125 mm (5 in.) thick reinforced topping slab.

As will be discussed below, the design of the panels used in the bridge project at I-225/Parker Road is extremely conservative. It is more interesting to evaluate the performance of panels designed to barely satisfy the minimum requirements of AASHTO. For this reason, two sets of panels are designed in this chapter to satisfy the minimum AASHTO requirements, one with steel strands and the other with CFRP tendons. The actual bridge panels designed by CDOT are based on the 16th Edition of AASHTO Standard Specifications (1996). For the sake of consistency, the design presented here will also follow the same standards.

Design techniques for the use of FRP are still in their development stages. Research performed by Dolan et al. (2000) has provided a good guidance for design using Leadline prestressing tendons. Their research will be consulted to supplement the specifications covered in the 16th Edition of AASHTO.

3.2 CDOT Panels

In the bridge project at I-225/Parker Road, a standard panel design used by CDOT has been adopted. The panel size is about 2950 mm (116 in.) wide and 2438 mm (96 in.) long. The width is defined as the dimension along the span of the panel in the direction perpendicular to that of traffic. The design is based on 9.5 mm (3/8 in.), Grade 270, low-relaxation seven-wire strands. Each panel has 20 steel strands at a center-to-center spacing of 121 mm (4.75 in.). The temperature steel is #3 bars (9.5 mm diameter) at a spacing of 305 mm (12 in.). They also serve as the distribution reinforcement. They satisfy the AASHTO requirement that a minimum of 71 mm^2 (0.11 in^2) of reinforcement be provided per 305 mm (12 in.) of panel width. The design has been used for a variety of span lengths and is very conservative for the span length used in this project.

Some of the panels in the bridge have CFRP tendons for prestressing and GFRP bars for the temperature reinforcement. In this case, the 3/8 in. (9.5 mm) steel strands are replaced by 10 mm (0.39 in.) CFRP tendons on a one-to-one basis, and the #3 (9.5 mm diameter) mild steel reinforcement is replaced by 13 mm (0.5 in.) GFRP bars at a spacing of 152 mm (6 in.), which is to account for the fact that GFRP bars have a much lower modulus of elasticity than steel. Since the CFRP tendons have a slightly larger diameter and significantly higher strength than the steel strands, the panels with the FRP reinforcement are perceived to be extremely conservative for this application.

The prestressing forces applied to the steel strands and the CFRP tendons are identical. Each tendon is jacked to 76 kN (17 kips).

The design of a typical panel is illustrated in Figure 3.2. All panels have straight tendons with an eccentricity of 12 mm (0.47 in.). This eccentricity is required to provide an additional factor of safety for the construction loads with the given tolerance for the placement of the tendons.

As mentioned in Chapter 2, Leadline is chosen by the contractor in this project mainly because it has a well-developed anchoring chuck for the ease of prestressing.

3.3 Strength Evaluation of Panels and Composite Slabs with FRP Tendons

An allowable stress approach is used for the design of the prestressed panels and the cast-in-place topping slabs. However, the ultimate strengths of the panels and composite slabs have to be checked after the design. These checks require the evaluation of the nominal moment capacities of the panels and the slabs. For panels/slabs with Leadline tendons, this requires extra attention as CFRP tendons deform linearly elastically up to rupture as opposed to steel strands which develop a significant nonlinear behavior before rupture. Even though the composite slabs in this case are under-reinforced, the panels themselves are over-reinforced. For members with FRP reinforcement, it is beneficial to be over-reinforced because of the brittle nature of the FRP bars. However, if the nominal capacity of a member is substantially higher than the design load, this is not an issue. Hence, in this project

and with FRP reinforcement in general, we have to consider different reinforcing scenarios.

Dolan et al. (2000) have proposed simplified formulas to evaluate the nominal moment capacity of members prestressed with CFRP under different reinforcing scenarios. These are summarized below.

3.3.1 Nominal Moment Capacity with Dolan's Method

Dolan et al. (2000) classify the behavior of a member prestressed with CFRP using a brittleness ratio (ρ_{br}), which is defined as the reinforcement ratio at which the concrete strain reaches 0.003 at the same time as the rupture of the FRP bars. This ratio, as given in equation 3.1, is similar to the balanced strain ratio in concrete with steel reinforcement but is defined in terms of the rupture strength of FRP bars (f_{pu}).

$$\rho_{br} = 0.85\beta_1 \frac{f_c^{'} c}{f_{pu} d_p} \qquad (3.1)$$

where β_1 = factor for the length of the rectangular stress block

$$= 0.85 - 0.05 \cdot \left(\frac{f_c^{'} - 4000}{1000} \right)$$

c = distance of the neutral axis from the extreme compression fiber

d_p = effective depth of the section

This ratio can also be expressed in terms of strain quantities as shown in equation 3.2. Note that the decompression strain is normally an order of magnitude less than the flexural strain and is therefore eliminated to simplify the computation.

$$\rho_{br} = 0.85\beta_1 \frac{f_c^{'}}{f_{pu}} \left(\frac{\varepsilon_{cu}}{\varepsilon_{cu} + \varepsilon_{pu} - \varepsilon_{pe}} \right) \qquad (3.2)$$

where ε_{cu} = concrete compressive strain at failure (0.003)

ε_{pu} = ultimate tensile strain of tendons

ε_{pe} = effective prestress strain

Based on the definition of the brittleness ratio in equations 3.1 and 3.2, Dolan et al. (2000) define three behavioral scenarios. First, if the reinforcement ratio $\rho \geq \rho_{br}$, the member will fail by the compression of the concrete with no failure of the tendon. Second, if $0.5\rho_{br} \leq \rho \leq \rho_{br}$, the tendon will rupture and the concrete compressive stresses will be significantly non-linear. For this case, an equivalent rectangular stress distribution can be used to predict the member strength. Third, if $\rho \leq 0.5\rho_{br}$, then the member is under-reinforced and the concrete stress is governed by a linearly elastic behavior up to tendon rupture. The use of $0.5\rho_{br}$ as the dividing point for the above scenarios was selected by Dolan without extensive validation. Further confirmation by experimental studies is recommended to validate this limit. The calculation of the nominal moment capacity for each scenario is summarized below.

MEMBERS WITH NORMAL REINFORCEMENT RATIO ($0.5\rho_{br} \leq \rho \leq \rho_{br}$)

For this case, the nominal moment capacity can be computed in the same way as specified in the 16th Edition of AASHTO. The only difference in Dolan's formula is that the ultimate strength of the FRP tendons (f_{pu}) is used in place of the computed stress in the steel strand at ultimate load (f_{ps}) as shown in the following equation.

$$M_n = \rho b d_p^2 f_{pu}\left(1 - \frac{\rho f_{pu}}{1.7 f_c'}\right) \qquad (3.3)$$

UNDER-REINFORCED MEMBERS ($\rho \leq 0.5\rho_{br}$)

For an under-reinforced member, the stress in the concrete is given by a linear stress-strain relation. The neutral axis is located at the centroidal axis of the transformed section. The distance from the compression face to the neutral axis can be defined as $c = kd_p$ where d_p is the depth of tendon in the concrete section. Based on the fact that the net axial force is zero, k can be calculated as follows.

$$k = \sqrt{(\rho n)^2 + 2\rho n} - \rho n \qquad (3.4)$$

where n = the ratio of the modulus of elasticity of the tendons to that of the concrete

The resulting nominal moment is shown in equation 3.5.

$$M_n = \rho b d_p^2 f_{pu}\left(1 - \frac{k}{3}\right) \qquad (3.5)$$

OVER-REINFORCED MEMBERS ($\rho \geq \rho_{br}$)

For an over-reinforced member, the tendons will remain elastic and undamaged at failure. Dolan first defines the neutral axis location as $c = k_u d_p$, the distance from the compression face of the section to the neutral axis. The strain in the prestressing tendon (ε_p) is equal to the effective prestressing strain (ε_{pe}) plus the flexural strain (ε_f). Again, the decompression strain is ignored here. Equation 3.6 allows one to calculate ε_p based on strain compatibility if the concrete strain at failure (ε_{cu}) is known. The strain ε_{cu} is assumed to be 0.003.

$$\varepsilon_p = \varepsilon_{pe} + \varepsilon_{cu}\frac{1 - k_u}{k_u} \qquad (3.6)$$

Knowing that the tendon stress is $f_{ps} = \varepsilon_p E_p$, and using the rectangular stress block assumption, the equilibrium of the forces in the cross section leads to equation 3.7.

$$\rho b d f_{ps} = 0.85 f'_c b \beta_1 k_u d_p \qquad (3.7)$$

Defining a material constant $\lambda = (E_p\varepsilon_{cu})/(0.85f'_c\beta_1)$ and combining equations 3.6 and 3.7, one arrives at equation 3.8 to obtain k_u.

$$k_u = \sqrt{\rho\lambda\left[\frac{\rho\lambda}{2}\left(1-\frac{\varepsilon_{pi}}{\varepsilon_{cu}}\right)\right]^2} - \frac{\rho\lambda}{2}\left(1-\frac{\varepsilon_{pe}}{\varepsilon_{cu}}\right) \qquad (3.8)$$

Finally, the nominal moment capacity of the over-reinforced section is determined by equation 3.9.

$$M_n = 0.85\, f'_c\, b\beta_1 k_u d_p^2\left(1-\frac{\beta_1 k_u}{2}\right) \qquad (3.9)$$

3.3.2 Nominal Moment Capacity of Composite Slabs

For the composite slabs considered here, the ultimate moment capacity is governed by the rupture of the tendons. In this case, a simple yet rigorous approach can be used to evaluate the moment capacity based on the strain compatibility between the tendons and concrete and the nonlinear stress-strain behavior of concrete. This method can be used to check the accuracy of the formulas proposed by Dolan et al. (2000) for members that are in the transition zone from under-reinforcement to normal reinforcement.

The incremental strain $\Delta\varepsilon_{ps}$ in the tendons from the effective prestress state to rupture can be calculated by equation 3.10.

$$\Delta\varepsilon_{ps} = \frac{f_{pu} - f_{pe}}{E_p} \tag{3.10}$$

With $\Delta\varepsilon_{ps}$ from equation 3.10 and assuming that the neutral axis location is known, one can express the strain in the concrete at the rupture of the tendons as follows.

$$\varepsilon_c(y) = \frac{\Delta\varepsilon_{ps}\, y}{d_p - c} \tag{3.11}$$

d_p = depth of tendon in concrete section

c = location of neutral axis as defined by the distance from the top of the section

y = distance along the vertical axis measured from the neutral axis

A model proposed by Kent and Park (1971) is used to represent the stress-strain behavior of concrete. In this model, the following sets of equations are used to define the compressive stress-strain relation of concrete.

For $0 < \varepsilon_c \leq 0.002$,

$$f_c(\varepsilon_c) = f'_c \left[\frac{2\varepsilon_c}{0.002} - \left(\frac{\varepsilon_c}{0.002} \right)^2 \right] \tag{3.12}$$

For $0.002 < \varepsilon_c \leq \frac{6+.002f'_c}{f'_c-1000}$, $\quad f_c(\varepsilon_c) = f'_c - \frac{0.5f'_c(\varepsilon_c - 0.002)}{\left(\frac{3+0.002f'_c}{f'_c-1000}\right) - 0.002}$ (3.13)

For $\varepsilon_c > \frac{6+.002f'_c}{f'_c-1000}$, $\quad f_c(\varepsilon_c) = 0.2f'_c$ (3.14)

In the above equations, stress is in psi. The neutral axis location *c* in equation 3.11 is determined by equating the compressive force in the concrete to the tensile force in the tendons. This is done in an iterative manner. The tensile stress in the concrete is assumed zero. By substituting equation 3.11 into equations 3.12, 3.13, and 3.14, the total force in the concrete can be determined by integration. The iterative procedure is presented as follows:

1. An initial guess for *c* is made that is less than half of the total section depth (*d*).
2. Based on this value for *c*, the integration limits for computing the compressive forces are determined.
3. Once the limits are computed, the force in the concrete is computed by integrating the stresses given by equations 3.12, 3.13, and 3.14.
4. The difference between the computed force in the concrete and the known tendon force is computed. This residual error is used to calculate a new value of *c* which further minimizes this residual error.

5. Repeat steps 2 through 4 until the compressive force in the concrete is equal to the tensile force in the tendons. Once this occurs, the residual error is zero, and the value for *c* is obtained.

Once equilibrium has been established with the correct value for *c*, the nominal moment capacity is computed by integration. This procedure is programmed using *Mathcad 2000.*

3.3.3 Comparison of Evaluation Methods

As discussed earlier, Dolan et al. (2000) have suggested that a reinforcement ratio of $0.5\rho_{br}$ be the transition point from the under-reinforced to normal-reinforced situation. Given the higher accuracy of the nominal moment capacity evaluated with the Kent and Park model for concrete presented in the previous section, this more refined approach is used to evaluate the formulas and the transition point proposed by Dolan et al. (2000). To this end, three separate methods are used to compute the nominal moment capacity for a 215 mm (8.5 in.) thick composite slab. They are the *refined method* presented in section 3.3.2, and the two formulas proposed by Dolan et al. for *normal-reinforced* and *under-reinforced* members, respectively. All variables are set equal for each case including the depth of the prestressing tendon d_p, the concrete strength f'_c, the ultimate tendon strength f_{pu}, and the effective prestress f_{pe}. The area of the prestressing tendons used is varied so that ratio of the reinforcement

ratio to the brittleness ratio (ρ/ρ_{br}) varies from 0.1 to 1.0. The results are summarized in Table 3.1. By comparing the results from Dolan et al.'s simplified formulas to those from the refined method, we can see that the simplified formulas are sufficiently accurate. However, the transition point for under-reinforcement to normal reinforcement is between $0.3\rho_{br}$ and $0.35\rho_{br}$.

Table 3.1 Comparison of strength evaluation methods (in-kips)

ρ/ρ_{br}	M_n (1) *Refined Method*	M_n (Dolan) (2) *Normal reinforced*	M_n (Dolan) (3) *Under-reinforced*	%Difference *(1) & (2)*	%Difference *(1) & (3)*
0.10	32.6	32.9	32.7	1.0	0.4
0.15	48.8	49.2	49.0	0.8	0.3
0.20	64.7	65.4	65.1	1.1	0.7
0.25	80.7	81.4	81.3	0.9	0.7
0.30	96.4	97.4	97.3	1.0	0.9
0.35	112.3	113.2	113.4	0.8	1.0
0.40	127.9	128.9	129.4	0.8	1.2
0.45	143.6	144.5	145.3	0.6	1.2
0.50	159.0	160.0	161.3	0.6	1.4
0.60	189.8	190.6	193.0	0.4	1.7
0.70	220.3	220.7	224.7	0.2	2.0
0.80	250.8	250.3	256.2	-0.2	2.1
0.90	280.6	279.5	287.6	-0.4	2.5
1.00	309.8	308.3	319.0	-0.5	3.0

3.4 Design Considerations for Panels with FRP Tendons

As stated earlier, the CDOT panels are extremely conservative. Their capacities are way beyond the AASHTO (1996) requirements. To explore the future use of Leadline in an economical fashion, panels that are designed to barely satisfy the minimum AASHTO requirements are evaluated experimentally. For this purpose, two sets of panel designs are considered here. One is with 9.5 mm (3/8 in.) steel strands, and the other is with 8 mm (0.315 in.) Leadline bars. Specific design

considerations for Leadline bars, namely, the allowable pretensioning stress, the relaxation losses, and the required development lengths are discussed.

3.4.1 Jacking Stress and Initial Prestress

The maximum allowable initial prestress (f_{pi}) is governed by the creep-rupture behavior of FRP tendons. As discussed by Dolan et al. (2000), this process has three stages: primary, secondary, and tertiary. In the primary stage, the strain steadily increases, but causes no permanent fiber damage. During the secondary stage, large sustained stresses cause weaker fibers in the tendons to break. Upon the initial fiber rupture, the excess load is transferred by way of the epoxy matrix to the other fibers in the tendon. If the stress level is low enough, fiber damage is confined to the secondary creep level and the tendon has an unlimited service life. However, if the stress level is too high, the creep process will move into the tertiary stage. As a result, the remaining fibers are overloaded, continuing this process until complete tendon failure. Tests reported by Dolan et al. (2000) were performed with the intention of finding the appropriate stress level that will not cause creep-rupture. In the tests, a concrete cylinder with a concentrically placed Leadline bar was used. The Leadline bar was first pretensioned and gripped at both ends with the concrete cylinder cast later. At one end, a compressed spring is placed between the grip and the supporting frame in order to apply a continuous load against the grip. This places a constant stress on the tendon during testing. All tests were performed for 12,000 hours in a sealed environmental chamber to simulate a concrete/alkaline environment

typical of prestressing applications. Time and rupture stress data were collected in the 12,000-hour tests. The rupture stress was plotted as a percent of the ultimate strength against time on a semi-logarithmic scale. Using this plot, the rupture stress data was then extrapolated to 1,000,000 hours. The predicted allowable stress level for CFRP prestressing tendons to achieve 100 years of service life is about $0.7f_{pu}$. Based on these tests, Dolan et al. (2000) recommend a maximum jacking stress of $0.65f_{pu}$ and a maximum initial prestress of $0.6f_{pu}$ after transfer.

3.4.2 Initial Prestress Losses

Elastic shortening and tendon relaxation are the main sources of initial prestress losses for pretensioned concrete. Elastic shortening loss can be computed in the same way as for normal prestressed concrete. Relaxation loss for CFRP prestressing tendons has not been clearly understood due to limited research in this area. Dolan et al. (2000) present a discussion to estimate this loss. The discussion identifies three sources that constitute tendon relaxation. First, after the jacking stress is applied, some of the load is carried by the resin matrix. This resin matrix relaxes releasing its portion of the load. For CFRP, this relaxation loss is estimated to be 0.6 to 1.2 percent of the initial prestress. This value is dependent on the ratio of the modulus of elasticity of the matrix to that of the carbon fibers. It also depends on the volume ratio of the epoxy matrix in the tendon. Second, the fibers in the pultruded section are never completely parallel; given time, the stress in the tendon will likely straighten the fibers out. This is a function of the quality control of the pultrusion process. A

relaxation loss of one to two percent of the initial prestressing force is estimated from this phenomenon. Third, each of the individual fibers may relax. However, CFRP tendons have negligible fiber relaxation. Total relaxation is a result of these three contributions. The study proposes an approximate value of one to three percent for the total relaxation loss in CFRP tendons.

Dolan et al. (2000) did some tests to quantify the initial losses with different FRP tendons and steel strands. Jacking stresses of 60 to 65 percent of the ultimate strength were applied to a series of tendons used in laboratory-scale beams. After the steel anchors were set and the tendons were allowed to relax for two hours prior to pouring concrete, prestress losses were noted to be between 9 and 14 percent. If the above estimates are correct, most of the losses must be contributed by factors other than the tendon relaxation. Both Leadline and steel strands were at the low end of this spectrum with Leadline CFRP tendons having the least initial loss. For the purpose of design in this report, a loss of ten percent will be applied before release of tendons as identified in the above study.

3.4.3 Development Length

The results of the pullout tests presented in Chapter 2 indicate that the development length equation in the ACI code will be too conservative for Leadline bars. Hence, a decision was made to use the equations developed by Mahmoud et al. (1999) for development length of CFRP tendons. The proposed equations incorporate the initial and matured strengths of the concrete in addition to the bar diameter. In

these respects, they are more refined than the formulas proposed by others. The development length proposed by Mahmoud et al. (1999) is given as the sum of the transfer and the flexural bond lengths shown in equations 2.4 and 2.5.

3.5 Design of Precast Panels and Composite Slabs

Two sets of precast panels were designed. One is prestressed with 8 mm (0.315 in.) Leadline CFRP tendons and the other with 9.5 mm (3/8 in.) steel strands. The minimum concrete strengths specified are 29.6 MPa (4300 psi) at release and 31 MPa (4500 psi) at 56 days. The design traffic load is a single wheel load given by an HS25-44 truck with alternate military loading. This AASHTO standard design truck consists of two 89 kN (20 kip) wheel loads spaced at 1.8 m (6 ft.). To evaluate their performance, a set of these panels were fabricated for subsequent testing as described in Chapter 4.

3.5.1 Prestressing Tendons

The design of the CFRP prestressed panels follows the AASHTO Specifications (1996) as well as the guidelines presented in Section 3.4 and is detailed in Appendix A. The final design uses fourteen 8 mm (0.315 in.) CFRP tendons symmetrically placed over the 2438 mm (96 in.) length.

The design of the steel prestressed panels follows AASHTO Specifications (1996). The design requires fourteen 9.5 mm (3/8 in.) seven-wire steel strands at the

same spacing as determined for the CFRP tendons. While the tendon spacing for both the steel prestressed panels and the CFRP prestressed panels is exactly the same, the area of a 9.5 mm (3/8 in.) steel strand is 55 mm^2 (0.085 in^2) while the area of an 8 mm (0.315 in.) Leadline tendon is 46.1 mm^2 (0.0715 in^2). Even though the total cross-sectional area of Leadline is smaller than that of steel, the former has a higher tensile strength. The layout of the tendons for both designs can be viewed in Figure 3.3.

The jacking force of 76 kN (17 kips) is determined based on the AASHTO limit of $0.75f_{pu}$ for steel strand. This jacking force is used for both CFRP tendons and steel strands in the design. However, for the CFRP tendons, this jacking force converts to a jacking stress of approximately $0.58f_{pu}$ and is conservative compared to $0.65f_{pu}$ recommended by Dolan et al. (2000).

The effective prestressing force for the CFRP tendons accounts for the ten percent loss before prestress release as discussed in Section 3.4.2, elastic shortening loss and also a fifteen percent loss after prestress release. This fifteen percent loss takes into account the low relaxation of FRP as compared to the twenty percent loss assumed for the steel strand.

It must be pointed out that the CDOT panels described in Section 3.2 use twenty 10 mm (0.39 in.) CFRP tendons placed uniformly as shown in Figure 3.2. The same jacking force of 76 kN (17 kips) is used for each tendon and since the area of a 10 mm (0.39 in.) CFRP tendon is 71 mm^2 (0.11 in^2), the initial jacking stress for the CDOT panel is much lower than that for the panel designed above.

3.5.2 Temperature/Shrinkage Reinforcement in Panels and Topping Slabs

The design of the temperature and shrinkage reinforcement in the panels followed the 16th Edition of AASHTO which requires a minimum of 71 mm^2 (0.11 in^2) of reinforcement per 305 mm (12 in.) width of panel. This serves as the temperature/shrinkage reinforcement requirement as well as the distribution reinforcement requirement. Hence, #3 (9.5 mm in diameter) epoxy-coated bars were placed at 305 mm (12 in.) spacing in the panel prestressed with steel.

In the ACI 440H draft document (2000), an adjustment of temperature reinforcement stipulated in ACI 318 for steel is proposed for FRP. The adjustment factor is based on the ratio of the yield strength of steel (f_y) to the ultimate strength of FRP (f_{pu}) and the ratio of the modulus of elasticity of steel (E_s) to that of FRP (E_f) as shown in the following equation.

$$\rho_{f,ts} = 0.0018 \cdot \frac{60}{f_{pu}} \cdot \frac{E_s}{E_f} \qquad (3.15)$$

In equation 3.15, 0.0018 is the steel ratio required by ACI 318 for mild reinforcement and 60 is the yield strength (f_y) of standard steel rebar (414 MPa/60 ksi). For this study, the AASHTO requirement of 71 mm^2 (0.11 in^2) of reinforcement per 305 mm (12 in.) of panel width was used in lieu of 0.0018. Based on this modification of

equation 3.15 and the C-BAR properties listed in Chapter 2, 13 mm (0.5 in.) C-BAR GFRP bars were spaced at 305 mm (12 in.) for the CFRP prestressed panels.

A 125 mm (5 in.) topping slab was used as in the original CDOT design as shown in Figure 3.4. Since the panels would be tested in a simply supported condition, in which the reinforcement in the topping slab had no load resisting function, the reinforcement was simply placed to satisfy the temperature/shrinkage requirement. In this case, 81 mm^2 (0.125 $in.^2$) of steel reinforcement per 305 mm (12 in.) width of panel is prescribed by AASHTO for both directions in the topping slab. This calls for #3 bars (9.5 mm diameter) at 305 mm (12 in.) spacing in both directions. Epoxy-coated steel bars were used in the topping slab for all panels as in the actual bridge. This is to avoid special handling requirements needed for FRP bars in the field.

3.5.3 Design Strengths

The nominal moment capacities, M_n, of the prestressed panels and panels with a topping slab are evaluated and compared to the factored design moments, M_u. The results are summarized in Table 3.2. The nominal moment capacities are evaluated with the methods presented in Section 3.3. For the panels alone, the nominal moment capacities M_n are governed by the flexural capacity of the section. However, as shown in Appendix A, the nominal moment capacities for the composite slabs are limited by the development length. In the case of the bare panels, the flexural capacity is limited by the compressive crushing of concrete rather than the strength of the tendons. In Table 3.2, the nominal moment capacities governed by the

development length are shown in parentheses. The M_u for the panels is due to the factored self-weight and construction loads only, while M_u for the composite slabs includes the factored HS25-44 wheel load in addition to the self-weight. The tendon stress at M_u, denoted f_{Mu}, for the FRP reinforced composite section is computed using the strain compatibility, equilibrium of the tensile and compressive forces in the slab cross-section, and elastic concrete behavior. The last assumption is an approximation stemming from the fact that the composite section is under-reinforced and that M_u is significantly lower than the nominal moment capacity of the slab governed by tendon failure. The tendon stress is not computed for the panels alone, as it is not a major concern under construction loads.

Table 3.2 Panel/slab design comparison

(1 in-kips = 113 N-m / 1 ksi = 6.9 MPa)

Specimen Type	M_n in-kips	M_u / M_n	f_{Mu} ksi	f_{Mu} / f_u
Steel Prestressed Panel	65.9	0.65	NA	NA
FRP Prestressed Panel	64.3	0.66	NA	NA
Steel Prestressed Composite Slab	261.6 (255.5)	0.81 (0.83)	NA	NA
FRP Prestressed Composite Slab	339.7 (278.6)	0.62 (0.76)	253	0.62

Note: The numbers in parentheses reflect a reduction governed by the development length.

The results show that the panels with steel and CFRP tendons have similar nominal moment capacities. However, the nominal moment capacities of the panels with the composite topping slabs are significantly different. The ratio of M_u to M_n is

much lower for the CFRP prestressed composite slab than for the steel prestressed composite slab. The difference is reduced when considering the development length limitations; however, it still remains significant. Hence, the slabs with CFRP tendons are extremely conservative. This is mainly because of the low prestressing force used in comparison to the high tensile strength of the CFRP tendons.

Given that the maximum allowable tensile stress in a Leadline CFRP tendon is 2,822 MPa (409 ksi), the tendon stress at M_u (f_{Mu}) for the composite slab prestressed with CFRP is only 62 percent of the guaranteed ultimate strength f_u. A large amount of reserve capacity exists in the tendon, adding to the safety of the design.

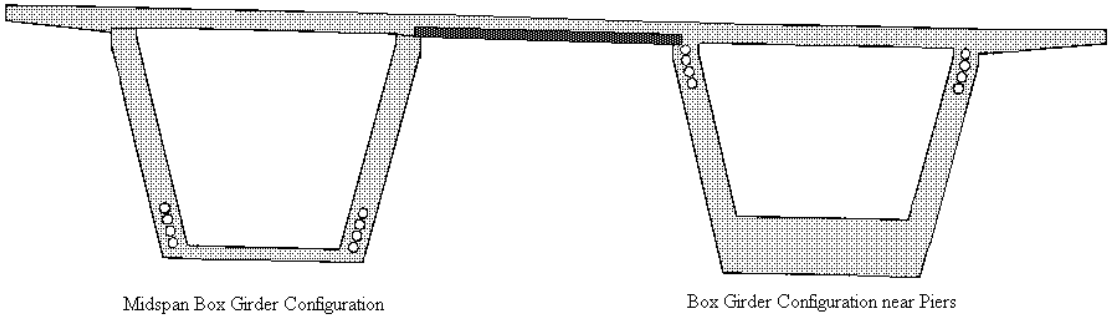

Figure 3.1 Cast-in-place, post-tensioned box girders with precast panel (darkened portion)

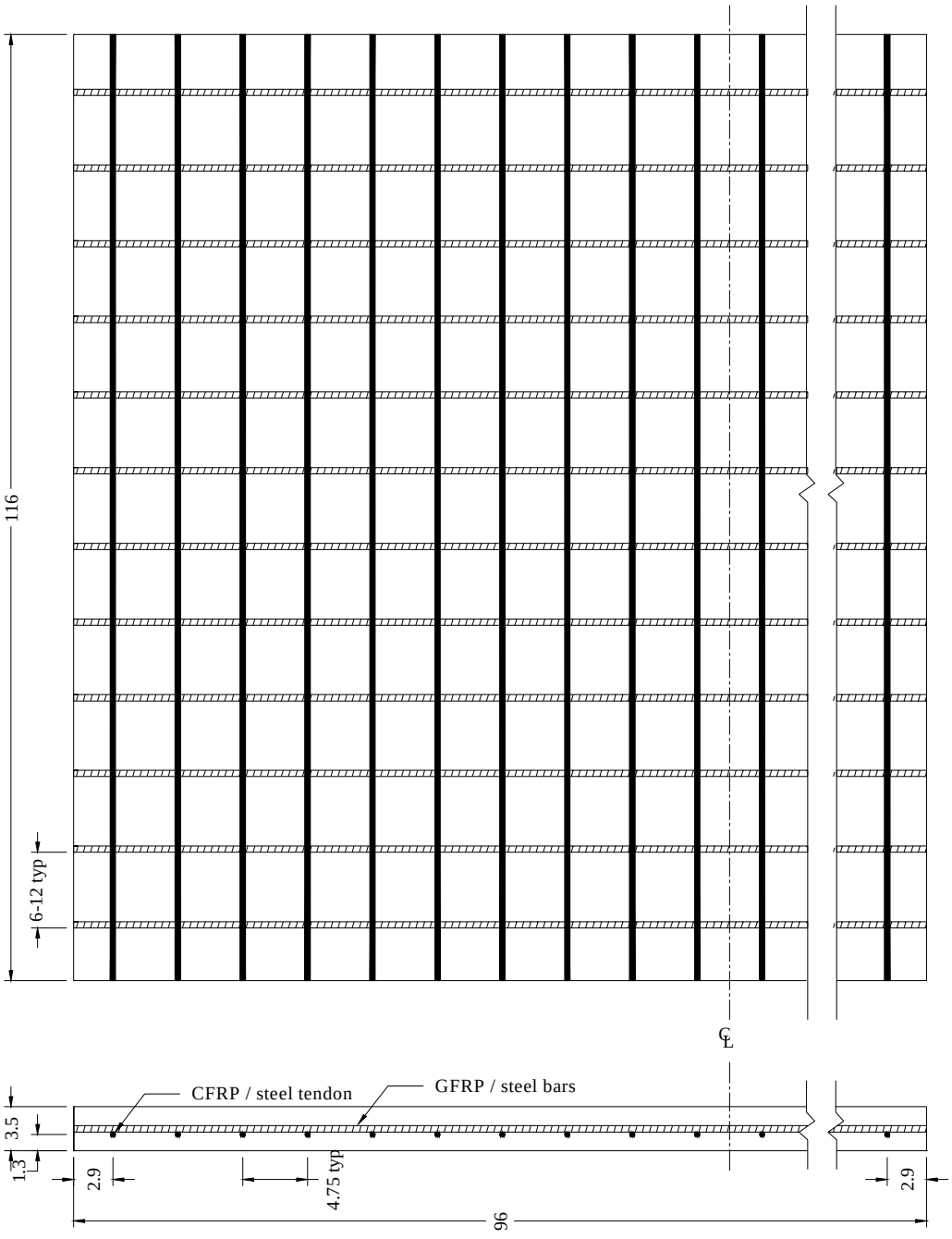

Figure 3.2 CDOT panel cross-section and plan view (all values in inches) (1 in. = 25.4 mm)

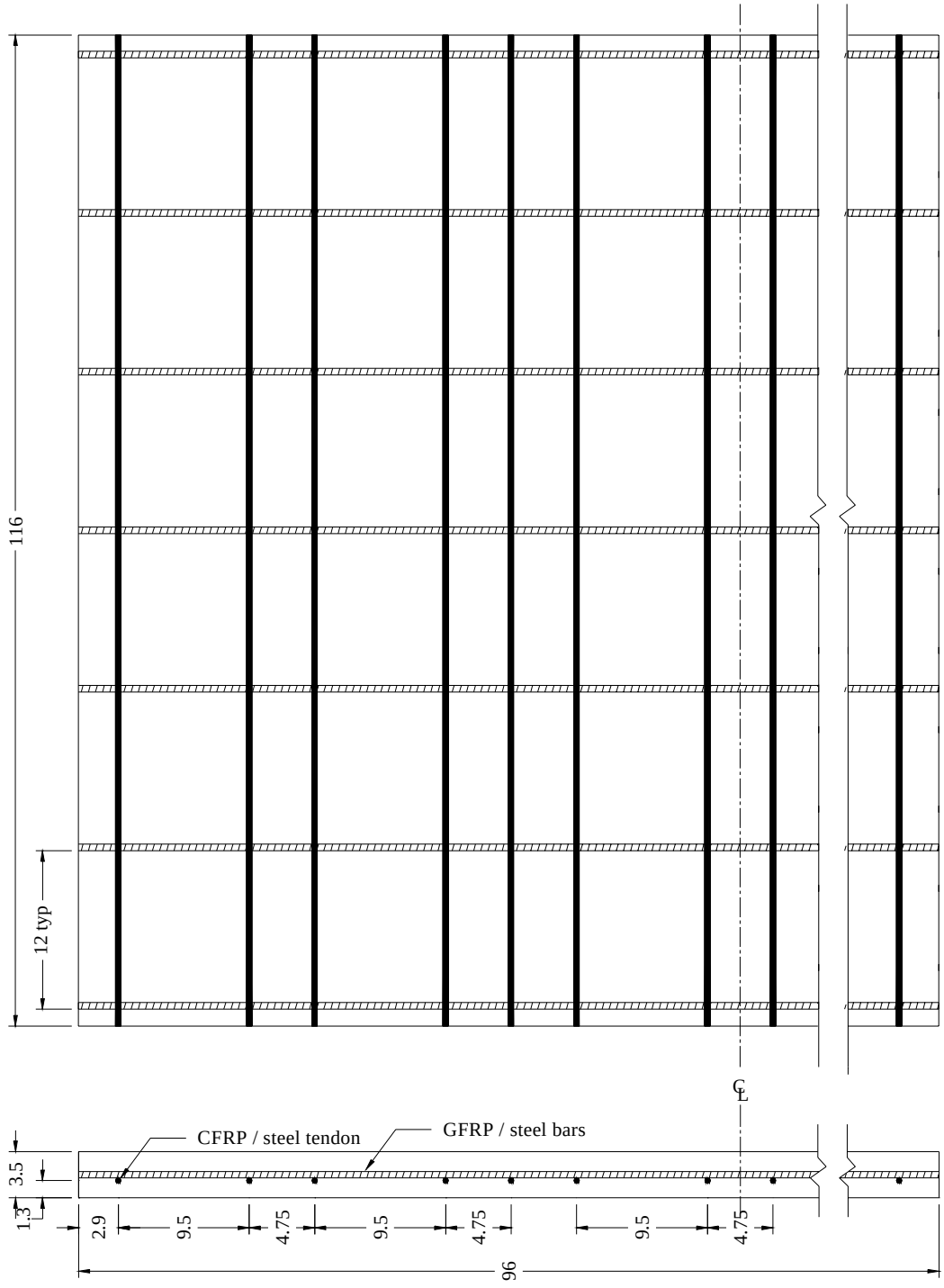

Figure 3.3 Cross-section and plan view of test panels (all values in inches) (1 in. = 25.4 mm)

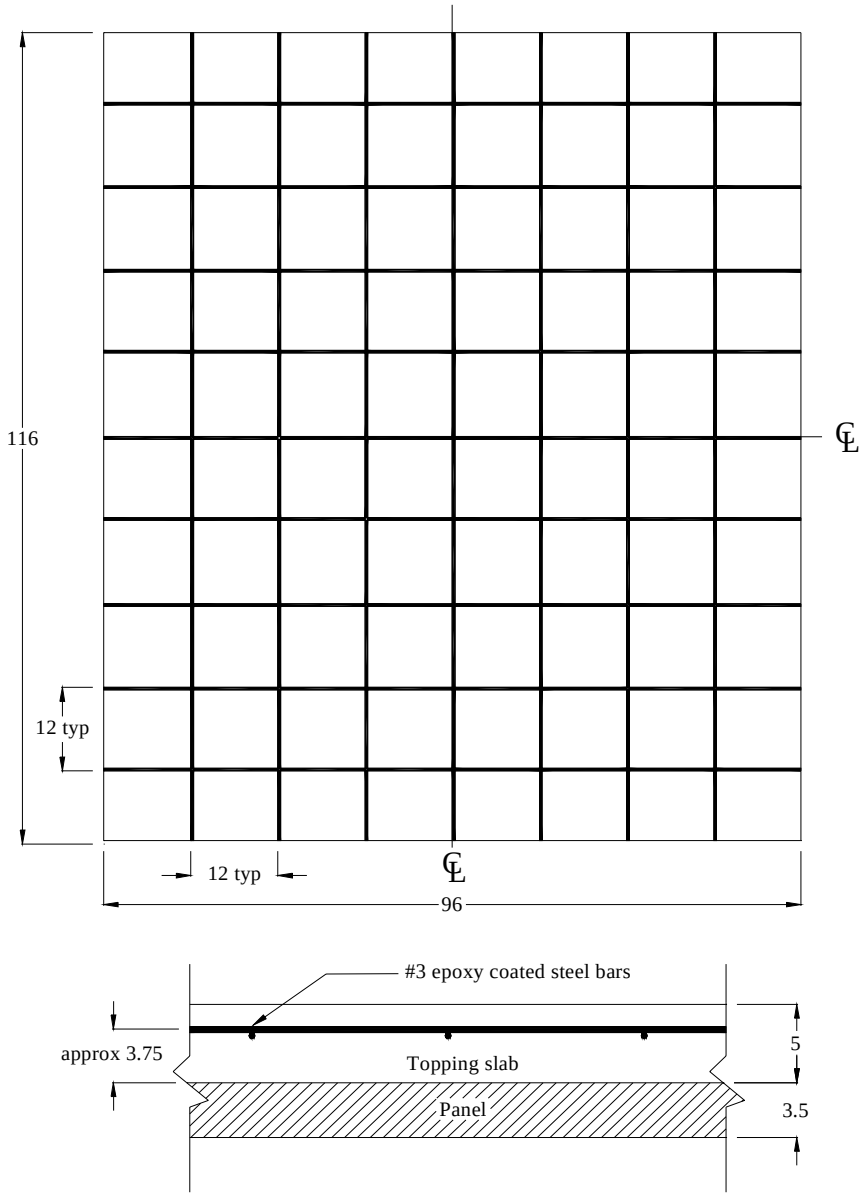

Figure 3.4 Cross-section and plan view of panel and topping slab (all values in inches) (1 in. = 25.4 mm)

4. Experimental Program

4.1 Scope of Test Program

Four pretensioned panels of similar design were fabricated for testing. Two of the panels were pretensioned with fourteen 8 mm (0.31 in.) Leadline prestressing tendons, while the other two were pretensioned with fourteen 9.5 mm (3/8 in.) seven-wire prestressing strands. The design is shown in Figure 3.3. Additionally, a fifth panel that was designed by CDOT for the actual bridge deck was tested. This panel was prestressed with twenty 10 mm (0.39 in.) Leadline tendons as shown in Figure 3.2.

One CFRP prestressed panel and one steel prestressed panel were tested as constructed. The other two were tested with the addition of a 125 mm (5 in.) reinforced composite topping slab as shown in Figure 3.4.

For the first set of tests on the panels with no composite topping slab, a line load was applied at the midspan as shown in Figure 4.1a. For the second set of tests on the composite panels, the load was applied with a 508 mm (20 in.) by 508 mm steel plate as shown in Figure 4.1b. The intention of these tests was to look at the distribution of a plate load throughout a panel to evaluate the effective width given by AASHTO [LRFD] equation 4.6.2.1.3.

This chapter will describe the test setup, instrumentation, and procedures used in the testing program.

4.2 Specimen Fabrication

The panel specimens were fabricated by CSR Hydroconduit in Denver, Colorado. The two FRP prestressed panels were fabricated six days before the steel prestressed panels.

4.2.1 Formwork and Tendon Placement

A panel prestressing bed was used with the width set to 2468 mm (96 in.). The tendon spacing allowed by the bulkhead was in increments of 121 mm (4.75 in.). To comply with this requirement, the tendon layout for the panels is shown in Figure 3.3. Each CFRP tendon was encased in a plastic sheath in order to protect the tendon from damage during placement in the casting bed. The sheaths were removed later before casting. Figure 4.2 shows the casting bed in which the panels were poured.

4.2.2 Pretensioning Procedure

CSR Hydroconduit had to modify their standard prestressing procedure in prestressing the panels with Leadline tendons. The manufacturer of Leadline, Mitsubishi Chemical Corporation, has patented a modified wedge system to anchor the tendons. Figure 2.2 shows the components of the wedge system. First, an aluminum sleeve was placed over the end of the Leadline tendon. Then, two wedge pieces were placed over the aluminum and pushed into a tapered steel socket with a

hydraulic jack as shown in Figure 4.3. CSR Hydroconduit used this method to fix the anchors to the CFRP tendons.

The CFRP tendons cannot be directly jacked without causing damage. Thus, a coupling device borrowed from The Prestressed Group in Michigan was used to attach the CFRP tendons to standard steel strand. This device is shown in Figure 4.4. This way, the hydraulic jack could be applied to the steel strand and used in a standard fashion.

A further unforeseen problem in the prestressing process resulted from the tendency of seven-wire steel strand used between the coupler and hydraulic jack to twist when stressed. For this construction, only two three-meter CFRP prestressed panels were poured in a bed that extended over thirty meters. With the CFRP coupled to the steel strand at the end of the panels, the long length of steel strand developed a certain amount of twist even though restrainers were used to prevent the rotation of the couplers. As a result, two of the Leadline tendons had surface damage, but the damage did not appear severe enough to require tendon replacement. However, it was perceived that this problem would not be an issue if the entire length of the bed was used for panel construction. This proved to be true in later large-scale pours for the CDOT bridge panels.

The application of the load to the tendons was done in three stages: 13 kN (3 kips), 49 kN (11 kips), and finally 76 kN (17 kips). These three values approximately represented 10 percent, 38 percent, and 58 percent of the maximum tensile strength of Leadline CFRP tendons.

4.2.3 Concrete Placement

After prestressing, mild reinforcement was placed on top of the tendons, perpendicular to the direction of prestressing at a spacing of 305 mm (12 in.). The panels prestressed with seven-wire prestressing strand had #3 epoxy-coated bars (10 mm diameter) and the panels prestressed with CFRP tendons had 13 mm (0.5 in.) C-BAR. Once this was finished, concrete placement began. The panel concrete was batched on-site at the fabricator's batch plant. The mix design shown in Table 4.1 was used. It was developed at the University of Colorado to attain a minimum 56-day strength of 31 MPa (4.5 ksi). The mix is intended to have low cracking tendency and low permeability.

Table 4.1 Panel concrete mix design

Major components	*kg/m^3*	*lbs/yd^3*
Cement	285	480
w/c (total)	0.384	0.384
Sand	798	1345
Gravel	1115	1880
Fly ash (Class F)	53	90
Silica fume	15	25
Additives	*ml/m^3*	*ounces/yd^3*
MRWR, DC- 55	3210	83
Air entraining agent	39	1.0

Concrete was taken to the prestressing beds in 3 cubic meter buckets and placed directly into the beds. Concrete cylinder samples were taken and slump tests were

performed on each batch. Although the mix designs were nearly identical, the concrete strength and slump values differed significantly for the panels prestressed with CFRP and steel tendons. Table 4.2 shows the values obtained.

Table 4.2 Panel concrete data (1 in. = 25.4 mm / 1 psi = 6.9 kPa)

	Concrete Age	**CFRP Prestressed Panel Concrete**	**Steel Prestressed Panel Concrete**
Date poured	0	1/4/01	1/10/01
Slump *inches*		6.5	2.25
Prestress release strength *psi*	1.5	2600	4500
28-day - fog cure *psi*	28	4464	5391
28-day – air cure (same conditions as panels) *psi*	28	3549	4918
Test date-steel prestressed	56		3/7/01
Test date-CFRP prestressed	62	3/7/01	
Test day - fog cure *psi*	62/56 (CFRP/steel)	5543	5913
Test day - air cure (same conditions as panels) *psi*	62/56 (CFRP/steel)	3661	5754

It is uncertain why there were discrepancies in the concrete strengths given in Table 4.2. One probable cause is that additional water was added to the batch used for the CFRP prestressed panels to increase concrete workability. No documentation exists for this to identify the exact water content. This would explain the large slump

and the much lower strength for the CFRP panels. However, it is difficult to state whether this alone would account for such a large difference in concrete strengths.

4.2.4 Composite Topping Slab Placement

Both sets of panels were delivered to the laboratory at the University of Colorado after the steel prestressed panels were poured and partially cured. Forms were built around two of them to add a 125 mm (5 in.) composite topping slab. In addition, epoxy-coated #3 bars (10 mm diameter) were placed in the composite topping slab in a grid as described earlier (See Figure 3.4).

Strain gauges were attached to the reinforcing steel placed in the composite slab. Knowing that the reinforcing bars would be subject to slight bending, two gauges were placed on opposite sides of the bar with the intention of averaging out the bending effect. A smooth surface was ground out on opposite sides of a bar to give an adequate application area. Once the gauges were applied, an additional layer of protection was used in order to seal the gauges against water and further damage during the construction process. The strain gauge wires were pulled through half-inch plastic tubing to provide protection during construction and testing. Figure 4.5 shows one panel ready for pouring concrete.

The concrete mix design used for the composite topping slab is similar to the design used in the panel construction. Table 4.3 gives the exact mix design used by the ready-mix provider. The concrete delivery truck was delayed in getting to the

laboratory making the concrete over three hours old when applied. The slump was found to be still adequate, so the pour proceeded.

Table 4.4 gives the concrete properties.

Table 4.3 Topping slab concrete mix design

Major components	*kg/m^3*	*lbs/yd^3*
Cement	279	470
w/c	0.42	0.42
Sand	742	1250
Gravel	1056	1780
Fly ash (Class C)	53	90
Silica fume	15	25
Additives	*ml/m^3*	*ounces/yd^3*
MRWR, DC-55	2714	70.2
Air entraining agent	112	2.9

Table 4.4 Topping slab concrete data (1 in. = 25.4 mm / 1 psi = 6.9 kPa)

	Concrete Age	**Strength**
Date poured	0	1/31/01
Slump *inches*		3.5
28-day – fog cure *psi*	28	3637
28-day – air cure (same conditions as panels) *psi*	28	3477
Composite slab test date	50	3/22/01
Test day - fog cure *psi*	50	4074
Test day - air cure (same conditions as panels) *psi*	50	3553

4.3 Test Setup

4.3.1 Loading Setup

Figures 4.1a and 4.1b show the basic setup used to support and load the panels. The simple supports at the ends were constructed using a W14X145 steel beam with a 50 mm (2 in.) diameter steel bar welded to the top. In order to keep the panel from local damage at the support, a 13 mm (0.5 in.) steel plate was placed along the panel width between the panel and the simple support. Two 490 kN (110 kip) MTS loading actuators were hung from a loading frame centered over the top of the test panel. With only a 254 mm (10 in.) stroke, the design of the setup had to be very precise in order to optimize the limited motion of the actuators.

For the panel tests, a W14X145 steel beam was attached to the base of the two actuators as shown in Figure 4.6. On the panel surface, a 13 mm (0.5 in.) rubber pad was placed to distribute the load more uniformly. The loading beam was 381 mm (15 in.) wide and 2438 mm (96 in.) long to provide a line load.

For the composite slab tests, a 51 mm (2 in.) thick, 508 mm (20 in.) by 508 mm plate was placed beneath the beam as shown in Figure 4.7. The plate length dimension is given by equation 4.1, as specified in AASHTO [LRFD] 3.6.1.2.5.

$$l = \frac{P\gamma}{2.5}\left(1 + IM/100\right) \qquad (4.1)$$

where IM = dynamic load allowance (= 33 from AASHTO [LRFD] 3.6.2.1)

γ = load factor (= 1.75 from AASHTO [LRFD] 3.4.1)

P = HS 25-44 wheel load, which is 89 kN (20 kips)

The width dimension is given by AASHTO as 508 mm (20 in.). A 13 mm (0.5 in.) rubber pad was fitted under the plate.

4.3.2 LVDT Placement

Linear voltage differential transducers (LVDTs) were used to measure deflection at the mid-span of the panels. The LVDTs were attached to both sides of the panels with glue. The LVDTs measured the distance between the attachment point of the panel and the floor of the lab. In addition to the external LVDTs, each actuator contained an internal LVDT that was used to check all data.

4.3.3 Strain Gages

Prior to placement of the composite slab, strain gauges were mounted on the reinforcing steel as shown in Figure 4.8. Also displayed in the figure is the elevation view of the reinforcing grid on which the gages were mounted. One layer was placed directly on the panel surface and another layer was raised 3-4 in. off the panel. The vertical distance measured from the top of the panel to the two strain gages placed at each numbered location is shown in Table 4.5 for the composite slab.

Table 4.5 Strain gage elevation measured from the top of the slab (inches)

Strain gage location #	Composite slab with CFRP	Composite slab with steel
1	0.25	0.5
2	0.25	0.5
3	0.75	1.25
4	0.625	0.75
5	0.75	0.875
6	3.25	3.5
7	3.375	3.625
8	3.75	4
9	3.75	3.75
10	3.75	3.875

4.3.4 Data Acquisition

LabVIEW instrumentation software developed by National Instruments was used to gather all data. LabVIEW uses a virtual instrumentation concept to take data, analyze it, and present results in a table format. The advantage of this software is that all output can be viewed on the computer monitor while the test is taking place. Given the length of the test, LabVIEW was programmed to take data readings at the click of the mouse.

Sixteen channels were monitored and they included the following: calibrated load cells and internal LVDTs for both actuators, two external LVDTs, and ten pairs of strain gages. The two gages on each bar are connected to a single channel to get an average reading. The output voltage from each wheatstone bridge was divided by two and read by LabVIEW as a quarter bridge in order to compute strain.

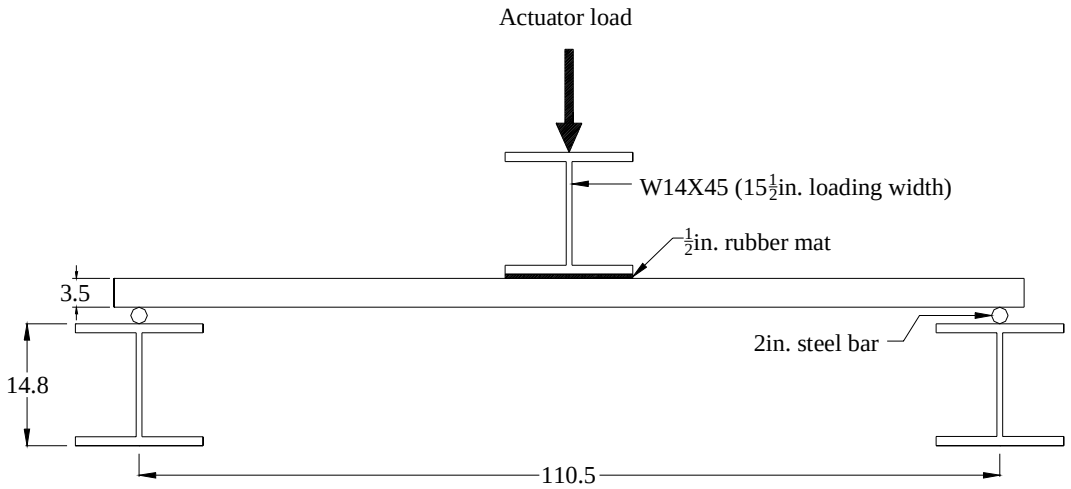

(a)

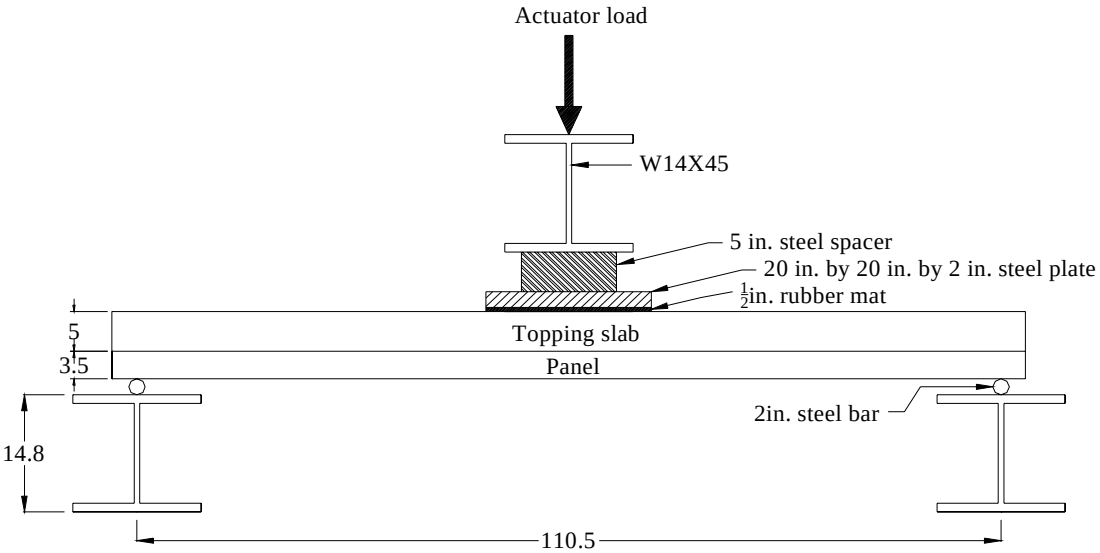

(b)

Figure 4.1 Loading setups for (a) panel test (b) composite test (values in inches)

Figure 4.2 FRP prestressed panel construction

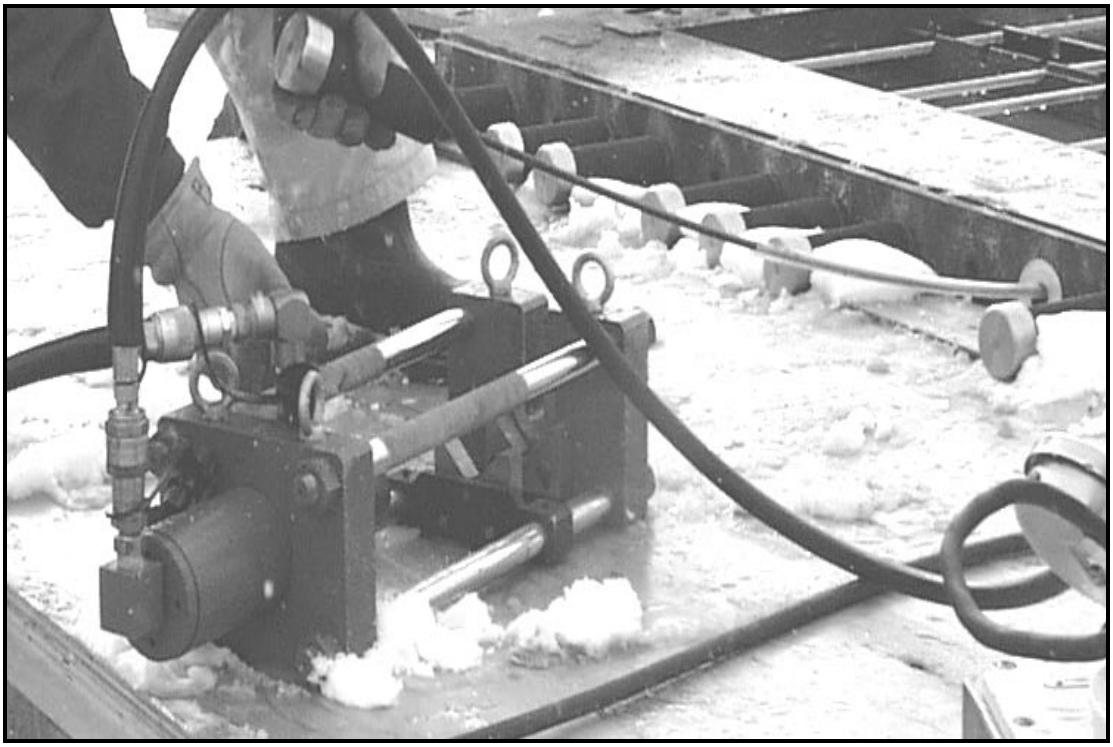

Figure 4.3 Leadline anchor application using a hydraulic jack

Figure 4.4 Coupler application

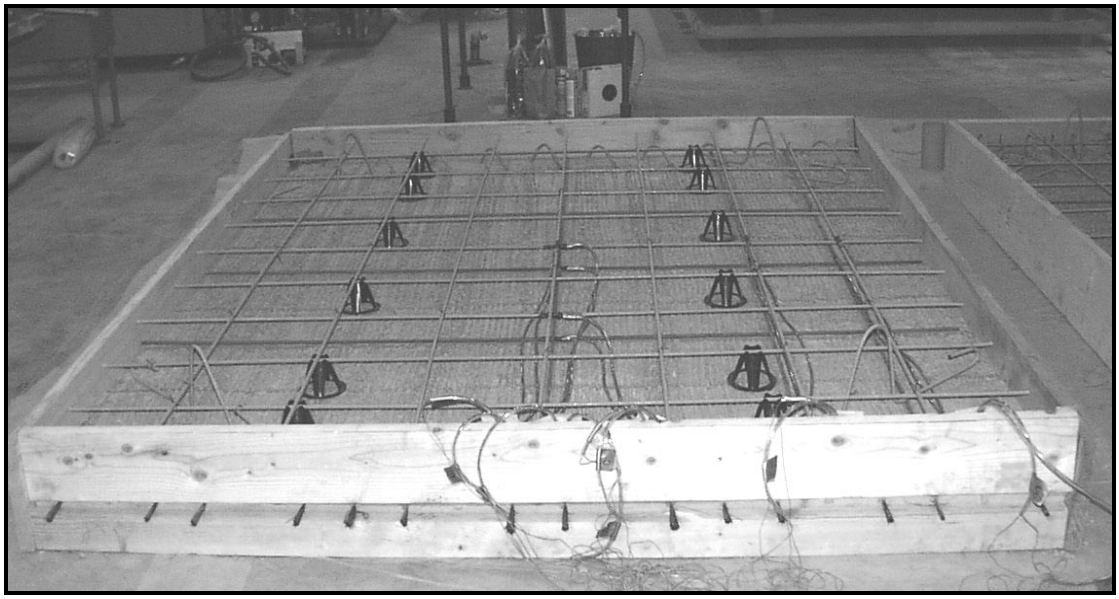

Figure 4.5 Panel with rebar ready for topping slab pour

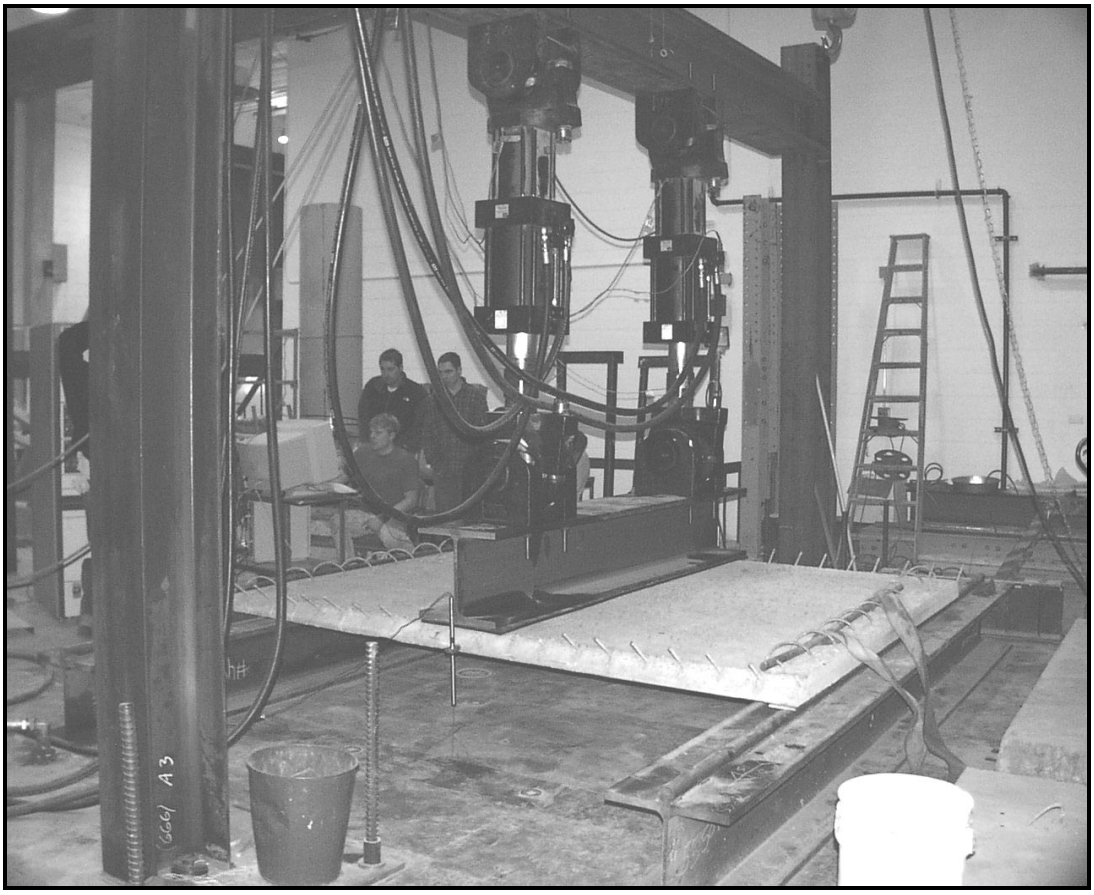

Figure 4.6 Line load testing setup for panel tests

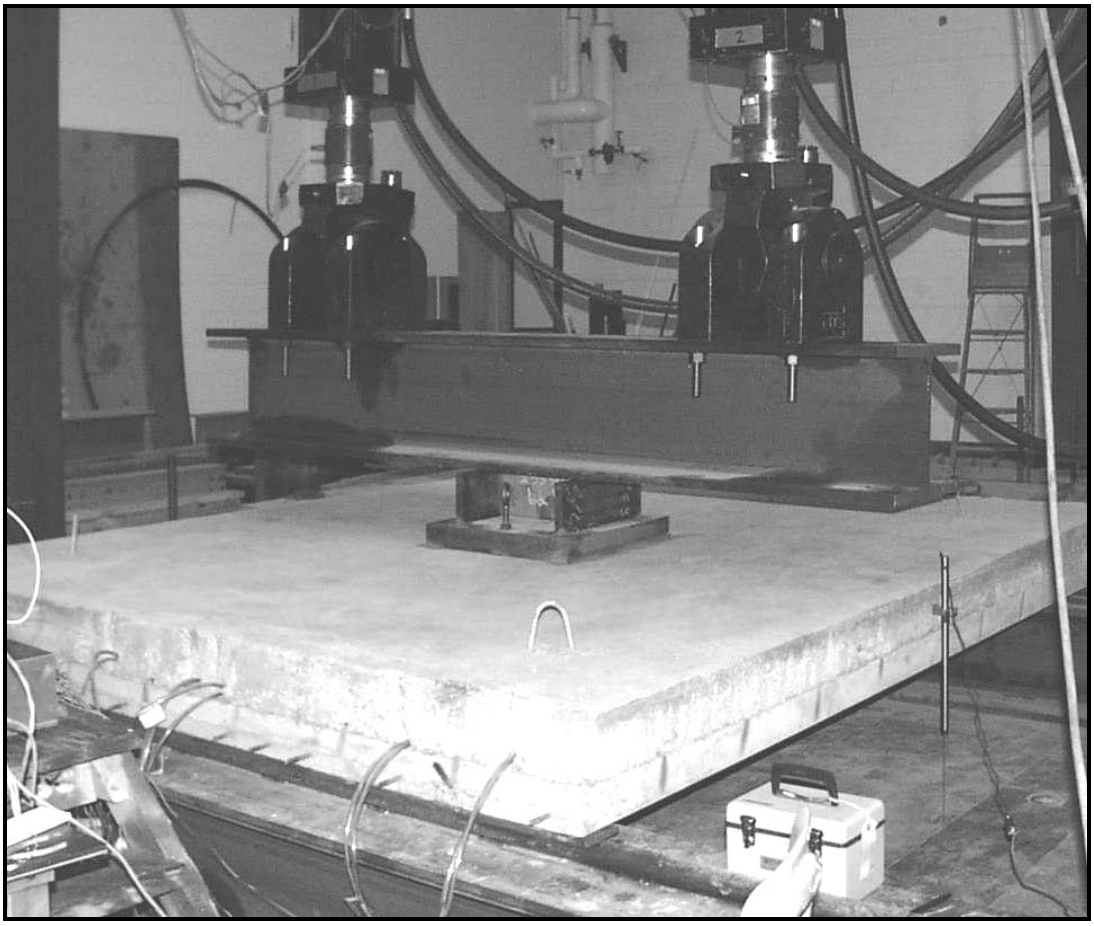

Figure 4.7 Plate load testing setup for composite slab tests

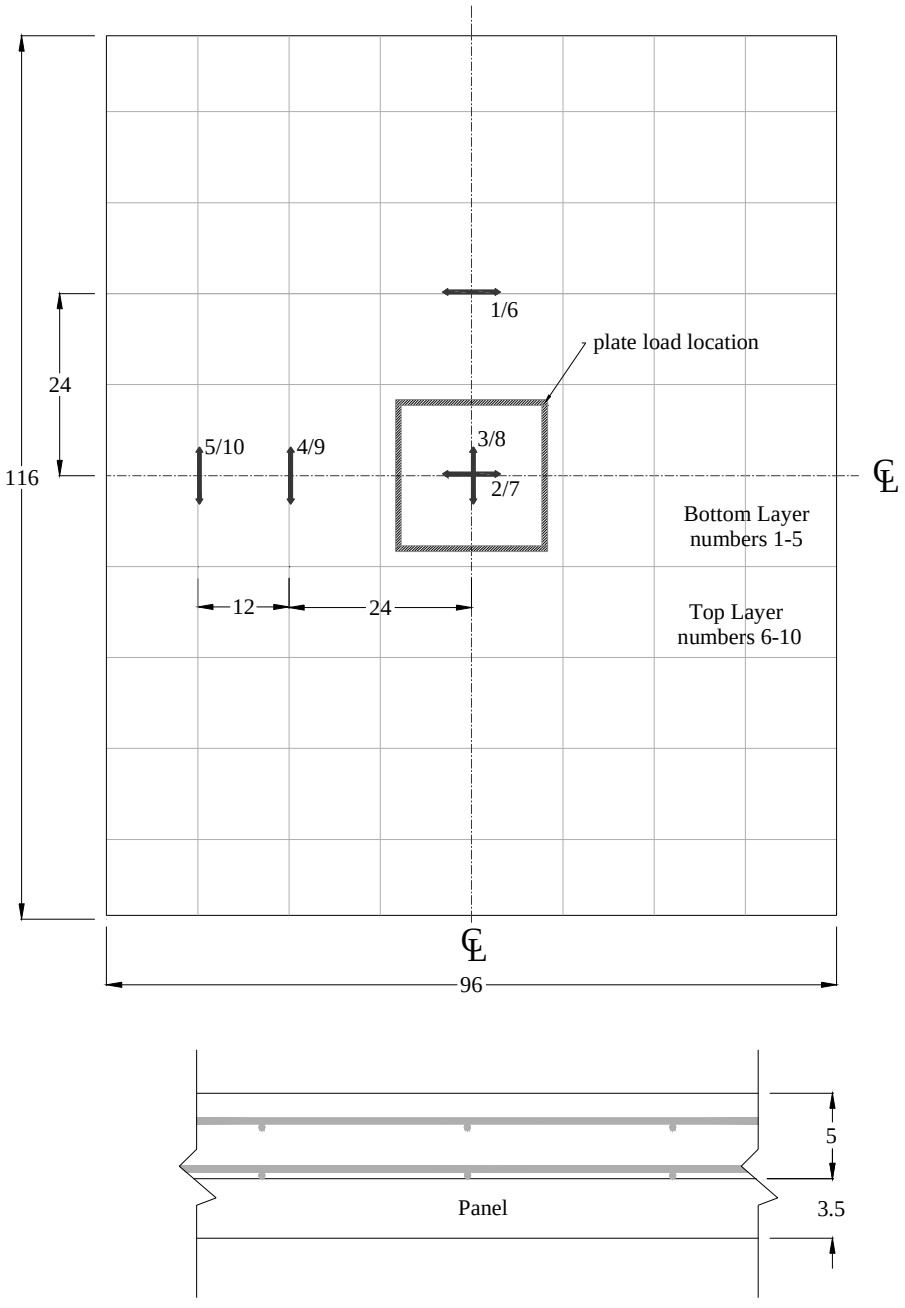

Figure 4.8 Strain gage layout (all values in inches) (1 in. = 25.4 mm)

5. Results of Panel/Slab Tests

5.1 Panel Tests

In the panel tests, the data recorded was load and deflection. In order to compare the nominal resistance of the panels to the actual load resistance developed in the tests, it is necessary to calculate the load carrying capacity of the panels from the nominal moment resistance. The panels were simply supported with a line load at midspan. The width of the loaded area is b = 381 mm (15 in.). Hence, assuming that the load within the loaded area is uniform, we can compute the nominal load capacity P_n from the nominal moment capacity M_n as

$$P_n = \frac{4 \cdot \left(M_n - M_{self-wt}\right)}{L - \frac{b}{2}} \qquad (5.1)$$

where L is the span length. Note that the nominal moment capacity is reduced by the moment $M_{self\text{-}wt}$ induced by the self-weight of the panel.

5.1.1 CFRP Prestressed Panel

Immediately upon delivery of the CFRP prestressed panels, small cracks were observed originating at each prestressing tendon as shown in Figure 5.1. Many of the cracks crossed the entire panel as visible on both the top and the bottom surfaces.

The cracks are suspected to be caused by the low strength of the concrete (17 MPa / 2500 psi) at stress transfer. When a tendon is prestressed, the diameter reduces due to Poisson's effect. Upon prestress release, the bars expand laterally and induce tensile stresses in the concrete. In this case, the force produced by the tendon expansion might have been too high for the concrete. These cracks were observed only on the CFRP prestressed panels. The steel reinforced panels had adequate concrete strength (31 MPa / 4500 psi) when the prestressing force was released, and no cracks were observed.

The CFRP prestressed panel failed in a typical over-reinforced fashion in which the concrete in the top half of the slab crushed before any tendon failure was observed. However, at some point during the test, the load carrying capacity dropped significantly because of excessive bond slip. This poor bonding can be attributed to the cracks in the vicinity of the tendons as mentioned above. No elastic rebound was observed after release of the load. The load-displacement curve for this test is shown in Figure 5.2.

Compared to the nominal strength calculated with the design specifications, the CFRP panel under-performed considerably. The maximum load was 44 kN (9.9 kips). This was considerably less than the expected design load of 80.1 kN (18 kips). This can be attributed to the several discrepancies between the design specifications and the actual panel. First, the strength of the concrete on the day of the test was 24.8 MPa (3600 psi) which is considerably lower than the 31 MPa (4500 psi) strength specified in the design. This has a significant impact on an over-reinforced panel.

Second, the depth of the panel was found to be slightly less than the 90 mm (3.54 in.) specified in the design. The actual depth was 87 mm (3.4 in.). Finally, the location of the strand was found to be at 43 mm (1.7 in.) from the base on the average. This essentially eliminates the eccentricity specified in the design. Based on these three findings, the load carrying capacity of the panel is recomputed and found to be 45.4 kN (10.2 kips). This value could be further reduced by the slip of the tendons. In any respect, the calculated value is very close to the test result as shown in Figure 5.2.

5.1.2 Steel Prestressed Panel

For the steel prestressed panel, the strength of the concrete on the day of the test was 40 MPa (5800 psi) which is significantly higher than the design strength of 31 MPa (4500 psi). This increased the load capacity from 81.8 kN (18.4 kips) to 89 kN (20 kips). The location of the steel strand was fairly precise. The panel failed at a maximum load value of 96.1 kN (21.6 kips). The failure mode was typical for an over-reinforced member in that the steel strand never ruptured. Upon reaching the maximum stroke of the actuators at 152 mm (6 in.), the load was released. This was followed by an elastic rebound of a few inches. The load-displacement curve is shown in Figure 5.2.

5.1.3 CFRP Prestressed Panel from the Bridge

It was not initially in the test program to test an actual panel from the bridge. The results of the aforementioned two panels were supposed to have validated the performance of a CFRP prestressed panel. However, because of the deficiency of the CFRP prestressed panel, it was deemed necessary to test another panel from the bridge. Thus, a panel was removed from the I-225/Parker Road construction site and brought to the laboratory. The design of this panel is presented in Section 3.2. It had twenty CFRP tendons, whereas the first two panels had only fourteen tendons.

As shown in Figure 5.2, the CDOT panel showed a very high strength and a brittle failure. Upon reaching the maximum load of 188.2 kN (42.3 kips), the panel cracked in half with complete rupture of the CFRP tendons and dropped to the floor. The tendon rupture is suspected to be caused by the excessive bending of the tendons under a large panel deflection. Unlike the first CFRP prestressed panel, no signs of tendon-concrete bond failure were observed. Figure 5.3 shows the CDOT panel after failure.

From theoretical calculations, the concrete strength should have significantly exceeded 55 MPa (8000 psi) to reach the panel strength obtained in the test. Unfortunately, the cylinder test result from a field specimen is inconclusive.

Figure 5.2 shows the comparison of the test results to the theoretical load carrying capacities of the panels. In addition, the uniformly distributed construction load specified in the design is converted to an equivalent line load. The equivalent load is

22.2 kN (5 kips). It is clear that all panels, including the first CFRP prestressed panel, can adequately meet this construction load requirement.

5.2 Composite Slab Tests

As described in Chapter 4, a plate load was used for the composite slab tests. This plate load is intended to simulate a wheel load of a design truck and to check the validity of the Equivalent Width Strip adopted in the AASHTO LRFD Specifications (1998). The Equivalent Width Strip provides an equivalent width over which a load is distributed as shown in Figure 5.4. The equivalent width is determined by the equations in Table 4.6.2.1.3-1 of AASHTO. The value of the equivalent width for the composite panels tested in this report can be calculated with equation 5.2 below, and cannot exceed 144 inches under the consideration of multilane loading.

$$EW = 26 + 6.6S \qquad (5.2)$$

In this empirical formula, the variable S is the center-to-center spacing (ft.) of support components. The equivalent width (EW) is in inches. Once the equivalent width is computed, the slab can then be analyzed by classical beam theory with the supporting components being assumed rigid and the span length taken as the center-to-center distance between girders. This formula is intended for a load area which satisfies the *tire contact area* defined in AASHTO [LRFD] 3.6.1.2.5. The formula to calculate

this area is shown in equation 4.1. For the composite slabs, the tire contact area is computed to be 508 mm (20 in.) by 508 mm (20 in.).

To examine the validity of the Equivalent Width Strip, one can compare the nominal load resistances of the slabs calculated with the entire slab width and with the equivalent width, respectively, to the experimental results. Such calculations can be carried out with equation 5.1. In this case, b = 20 in. This comparison can be especially meaningful for identifying the conservatism of the equivalent strip if the actual slab width is larger than the equivalent width. In this case, the composite slab width is 2438 mm (96 in.) and the calculated equivalent width based on the 2806 mm (110.5 in.) test span is 2205 mm (86.8 in.).

The nominal moment capacity of the composite slabs is calculated with the method in Section 3.3.2 based on the concrete strength of the topping slab as the compression block is expected to be in that region. The concrete strength of the topping slab on the day of the slab tests was 24.5 MPa (3550 psi) as opposed to the design specification of 31 MPa (4500 psi). Nevertheless, since the composite slabs were under-reinforced, this discrepancy in concrete strength was not expected to affect the nominal moment capacity significantly.

5.2.1 Steel Prestressed Composite Slab

The load-displacement curve for the composite slab with steel strands is shown in Figure 5.5. The maximum load reached was 429.7 kN (96.6 kips). The theoretical nominal load capacity is 338.5 kN (76.1 kips) considering the entire width of the slab

and is 306 kN (68.8 kips) considering the equivalent width of AASHTO. This capacity is computed assuming that there is no slip between the steel strands and the concrete.

The failure of the steel prestressed composite slab was exactly as expected. The slab was under-reinforced meaning that the steel would yield well before the concrete reached crushing levels. As shown in Figure 5.5, the steel reached its plastic regime and retained strength for a considerable duration. Then, without warning, the strands ruptured and the slab cracked into two halves and fell to the floor. Although development length was the governing criterion for the design giving nominal load capacities of 335 kN (75.3 kips) considering the entire width of the slab and 303 kN (68.1 kips) considering the equivalent width of AASHTO, no bond slip occurred.

5.2.2 CFRP Prestressed Composite Slab

For the CFRP prestressed composite slab, the load-displacement curve is shown in Figure 5.5. The actual maximum load achieved in testing was 362.1 kN (81.4 kips). The theoretical nominal load carrying capacity is 438.5 kN (98.6 kips) considering the entire width of the slab and 396.4 kN (89.1 kips) considering the equivalent width. This capacity is computed assuming that there is no slip between the CFRP tendons and the concrete. If equations 2.4 and 2.5 (Mahmoud et al., 1999) are used to estimate the required development length, the stress that can be developed in the CFRP tendon is significantly reduced because of the limited embedment length available. The theoretical nominal load carrying capacity based on the reduced

tendon stress due to debonding is 369 kN (83 kips**)** considering the entire width of the slab and 334 kN (75 kips) considering the equivalent width.

Numerous observations were made during the testing of the CFRP reinforced composite slab. Once the maximum load was reached, bond slip occurred in a few of the prestressed tendons. This caused a momentary drop in the load resistance of the slab. Then the strength increased again slightly until the next pullout occurred. This process repeated itself. At the end, the panel did not fail completely and was able to support its self-weight. This is shown in Figure 5.5.

5.3 Summary of Test Results

Table 5.1 compares the calculated load capacities of the panels and composite slabs with the experimental results and design loads. The *nominal design strength* in the second column is calculated according to the design specifications, while the *theoretical strength* is based on the as-built conditions with the actual concrete strengths on the day of testing. In the last column, the *design loads* are the specified construction load for the case of panels without a topping slab and the wheel load of an HS25-44 truck considering only the impact factor for the case of composite slabs.

For the composite slabs, two numbers are listed in the nominal design strength and the theoretical strength columns. The first number is the equivalent load capacity using the AASHTO equivalent width. The second number is the equivalent load capacity using the full panel width. These capacities are calculated without the consideration of possible bond failure.

Furthermore, Table 5.1 compares the ductility of different panels. In this study, ductility is defined as the ratio of deformation of the panel at the peak load to that at the design load. This is obtained from the experimental load-deflection curves. It is interesting to see that the CDOT panel with FRP prestressing tendons had the highest ductility

Table 5.1 Panel ductility and comparison of design and theoretical strengths to test results

(1 kip = 4.45 kN)

Panel Type	**Nominal Design Strength** *kips*	**Theoretical Strength** *kips*	**Experimental Values** *kips*	**Ductility**	**Design Load** *kips*
CDOT Panel	NA	33.7	42.3	33	5
Steel Prestr. Panel	18.4	20.0	21.6	21	
FRP Prestr. Panel	18.0	10.2	9.9	8	
*Steel Prestr. Comp. Slab**	71.1 / 78.6	68.8 / 76.1	96.6	19	26
*FRP Prestr. Comp. Slab**	93.7 / 103.6	89.1 / 98.6	81.4	8	

* The two numbers listed represent the equivalent load capacity using the AASHTO equivalent width and the full panel width, respectively.

For the steel prestressed composite slab, the experimental load achieved in the test far exceeds the theoretical load capacity. For the FRP prestressed composite slab, the experimental load achieved is between the theoretical load capacities with bond slip considering the full and equivalent widths. It can be concluded that in this case, the slip of the tendons was the governing factor for failure.

For all five tests performed, the strengths satisfy the design loads with a large factor of safety. Furthermore, the results seem to indicate that the Equivalent Width Strip method of AASHTO is conservative.

5.4 Strain Results

The strain gage data recorded in the two composite slabs were notably consistent with each other giving an impression of reliable results. With the strain gage placement diagram in Figure 4.1, it can be seen that the results were consistent with expectations up to the point of severe cracking. The only strain value that did not appear to be correct was from strain gage 4 in the composite slab with steel tendons. It was discovered later that this strain gage had not been functioning. Looking at the layout of the strain gage grid, it was expected that the strain values predicted by gage 4 would be between those of gages 3 and 5. This was confirmed by the strain results obtained from the slab with CFRP tendons. The trends established by the slab with CFRP tendons, in terms of the values of the strains at different locations, were used to approximate the strain at gage 4 in the slab with steel strands. These approximated results for gage 4 were used along with the other recorded strain results for further analysis as described later in this section. Results from all gages, except gage 4 in the composite slab with steel, up to the maximum load applied are shown in Figures 5.6 and 5.7. It can be seen that results after cracking are difficult to interpret. The strain values before cracking are shown in Figures 5.8 and 5.9.

The strain gage results were used to examine the variation of the transverse bending moment in the slab with respect to the distance from the plate load. The transverse moment is the moment acting in a direction perpendicular to the span of the slab.

In each slab, the strain gages provided values of strains at two elevations for five separate locations. The transverse moments can be calculated from the strains in gages 3-8, 4-9, and 5-10, with the numbers shown in Figure 4.8.

The main assumptions used in this analysis are that there is a perfect bond between the concrete and reinforcement, and that the concrete is linearly elastic. These are reasonable assumptions since we consider only the strain readings before cracking and the slabs were under-reinforced. In this range, it is expected that the compressive stress in concrete is below $0.5f'_c$.

To estimate a moment value from the strain profile obtained, a simple elastic analysis is conducted. Knowing the total height of the composite slab and the vertical locations of the gages as reported in Table 4.5, two strain values are used to create a strain profile. With the strain profile, the elevation of the neutral axis can be identified. Knowing that the concrete stress would not exceed the limit of $0.5f'_c$, an elastic concrete stress-strain diagram is used based on the modulus of elasticity of the concrete. The modulus of elasticity is estimated from the load-displacement curves shown in Figure 5.5. The moment is then computed from the stress in the concrete and the reinforcement assuming that the concrete in tension is not cracked. The

compression reinforcement is also considered. Only the incremental stress due to the applied load needs to be considered for the prestressing tendons.

The modulus of elasticity determined for the load displacement curves of the composite slab is 14.5 GPa (2100 ksi). This is low compared to the modulus of elasticity of 23.4 GPa (3396 ksi) predicted with the ACI 318 equation (ACI 318 8.5.1) using the actual compressive strength of concrete. However, test results reported by Shing and Abu-Hejleh (1999) show that a low modulus of elasticity can be expected for a concrete containing a substantial amount of fly ash. Their results show that at 28 days, the modulus of elasticity of a concrete with 20 percent fly ash by weight of cement can be considerably lower than that of a concrete that had comparable compressive strength but no fly ash. This is even true at an age of 90 days where the difference in the modulus of elasticity can be as high as 20 percent.

Before the moments are calculated, a check of the equilibrium between the force from the concrete and the reinforcing bar in the compression zone and the force from the concrete and prestressing tendon/strand in the tension zone is made. This is a preliminary check to determine the accuracy of the strain gage results. It is noted that the force in the compression zone is consistently higher than in the tension zone. For the composite slab with CFRP tendons, the compression force is 15 to 25 percent higher. For the composite slab with steel, the compression force is 20 to 35 percent higher. This increase in compression could be a result of the axial force induced in the composite slab by the support restraints. The nominal moment is computed by taking the moment about the centroid of the slab for each of the four force

components from the reinforcing bar, prestressing tendon/strand, compression concrete, and tension concrete, individually.

The moment values computed from the strain data are then compared with the moments calculated from the load attained in the experiment assuming perfect one-way bending using the entire width of the slab. However, based on the section forces observed above, it is estimated that ten percent of the loads applied in the tests were resisted by the frictional forces at the supports. Hence, for more exact comparison, the slopes of the experimental lines in Figures 5.10 and 5.11 should be increased by ten percent, which is not shown here. The results are compared in Figure 5.10 and Figure 5.11. A tabulated summary of the results for different gage locations is given in Tables 5.2 through 5.7.

Table 5.2 Moment calculations for composite slab prestressed with steel strand (strains 3 and 8)

Load *kips*	M_{load} *inch-kips*	Strain 3 $\mu\varepsilon$	Strain 8 $\mu\varepsilon$	M_{strain} *inch-kips*	$\frac{M_{load} - M_{strain}}{M_{load}}$
11.06	35.0	-18.8	-86.1	33.6	-4.0%
19.15	60.4	-32.9	-156.2	61.3	-1.5%
28.37	89.5	-44.2	-243.3	98.4	-9.9%
39.56	124.9	-56.5	-350.5	145.0	-16.1%
53.52	168.9	-37.7	-520.2	241.3	-42.9%
62.90	198.5	113	-691.3	448.2	-125.8%

Table 5.3 Moment calculations for composite slab prestressed with steel strand (strains 4 and 9)

Load *kips*	M_{load} *inch-kips*	Strain 4 $\mu\varepsilon$	Strain 9 $\mu\varepsilon$	M_{strain} *inch-kips*	$\frac{M_{load} - M_{strain}}{M_{load}}$
11.06	35.0	-8	-63.1	25.6	26.9%
19.15	60.4	-16	-120.5	48.6	19.5%
28.37	89.5	-26	-195.7	79.0	11.7%
39.56	124.9	-35	-283.2	114.9	8.0%
53.52	168.9	-45	-412.1	168.8	0.1%
62.90	198.5	-35	-539.1	228.5	-15.1%

Table 5.4 Moment calculations for composite slab prestressed with steel strand (strains 5 and 10)

Load *kips*	M_{load} *inch-kips*	Strain 5 $\mu\varepsilon$	Strain 10 $\mu\varepsilon$	M_{strain} *inch-kips*	$\frac{M_{load} - M_{strain}}{M_{load}}$
11.06	35.0	-10.4	-55.1	21.2	39.4%
19.15	60.4	-18.8	-106.8	41.4	31.5%
28.37	89.5	-29.2	-182.1	71.2	20.4%
39.56	124.9	-38.6	-262.1	103.3	17.3%
53.52	168.9	-48.0	-384.4	154.0	-8.8%
62.90	198.5	-30.1	-492.5	208.8	-5.2%

Table 5.5 Moment calculations for composite slab prestressed with CFRP tendons (strains 3 and 8)

Load *kips*	M_{load} *inch-kips*	Strain 3 $\mu\varepsilon$	Strain 8 $\mu\varepsilon$	M_{strain} *inch-kips*	$\frac{M_{load} - M_{strain}}{M_{load}}$
9.39	29.6	-4.7	-74.8	31.5	-6.4%
14.9	47.0	-9.4	-128.0	53.4	-13.6%
23.3	73.4	-18.4	-211.7	87.3	-18.9%
31.9	100.8	-18.8	-309.6	130.4	-29.4%
43.0	135.7	18.8	-464.3	215.6	-58.8%
53.1	167.7	306	-693.7	505.6	-201.5%

Table 5.6 Moment calculations for composite slab prestressed with CFRP tendons (strains 4 and 9)

Load *kips*	M_{load} *inch-kips*	Strain 4 $\mu\varepsilon$	Strain 9 $\mu\varepsilon$	M_{strain} *inch-kips*	$\frac{M_{load} - M_{strain}}{M_{load}}$
9.39	29.6	0	-47.1	20.2	31.8%
14.9	47.0	-4.0	-80.0	33.0	29.8%
23.3	73.4	-8.0	-141.2	57.9	21.1%
31.9	100.8	-12.0	-215.2	88.3	12.4%
43.0	135.7	0	-315.3	135.2	0.3%
53.1	167.7	56.2	-451.7	218.7	-30.4%

Table 5.7 Moment calculations for composite slab prestressed with CFRP tendons (strains 5 and 10)

Load *kips*	M_{load} *inch-kips*	Strain 5 $\mu\varepsilon$	Strain 10 $\mu\varepsilon$	M_{strain} *inch-kips*	$\frac{M_{load} - M_{strain}}{M_{load}}$
9.39	29.6	-0.5	-42.4	18.7	36.8%
14.9	47.0	-5.2	-70.6	29.4	37.4%
23.3	73.4	-9.9	-127.1	52.8	28.1%
31.9	100.8	-14.6	-188.2	78.2	22.4%
43.0	135.7	-9.9	-277.6	119.5	11.9%
53.1	167.7	51.3	-390.5	200.6	-19.6%

Tables 5.2 to 5.7 and Figures 5.10 and 5.11 show that the moments calculated with the strain values for the two composite slabs are reasonably close to the moment calculated from the experimentally obtained load assuming perfect one-way bending, except for load levels that exceed the cracking loads. After cracking, the calculated moment far exceeds the experimental value. This is probably due to the fact that concrete is assumed uncracked in the calculations. Hence, the calculated moment values shown in Figures 5.10 and 5.11 are unreliable after the cracking load is

reached. This is especially true for moments calculated with gages 3 and 8, which were directly under the plate load.

Since the plate load was acting directly in the center, it is expected that the moment computed from strains 3 and 8 will exceed the theoretical value. Moments computed from strains 4-9 and 5-10 are expected to be slightly lower as they are further away from the load application. This is confirmed by the results shown. The comparison will look better if we increase the slopes of the experimental results by 10% as mentioned previously. The average moment from these locations more or less coincides with the experimental value assuming uniform moment along the length. This is an indication of the accuracy of the calculated moments. Figures 5.10 and 5.11 show that the steel reinforced slab slightly better distributes the load in the transverse direction than the FRP reinforced slab. This could imply that the GFRP bars might not be as effective as the steel bars in distributing the load. Hence, the recommendation in the ACI 440H draft report for FRP temperature reinforcement (equation 3.2) might not be adequate for load distribution purposes in the slab. In particular, it seems more appropriate to eliminate the strength ratio in equation 3.2 since stiffness of the reinforcement is more relevant to load distribution in a slab.

For the slab with steel reinforcement, the variation of moment with distance seems small enough to assume that the entire length within the gage location is uniformly effective in carrying the load. The gages cover a slab length of 1829 mm (72 in.), considering symmetry, whereas the equivalent width according to AASHTO is computed to be 2205 mm (86.8 in.). However, with extrapolation of the strain

readings, we can see that the AASHTO equivalent width equation is conservative. This is further assured by the fact that this panel had a load resistance that is significantly higher than the theoretical strength based on the entire length of the slab. However, part of this could be due to the support restraints as mentioned before.

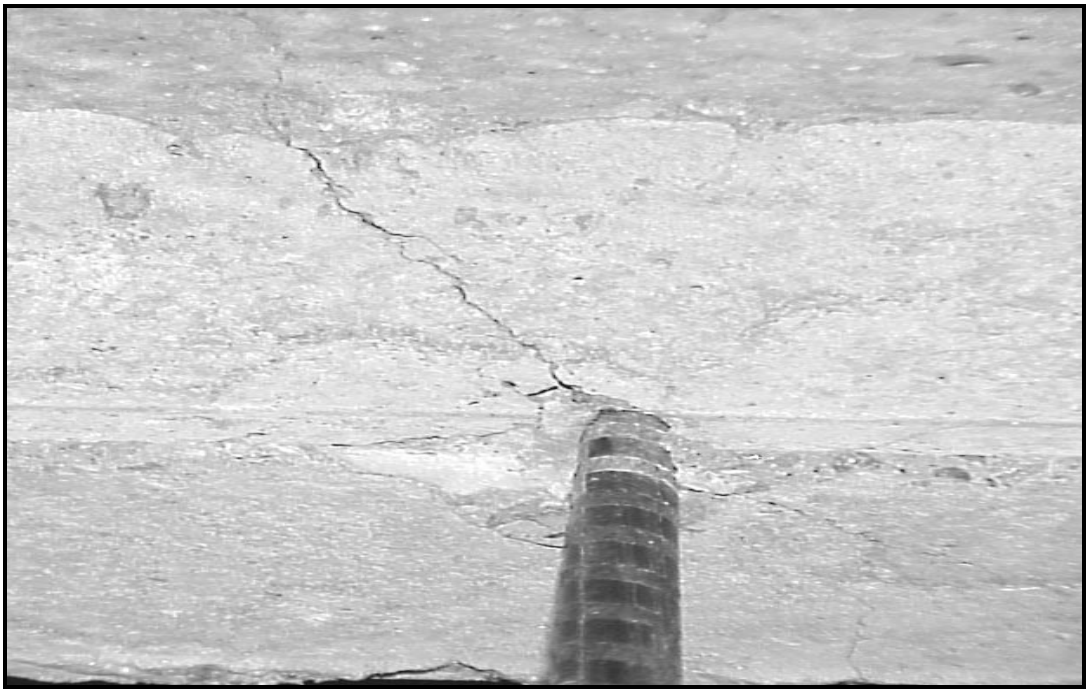

Figure 5.1 Initial cracking surrounding the prestressed CFRP tendons

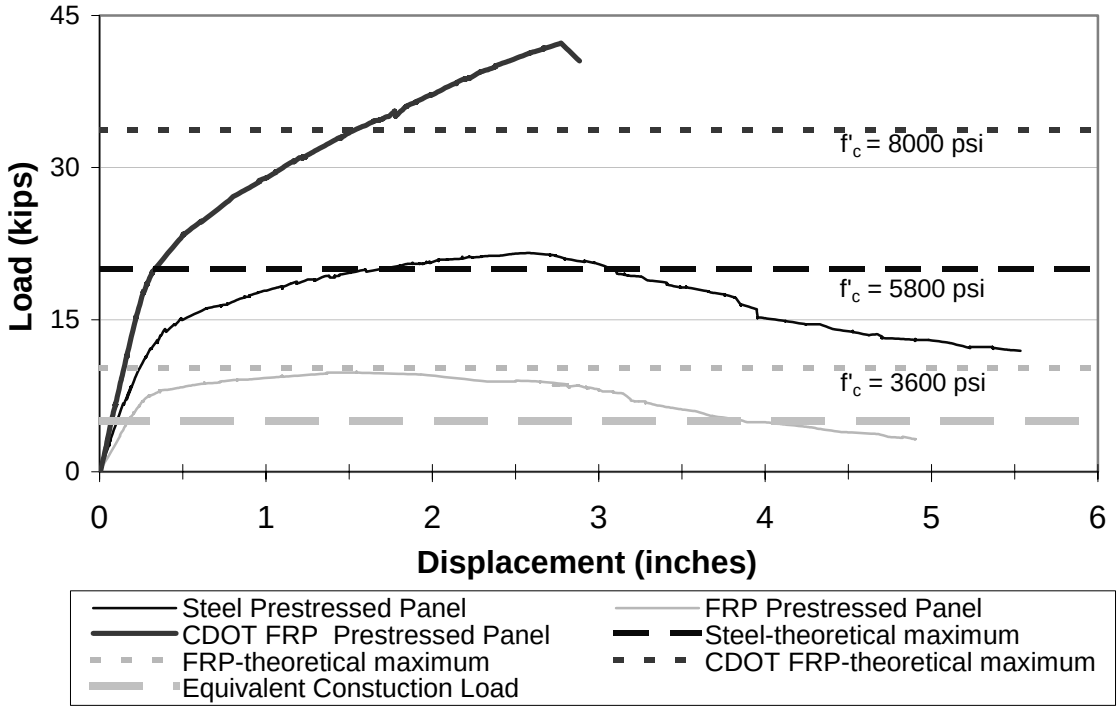

Figure 5.2 Load vs. displacement for three panels

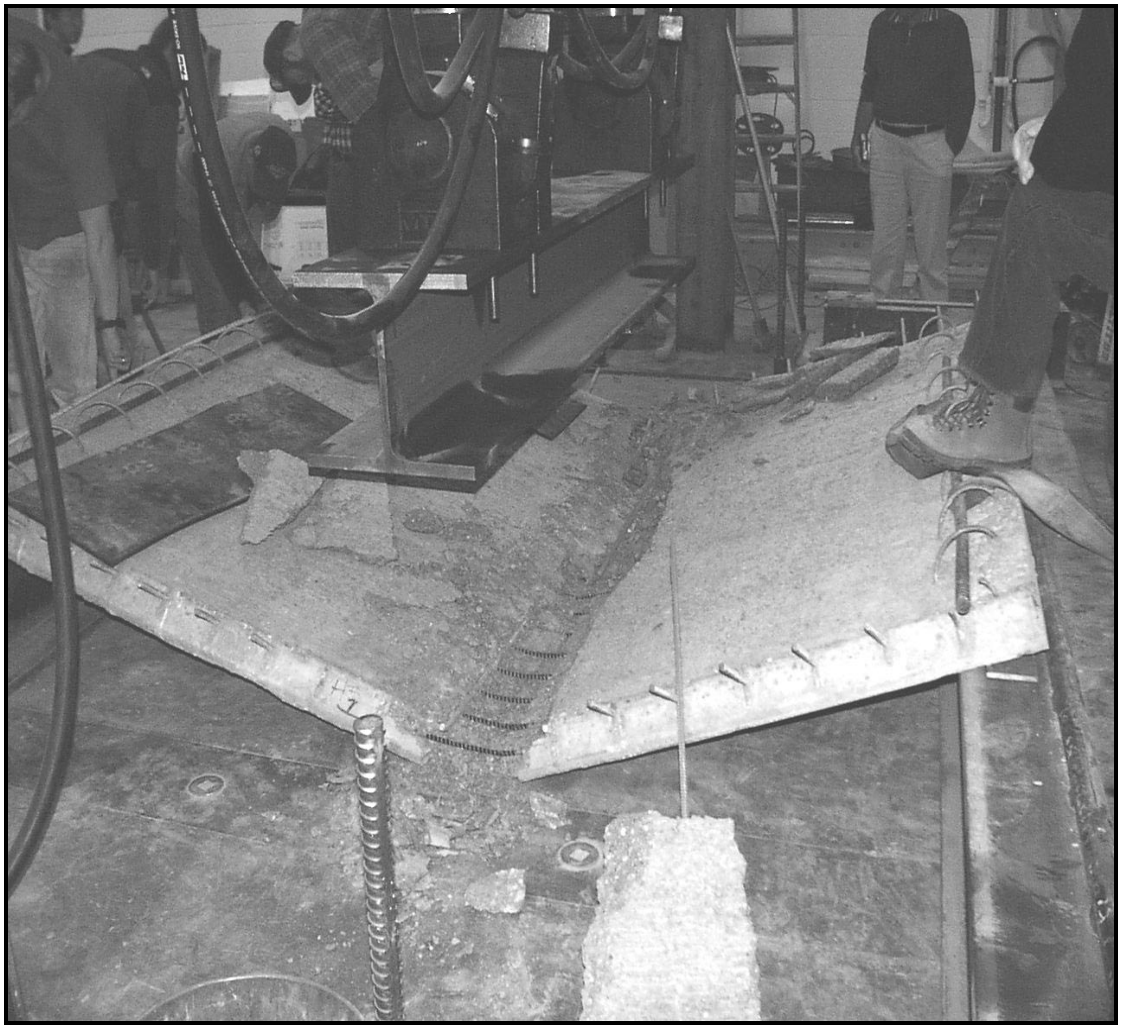

Figure 5.3 CDOT panel failure

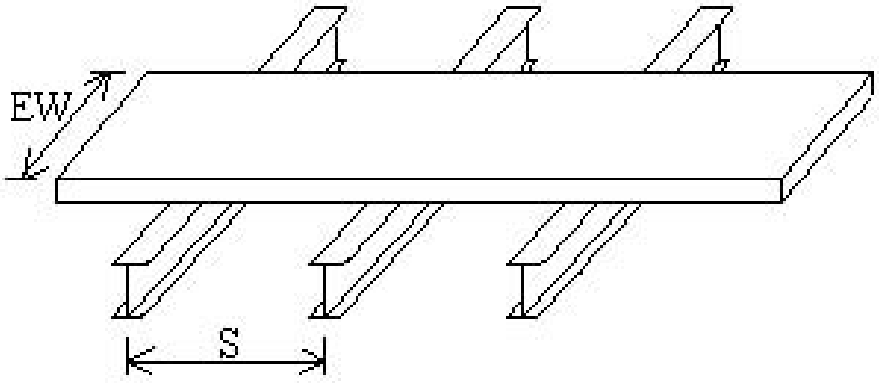

Figure 5.4 Design strip for the Equivalent Strip Method (Barker and Puckett 1997)

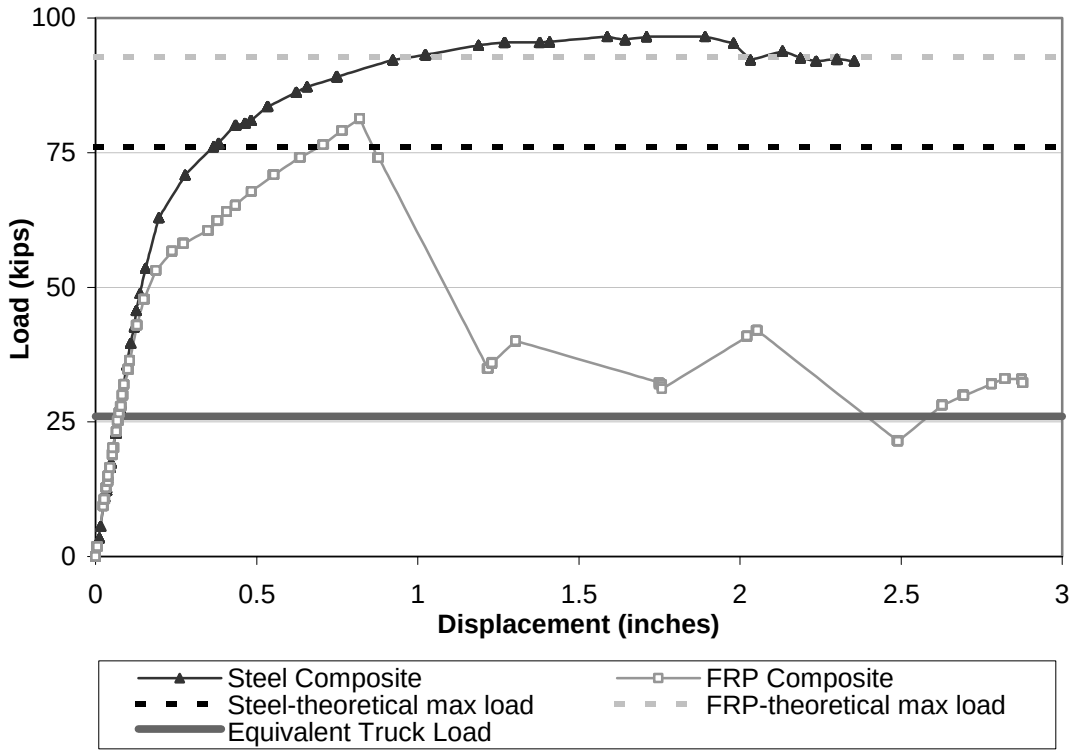

Figure 5.5 Load vs. displacement curves for the composite slabs (the theoretical maximum loads are calculated with a full panel width)

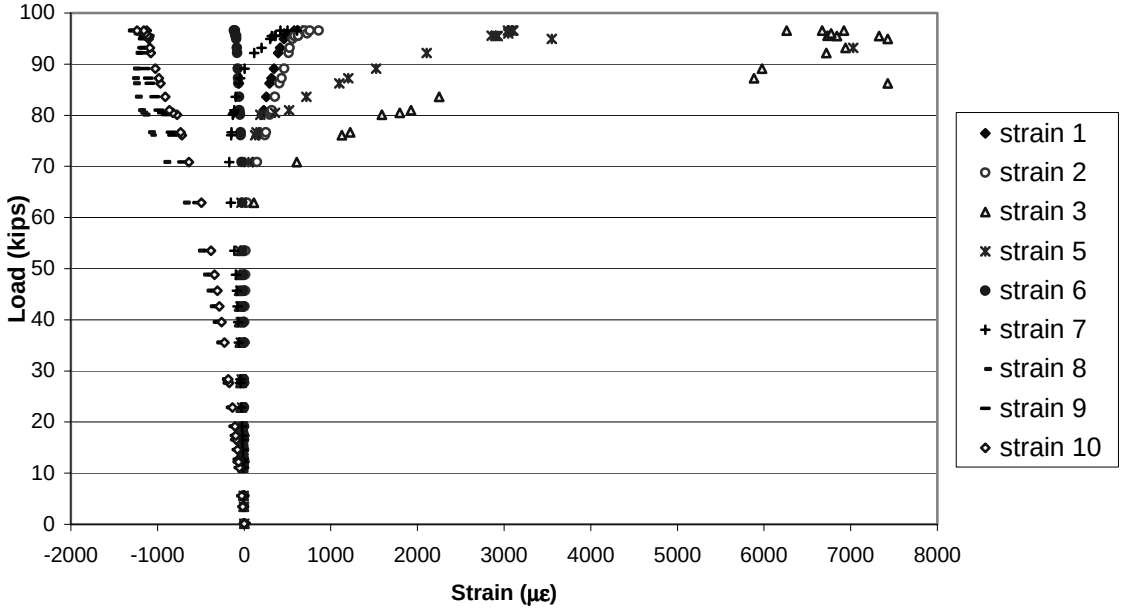

Figure 5.6 Load vs. strain values for composite slab prestressed with steel loaded beyond cracking

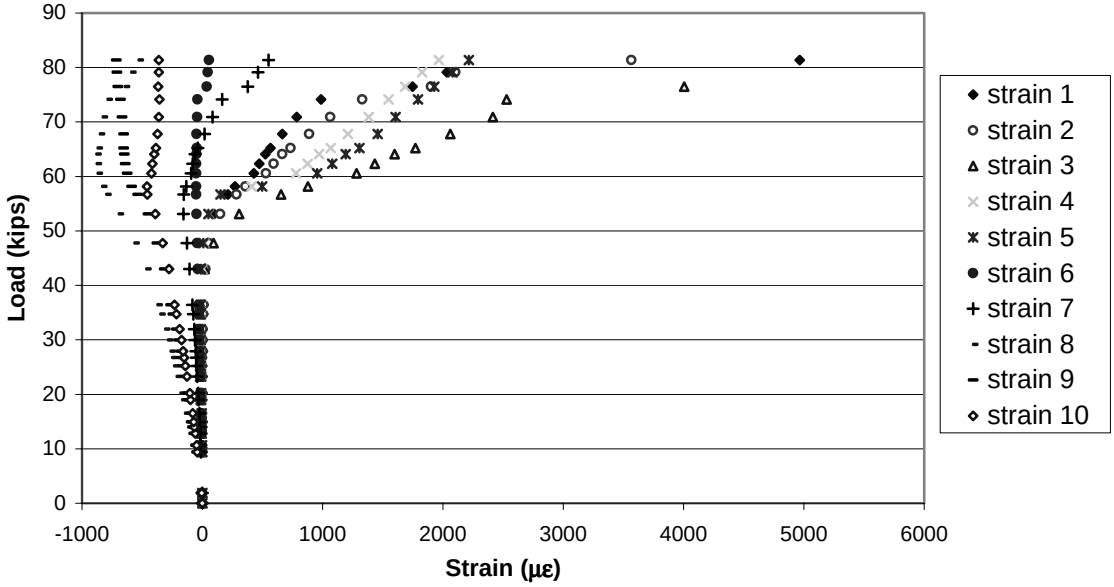

Figure 5.7 Load vs. strain values for composite slab prestressed with CFRP loaded beyond cracking

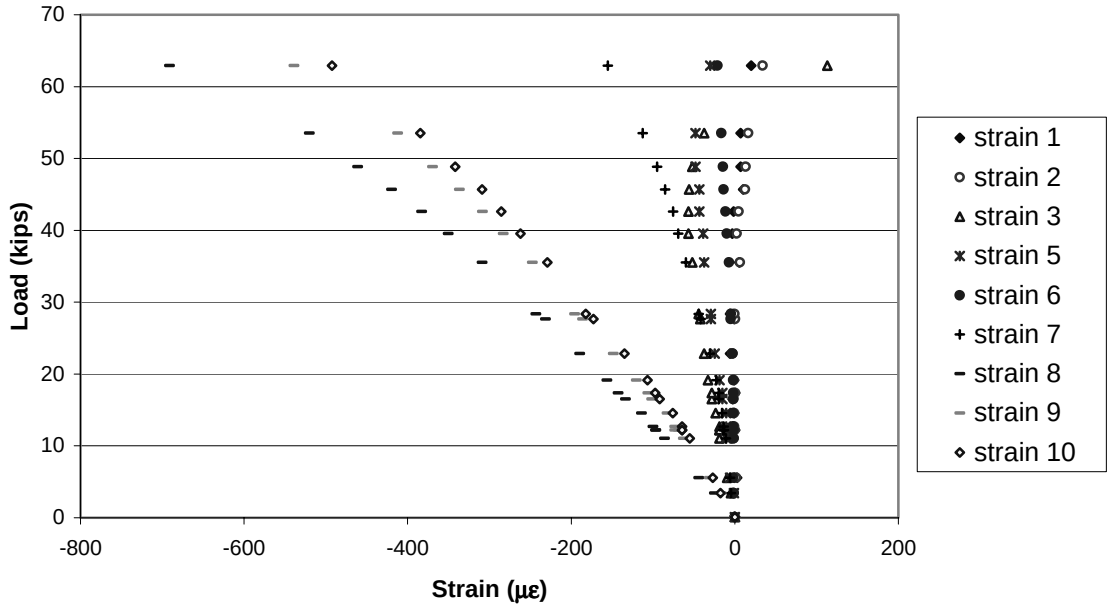

Figure 5.8 Load vs. strain values for composite slab prestressed with steel before cracking

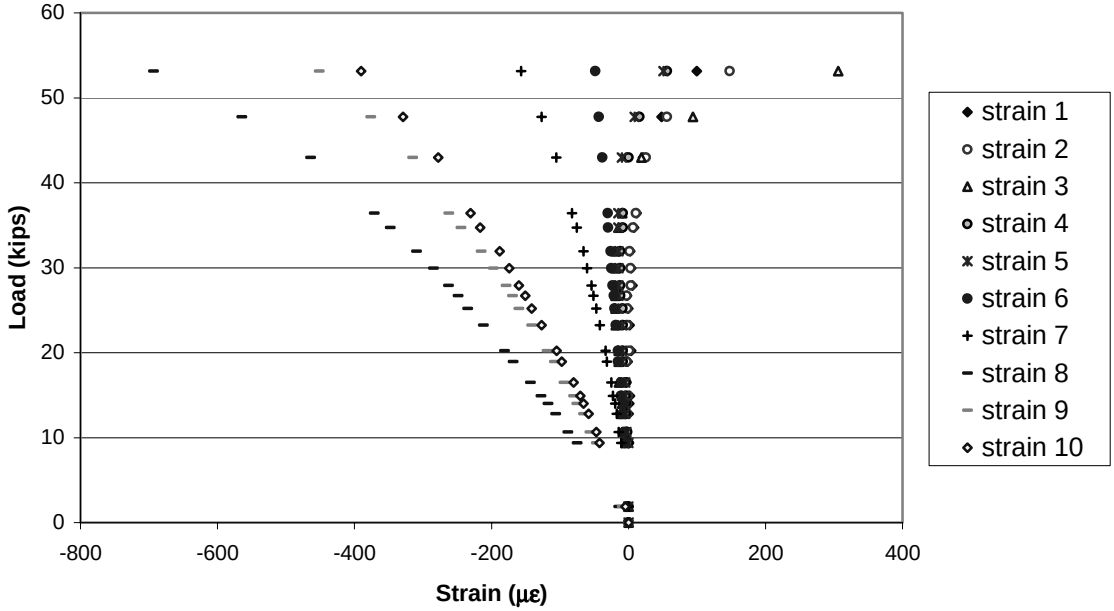

Figure 5.9 Load vs. strain values for composite slab prestressed with CFRP before cracking

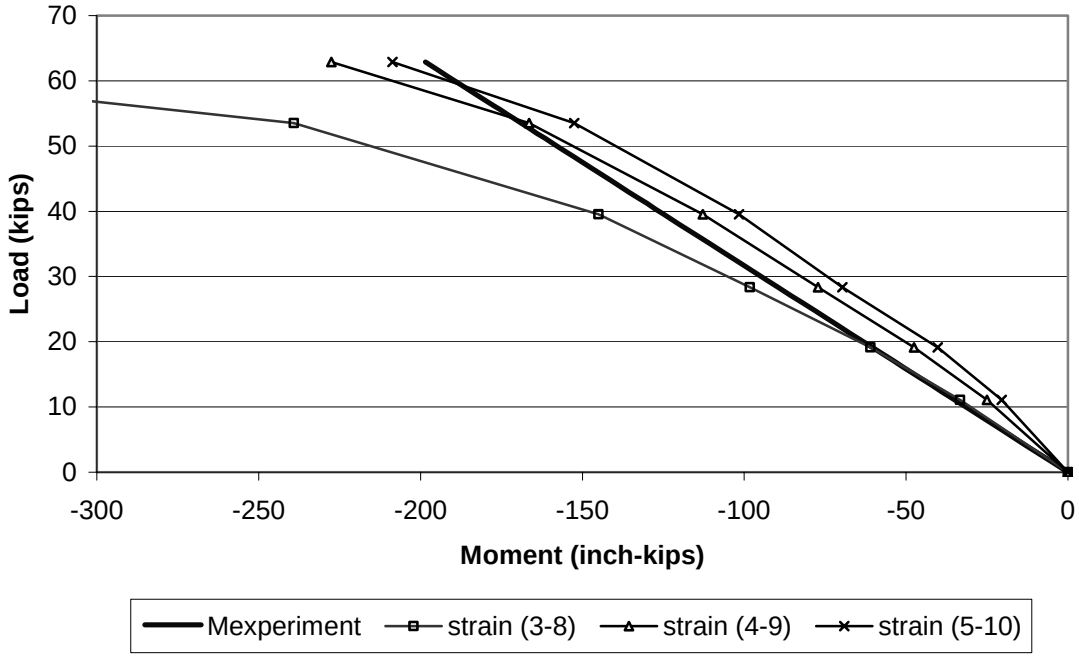

Figure 5.10 Load vs. moment for composite slab prestressed with steel

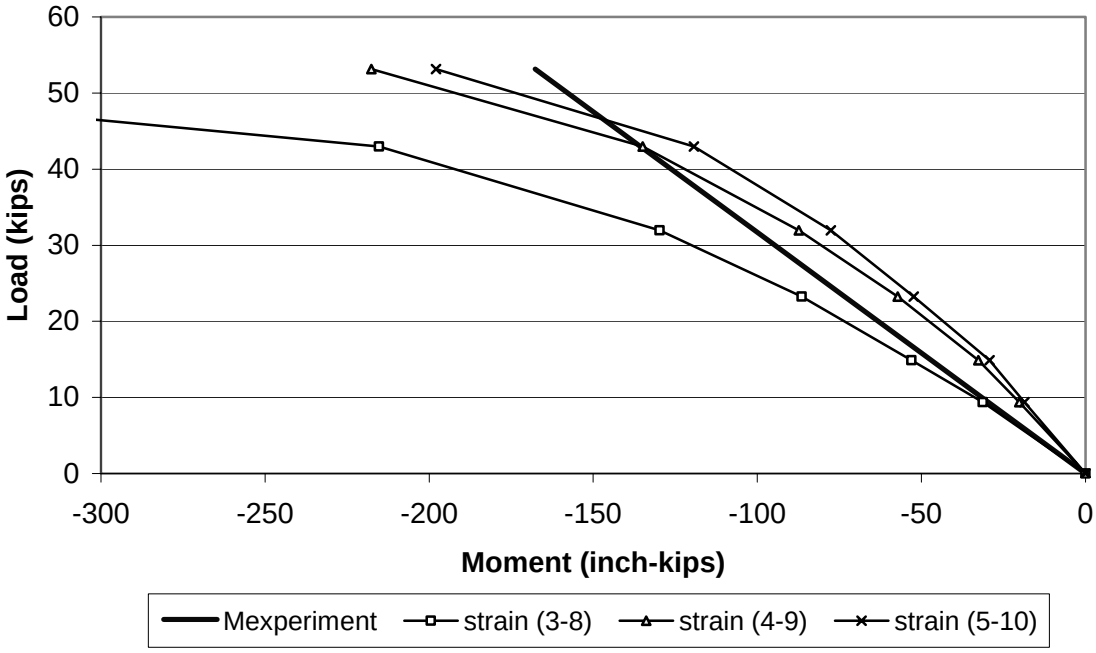

Figure 5.11 Load vs. moment for composite slab prestressed with CFRP

6. Summary and Conclusions

6.1 Summary

This study compares the strengths of precast panels and composite slabs prestressed with CFRP tendons and steel strands. The strengths of individual panels as well as those constructed with the addition of a 125 mm (5 in.) topping slab are investigated.

The panels were designed using the 16th Edition of AASHTO (1996) with additional considerations for CFRP tendons.

The panels were 90 mm (3.5 in.) deep, 2950 mm (116 in.) wide, and 2438 mm (96 in.) long. The panel width of 2950 mm was selected to span two precast, post-tensioned concrete box girders in a direction perpendicular to the flow of traffic. Each panel was prestressed with 14 tendons spaced symmetrically over the 2438 mm length. Perpendicular to the prestressing tendons, reinforcing bars were placed at 305 mm (12 in.) spacing. One set of panels was prestressed with 8 mm (0.315 in.) Leadline CFRP tendons and reinforced with 13 mm (0.5 in.) C-BAR GFRP reinforcing rods. The other set was prestressed with 9.5 mm (3/8 in.) seven-wire, low relaxation prestressing strand and reinforced with #3 steel bars (9.5 mm diameter).

One panel in each set was tested as it was. The other panel in each set had a 125 mm (5 in.) composite topping slab cast with one mat of #3 (9.5 mm) steel reinforcing bars spaced at 305 mm (12 in.) in each direction. The steel reinforcement in the grid was fitted with strain gages to obtain load distribution data for the slabs.

A third panel type was also tested. This panel was designed by CDOT and used in the bridge at I-225/Parker Road. The CDOT panel had the same overall dimensions as the other tested panels. However, the reinforcement was considerably different. Each panel was prestressed with twenty 10 mm (0.39 in.) diameter CFRP tendons spaced symmetrically over the 2438 mm (96 in.) length. GFRP reinforcing bars with a 13 mm (0.5 in.) diameter were placed at 152 mm (6 in.) spacing perpendicular to the prestressing tendons. Hence, the panel was more conservatively designed than the others.

The panels were loaded with a beam that spanned the entire 2438 mm (96 in.) length of the panel. The composite slabs were loaded with a 508 mm (20 in.) by 508 mm steel plate to model the tire contact area recommended by AASHTO.

Furthermore, a series of pullout tests were performed on Leadline CFRP tendons, seven-wire steel strand, C-BAR GFRP reinforcing rods, and #4 black steel bars to attain a better understanding of bonding between these materials and concrete.

6.2 Conclusions

The conclusions of this study are as follows:

1. Pullout test results show that 13 mm (0.5 in.) C-BAR reinforcing rods provided higher bond strength than that of #4 (13 mm diameter) black reinforcing steel. The average bond strength of the C-BAR with an embedment of $5d_b$ was 21.7 MPa (3.15 ksi). The average bond strength of the reinforcing steel with an embedment of $6d_b$ was 20 MPa (2.9 ksi).

2. Pullout test results show that 10 mm (0.39 in.) Leadline prestressing tendons provided higher bond strength than that of 9.5 mm (3/8 in.) steel prestressing strand. The average bond strength of the Leadline with an embedment of $10d_b$ was 10.9 MPa (1.58 ksi). The average bond strength of the steel strand with an embedment of $20d_b$ was 6.8 MPa (0.99 ksi).

3. The anchor chuck developed by Mitsubishi Chemical Corporation used in the prestressing of Leadline tendons provided adequate gripping capacity to attain a prestressing force equal to 60 percent of its maximum strength. Possible difficulties in the prestress process using this anchor are discussed. If using a coupler to attach the Leadline anchor to a steel strand, the twist produced by the steel strand during prestressing may induce large stresses on the CFRP tendons over long bed lengths. It is important to keep the length of steel strand used to a minimum in order to reduce the amount of twist that may develop.

4. The panels prestressed with CFRP cannot be directly compared to those prestressed with steel due to the abnormalities in the construction of the CFRP prestressed panels. In the construction, the placement of the CFRP tendons in the panels nearly wiped out all eccentricity specified in design. Also, the panel depth was reduced by 4 mm (0.1 in.). Finally, the concrete strength on the day of testing was 24.8 MPa (3600 psi) instead of the specified 56 day strength of 31

MPa (4500 psi). Lastly, cracks developed near the CFRP prestressing tendons before testing. The prestressing force was released while the concrete strength was at 17.2 MPa (2500 psi) which was very low compared to the specified release strength of 29.7 MPa (4300 psi). This could be very likely the cause of the cracks. With all of the above problems, the load carrying capacity of the panel was 44.0 kN (9.9 kips) which is much lower than expected.

The steel prestressed panels did not have any of the construction problems discussed for the CFRP prestressed panels. In fact, the concrete strength for the steel prestressed panels was 40 MPa (5800 psi) on the panel testing day. This was significantly larger than the 31 MPa (4500 psi) strength specified in design. The actual load carrying capacity reached was 96.1 kN (21.6 kips) in the panel test.

A careful analysis has indicated that the CFRP panel should have performed satisfactorily if it was constructed properly.

5. The testing of a CDOT panel added a great deal of confidence in the performance of a properly constructed CFRP prestressed panel. Unlike the first CFRP panel discussed above, the load carrying capacity obtained in testing was larger than the theoretical load carrying capacity.

6. Each panel that was tested showed a load carrying capacity greater than the equivalent construction load of 22.2 kN (5 kips). The CFRP prestressed panel, steel prestressed panel and the CDOT CFRP prestressed panel (I-225/Parker Road

project) had load carrying capacities of 44 kN (9.9 kips), 96.1 kN (21.6 kips), and 188.2 kN (42.3 kips), respectively.

7. In the case of the two composite slabs, the load carrying capacities attained in the tests were either greater than or close to the theoretical load carrying capacities. The load carrying capacities for the steel prestressed composite slab and the CFRP prestressed composite slab were 429.7 kN (96.6 kips) and 362.1 kN (81.4 kips), respectively. As a result of the problems mentioned above, the failure of the CFRP prestressed slab was governed by tendon slip, and, therefore, had a lower resistance than the steel prestressed slab. The wheel load of the HS25-44 AASHTO design truck with alternate military loading and an impact factor is 115.7 kN (26 kips).

8. The results of the moment analysis using the strain data show that the steel reinforced slab better distributed the loading in the transverse direction than the FRP reinforced slab. This would imply that the GFRP bars in the panels might not be as effective as the steel bars for distributing the load. Hence, the recommendation in the ACI 440H draft report for FRP temperature reinforcement (equation 3.2) may not be adequate for distribution reinforcement. In particular, it seems more appropriate to eliminate the strength ratio in equation 3.2 since stiffness of reinforcement is more relevant to load distribution in the slab.

APPENDIX A: DESIGN OF FRP PRESTRESSED PANELS AND COMPOSITE SLABS

This appendix documents the detailed design calculations for the FRP prestressed panels that were tested in this study.

The panel dimensions and tendon eccentricity are the same as the CDOT panel shown in Figure 3.2. The primary design variables are the spacing and sizing of the prestressing tendons. For the following calculations, a unit width of 305 mm (12 in.) is used throughout.

PANEL AND COMPOSITE SLAB DIMENSIONS

Clear span:	2860 mm (9.38 ft.)
Design span:	2905 mm (9.53 ft.)
Panel thickness:	90 mm (3.5 in.)
Topping slab thickness:	125 mm (5 in.)
Panel length:	2438 mm (96 in.)
Panel width:	2950mm (116 in.)
d_{pp} = depth of prestressing tendons in panel:	57 mm (2.33 in.)
d_p = depth of prestressing tendons in composite slab:	182 mm (7.17 in.)
e_c = eccentricity of tendons in the panel:	12 mm (0.47 in.)
$A_{c\text{-}pan}$ = panel cross-sectional area:	27408 mm^2 (42.5 in^2)
$A_{c\text{-}com}$ = composite slab cross-sectional area:	65500 mm^2 (101.5 in^2)

LINE LOAD FOR A 305 mm (12 in.) STRIP

Non-composite panel loading (panel only)

Construction loading: 5600 Pa (0.812 psi) = 1.71 kN/m (116.9 plf)

Panel self-weight: 0.65 kN/m (44.3 plf)

Slab self-weight: 0.90 kN/m (61.5 plf)

Moments due to construction loads and self-weight

M_{constr} = 0.125(1710 N/m)(2.905 m)^2 = 1804 N-m (15.9 inch-kips)

M_{panel} = 0.125(650 N/m)(2.905 m)^2 = 686 N-m (6.0 inch-kips)

M_{slab} = 0.125(900 N/m)(2.905 m)^2 = 949 N-m (8.4 inch-kips)

Composite slab loading (Assuming no overlay)

HS25-44 and alternate military loading

M_{truck} = *DF* (*IF*) (*CF*) (wheel load) [US customary units]

DF = distribution factor = (span + 2)/32 = 0.356 [AASHTO 3.24.3.1]

IF = impact factor = 1.3 [AASHTO 3.8.2.1]

CF = continuity factor = 0.8 [AASHTO 3.24.3.1]

M_{truck} = 0.356(1.3)(0.8)(20 kips)(12 in./1 ft.) = 88.8 in-kips (10 kN-m)

MATERIAL PROPERTIES

Leadline Prestressing Tendon (as given by Mitsubishi Chemical Corporation)

diameter = 8 mm (0.315 in.)

f_{pu} = 2818 MPa (409 ksi)

A_{cs} = 46.1 mm^2 (0.0715 in^2)

E_p = 146.9 GPa (21320 ksi)

Concrete

f'_{ci} = 29.6 MPa (4300 psi)

f'_c = 31 MPa (4500 psi)

$E_c = 57000\sqrt{4500}$ psi = 3824 ksi (26.3 GPa) [ACI 8.5.1, units in psi]

$E_{ci} = 57000\sqrt{4300}$ psi = 3738 ksi (25.7 GPa)

ALLOWABLE STRESSES FOR CONCRETE AND CFRP TENDONS

Note: Positive stresses are in tension and negative stresses are in compression (all units in equations are in psi). Stress limits for concrete are defined in AASHTO 9.15.2.

In panels after prestress release

$-0.6\ f'_{ci}$ = -0.6(4300 psi) = -2580 psi (-17.8 MPa)

$3\sqrt{f'_{ci}}$ = $3\sqrt{4300}$ psi = 197 psi (1.4 MPa)

In panels during construction and pouring of topping slab

-0.6 f'_c = -0.6(4500 psi) = -2700 psi (-18.6 MPa)

6 $\sqrt{f'_c}$ = 6 $\sqrt{4500}$ psi = 402 psi (2.8 MPa)

In composite after curing of topping slab and subject to full service loads

-0.6 f'_c = -0.6(4500 psi) = -2700 psi (-18.6MPa)

6 $\sqrt{f'_c}$ = 6 $\sqrt{4500}$ psi = 402 psi (2.8 MPa)

CFRP tendon jacking limit

For CFRP tendons, Dolan et al. recommend a jacking stress (f_{pj}) of 0.65f_{pu} and an initial prestress (f_{pi}) of 0.60f_{pu}. To be on the conservative side, a jacking stress of approximately 0.60f_{pu} is used here.

SECTION PROPERTIES

Panel

$I_{panel} = bh^3/12$ = 18.5 x 10^6 mm^4 (44.4 in^4)

$c_t = c_b$ = 90 mm/2 = 45 mm (1.77in.)

$S_t = S_b$ = 18.5 x 10^6 mm^4/45 mm. = 4.1 x 10^5 mm^3 (25.1 in^3)

$r^2 = I_{panel}/A_{c\text{-}pan}$ = 675 mm^2 (1.045 in^2)

Composite slab

$I_{composite} = bh^3/12$ = 252 x 10^6 mm^4 (605.5 in^4)

$c_t = c_b = 215$ mm/2 = 107.5 mm (4.23 in.)

$c_{tp} = 107.5$ mm - 90 mm = 17.5 mm (0.69 in.)

$S_t = S_b = 252 \times 10^6$ mm^4 / 107.5 mm = 2.3×10^6 mm^3 (143.1 in^3)

$S_{tp} = 252 \times 10^6$ mm^4 / 17.5 mm = 14.4×10^6 mm^3 (877.5 in^3)

$r^2 = I_{composite}/A_{c\text{-}com} = 3847$ mm^2 (5.96 in^2)

STRESSES CAUSED BY GIVEN LOADING

f_t = stress at the top of the composite slab

f_b = stress at the bottom of the panel and the composite slab

f_{tp} = stress at the top of the panel

Non-composite panel loading

Construction loading: $f_{tp} = f_b = 1804$ N-m / 4.1×10^5 mm^3 = ± 4.4 MPa (± 635 psi)

Panel self-weight: $f_{tp} = f_b = 686$ N-m / 4.1×10^5 mm^3 = ±1.7 MPa (± 241 psi)

Slab self-weight: $f_{tp} = f_b = 949$ N-m / 4.1×10^5 mm^3 = ± 2.3 MPa (± 334 psi)

Composite slab loading

Service loading: $f_t = f_b = 10$ kN-m /2.3×10^6 mm^3 = ±4.3 MPa (± 621 psi)

$f_{tp} = 10$ kN-m /14.4×10^6 mm^3 = +0.7 MPa (+101 psi)

PRESTRESS DESIGN

The selection of the tendon size and spacing is based on an iterative design procedure. Based on the allowable stresses and the fact that the prestressing bed used by the panel precaster is set up to space the tendons at 121 mm (4.75 in.) intervals, a tendon configuration was developed that placed 14 tendons over the entire 2438 mm (96 in.) width. The configuration is shown in Figure 3.3. The jacking force was chosen to be at 76 kN (17 kips) per tendon. This results in a jacking stress of $0.58f_{pu.}$

Number of strands per unit width = 1.75

The total jacking force for a unit width (P_{pj}) is 132.3 kN (29.8 kips).

Total area of prestressing tendon per unit width (A_p) = 80.7 mm^2 (0.125 in^2)

DETERMINE TENDON STRESSES

P_{pj} = 132.3 kN (29.8 kips)	This is the initial jacking force applied per unit width.
$P_{pj\text{-}r} = 0.9P_{pj}$ = 119.2 kN (26.8 kips)	This 10 percent reduction in jacking force is based on observations made in tests by Dolan et al. (2000).

$$P_i = \left(\frac{P_{j-r}}{E_p A_p} + \frac{M_{pan} e}{I_p E_{ci}} \right) \left(\frac{A_c E_{ci} A_p E_p}{A_c E_{ci} + \left(1 + \frac{e^2}{r^2} \right) E_p A_p} \right)$$

The above equation for P_i accounts for the stress reduction due to elastic shortening. The following descriptions define the notations used:

P_{j-r}	= jacking stress reduced by relaxation and other factors
M_{pan}	= moment created by the self-weight of the panel alone
e_c	= eccentricity of the tendon in the panel
A_p, A_c	= cross sectional area of the CFRP tendon and the concrete, respectively (computed with the unit width)
E_{ci}, E_c	= Modulus of Elasticity of concrete at initial prestress release and 28 days, respectively
E_p	= Modulus of Elasticity of Leadline tendon
I_p	= moment of inertia of the panel using a unit width
r^2	= variable defined by the $I_p/A_{c\text{-pan}}$

The above equation results in:

P_i = 116.9 kN (26.3 kips)

f_{pi} = 116.9 kN / 80.7 mm^2 = 1449 MPa (210 ksi)

$P_e = P_i\,(0.85) = 99.3$ kN (22.4 kips)

$f_{pe} = f_{pi}(0.85) = 1232$ MPa (178.5 ksi)

Relaxation loss in CFRP is expected to be less than that of steel, thus a value of 15 percent is chosen for the total losses.

PANEL STRESSES DUE TO PRESTRESSING

stress in top of panel due to P_i:

$$\frac{-P_i}{A_{c-pan}}\left(1-\frac{e_c c_t}{r^2}\right) = \text{-126 psi}$$

stress in bottom of panel due to P_i:

$$\frac{-P_i}{A_{c-pan}}\left(1+\frac{e_c c_t}{r^2}\right) = \text{-1113 psi}$$

stress in top of panel due to P_e:

$$\frac{-P_e}{A_{c-pan}}\left(1-\frac{e_c c_t}{r^2}\right) = \text{-107 psi}$$

stress in bottom of panel due to P_e:

$$\frac{-P_e}{A_{c-pan}}\left(1+\frac{e_c c_t}{r^2}\right) = \text{-960 psi}$$

CHECK STRESS LIMITS

Table A.1 Design stress values in phases of construction (values in psi)

	At prestress release		During deck construction		Final service loading		
	f_{tp}	f_b	f_{tp}	f_b	f_{tp}	f_b	f_t
$P_{i,e}/A_c$	-126	-1113	-107	-960	-107	-960	
$M_{panel\ self\text{-}wt}$	-241	241	-241	241	-241	241	
Total	**-367**	**-872**					
Allowable	*-2580*	*-2580*					
$M_{slab\ self\text{-}wt}$					-334	334	
$M_{construciton}$			-635	635			
Total			**-983**	**-84**			
Allowable			*-2700*	*-2700*			
M_{LL+I}					101	621	-621
Total					**-581**	**236**	**-621**
Allowable					*-2700*	*402*	*-2700*

Table A.1 shows that all stress states are satisfied. At this stage, the allowable stress design is complete. It is now important to check the ultimate strengths of the panels and composite slabs.

MOMENT CAPACITY OF COMPOSITE SECTION

Ultimate moment

$M_u = 1.3[M_{DL} + 1.67(M_{LL+I})]$ [AASHTO 3.22.1]

$M_u = 1.3[686\ \text{kN-m} + 949\ \text{kN-m} + 1.67(10\ \text{kN-m})] = 23.8\ \text{kN-m}\ (211\ \text{in-kips})$

Nominal moment

Use the method presented in Section 3.3.2 to calculate the nominal moment capacity. With f_{pu} = 2822 MPa (409 ksi), we have

M_n = 38.4 kN-m (339.7 in-kips)

$\phi = M_u / M_n$ = 23.8 / 38.4 = 0.62

The moment capacity is recomputed using the method in Section 3.3.1. The reinforcement ratio is computed and compared with ρ_{br} to determine the reinforcement scenario.

ρ = 0.00145

ρ_{br} = 0.00169

Hence, the slab is normally reinforced and equation 3.3 is used to compute the nominal moment capacity.

M_n = 38.1 kN-m (337 in-kips)

$\phi = M_u / M_n$ = 23.8 / 38.1 = 0.63

DEVELOPMENT LENGTH FOR COMPOSITE SECTION

The equation for development length used here is developed by Mahmoud et al. (1999) and is shown below. A verification needs to be made to determine whether the development length governs the nominal moment capacity.

$$l_d = \frac{f_{pi} d_b}{\alpha_t f'^{0.67}_{ci}} + \frac{(f_{pu} - f_{pe}) d_b}{\alpha_f f'^{0.67}_{c}}$$

Assume that $f_{ps} = f_{pu}$ =2818 MPa (409ksi)

$$l_d = \frac{(1449MPa)(8mm)}{1.9(29.6MPa^{0.67})} + \frac{(2818MPa - 1232MPa)(8mm)}{1.0(31MPa^{0.67})} = 1901 \text{ mm (74.9 in.)}$$

Allowable l_d = 0.5 (2950 mm) = 1475 mm (58.1 in.)

Hence, the development length governs the moment capacity. Using the equation above with l_d = 1475 mm, replace f_{pu} with f_{ps} and solve for f_{ps}.

$$f_{ps} = \frac{\left[l_d - \frac{f_{pi} d_b}{\alpha_t f_{ci}^{0.67}} \right] \cdot \alpha_f f_c^{0.67}}{d_b} + f_{pe}$$

f_{ps} = 2294 MPa (333 ksi)

Now, recompute the nominal moment capacity at maximum tendon stress again using the nominal moment computation method described in section 3.3.2.

M_n = 31.5 kN-m (278.6 in-kips)

$\phi = M_u / M_n$ = 23.8 / 31.5 = 0.76

MOMENT CAPACITY OF PANEL

Ultimate moment

$M_u = 1.3[M_{DL} + 1.67(M_{LL+I})]$ [AASHTO 3.22.1]

M_u = 1.3[686 N-m + 1.67(1804 N-m)] = 4808 N-m (42.6 in-kips)

Nominal moment

The method presented in Section 3.3.1 is used to compute the nominal moment capacity of the over-reinforced section.

ρ = 0.0046

ρ_{br} = 0.00168

$$k_u = \sqrt{\rho\lambda + \left[\frac{1}{2}\rho\lambda\left(1 - \frac{\varepsilon_{pe}}{\varepsilon_{cu}}\right)\right]^2} - \frac{\rho\lambda}{2}\left(1 - \frac{\varepsilon_{pe}}{\varepsilon_{cu}}\right)$$

k_u = 0.402

Summing the moments about the tendon gives the nominal moment capacity:

$M_n = 0.85 f_c b \beta_1 k_u d_p^2 [1 - (\beta_1 k_u / 2)]$

M_n = 7234 N-m (64 in-kips)

$\phi = M_u / M_n$ = 4808 / 7234 = 0.66

Development length does not govern this situation because the concrete crushing strength will govern failure.

CHECK LOSS ASSUMPTIONS

The total prestress losses are checked with AASHTO Specifications. Elastic shortening was computed earlier, thus it will not be repeated here. The following values are for steel tendons and will be adjusted later on based on the modulus ratio between steel and Leadline.

f_{sh} = concrete shrinkage = 17000-(150RH) [AASHTO 9.16.2.1.1]

RH = relative humidity = 60 (for Denver area)

f_{sh} = 17000-(150)(60) = 8000 psi

$f_{c\text{-}cr}$ = concrete creep = $12f_{cir} - 7f_{cds}$ [AASHTO 9.16.2.1.3]

$f_{cir} = (-f_{pi}A_p/A_c)+M_{panel}/S_b$

f_{cir} = -(213.2 ksi)(0.125 in^2)/(42.5 in^2) + 6.03 in-kips/25.1 in^3 = -387 psi

f_{cds} = -330 psi(33 mm/45 mm) = -242 psi

$f_{c\text{-}cr}$ = 12(387 psi) – 7(242 psi) = 2880 psi

Based on research performed by University of Wyoming, assume Leadline relaxation losses after prestress release to be negligible.

Total losses = f_{sh} + $f_{c\text{-}cr}$

Total losses for steel = 8000 + 2880 = 10880 psi

Total losses for Leadline = 10880 psi x 21,329/28,000 = 8,284 psi

R = (210 –8.3)/ 210 = 96 %

This is small compared to the 85 percent used in design.

BIBLIOGRAPHY

[1] AASHTO, *Standard Specifications for Highway Bridges, LRFD. US Customary Units,* 2nd ed. (1998). American Association of State Highway and Transportation Officials, Washington D.C.

[2] AASHTO, *Standard Specifications for Highway Bridges,*16th ed. (1996). American Association of State Highway and Transportation Officials, Washington D.C.

[3] ACI Committee 318, *Building Code Requirements for Reinforced Concrete (ACI 318-99),* American Concrete Institute, Farmington Hills, MI., 1999.

[4] ACI Committee 440, "Guide for the Design and Construction of Concrete Reinforced With FRP Bars," American Concrete Institute, Farmington Hills, MI., November, 2000. (Draft)

[5] ASTM A 416 *Standard Specification for Steel Strand, Uncoated Seven-Wire For Prestressed Concrete,* American Society for Testing and Materials, 1999.

[6] ASTM A 882 *Standard Specification for Epoxy-Coated Seven-Wire Prestressing Steel Strand,* American Society for Testing and Materials, 1996.

[7] ASTM A 981 *Standard Test Method for Evaluating Bond Strength for 15.2mm (0.6") Diameter Prestressing Steel Strand, Grade 270, Uncoated, Used in Prestressed Ground Anchors,* American Society for Testing and Materials, 1997.

[8] Barker, R. M., and Puckett, J.A. (1997). *Design of Highway Bridges,* John Wiley and Sons, Inc.

[9] Brearley, L.M., and Johnston, D.W. (1990). "Pull-out Bond Tests of Epoxy Coated Prestressing Strand," *J. of Structural Engrg.*, Vol. 116, No. 8, August, pp. 2236-2252.

[10] Conrad, J., Bakis, C., Boothby, T., and Nanni, A. (2000). "Section F-Durability of Bond of Various FRP Rods in Concrete," Report Draft produced for Federal Highway Association.

[11] Cooke, D., Shing, P.B., and Frangopol, D. (1998). "Colorado Study on Transfer and Development Length of Prestressing Strand in High Performance Concrete Box Girders," *Report No. CDOT-DTD-R-98-7*, Colorado Department of Transportation, April.

[12] Dolan, C., Hamilton, H.R., Bakis, C., and Nanni, A. (2000). "Design Recommendations for Concrete Structures Prestressed with FRP Tendons," *Report No. DTFH61-96-C-00019*, Federal Highway Association, May.

[13] Eligehausen, R., Popov, E.P., and Bertero, V.V. (1983). "Local Bond Stress-Slip Relationships of Deformed Bars Under Generalized Excitations." *Report No. 83/23*, Earthquake Engrg. Res. Ctr. (EERC), Univ. of California – Berkely.

[14] Karlsson, M. (1997). "Bond Between C-BAR FRP Reinforcement and Concrete," *Ph.D. Thesis*, Division of Building Technology, Chalmers University of Technology, Goteborg, Sweden, March.

[15] Kent, D.C., and Park, R.(1971). "Flexural Members with Confined Concrete," *Journal of the Structural Division, ASCE*, Vol. 97, No. ST7, July, pp. 1969-1990.

[16] Lu, Z., Boothby, T., Bakis, C., and Nanni, A. (2000). "Section I-Transfer and Development Lengths of FRP Prestressing Tendons," Report Draft produced for Federal Highway Association.

[17] Mahmoud, Z., Rizkalla, S.H., and Zaghloul, E. (1999). "Transfer and Development Lengths of Carbon Fiber Reinforced Polymers Prestressing Reinforcement," *ACI Structural Journal*, Vol. 96, No. 4, July-August, pp. 594-602.

[18] Mostofa, T., and Zia, P. (1977). "Development Length of Prestressing Strands," *PCI Journal*, Vol. 22, No. 5, September-October, pp. 54-65.

[19] Nanni, A., Bakis, C.E., O'Neal, E.F., and Dixon, T.O. (1996). "Performance of FRP Tendon-Anchor Systems for Prestressed Concrete Structures," *PCI Journal*, Vol. 41, No. 1, January-February, pp. 34-45.

[20] Nilson, A.H. (1987). *Design of Prestressed* Concrete, 2nd ed., John Wiley and Sons, Inc.

[21] Nilson, A.H., and Winter, G. (1991). *Design of Concrete Structures*, 11th ed., McGraw-Hill Inc., pp. 177-191.

[22] Rizkalla, S. and Tadros, G. (1994). “A Smart Highway Bridge in Canada,” Concrete *International*, June.

[23] Rizkalla, S. (1997). “Material Properties of C-BAR Reinforcing Rods,” Technical Report produced for Marshall Industries Composites Inc., Published by ISIS Canada, University of Manitoba, Winnipeg, Manitoba, Canada, June.

[24] Shing, P.B., and Abu-Hejleh, N. (1999). "Cracking in Bridge Decks: Causes and Mitigation," *Report No. CDOT-DTD-R-99-8*, Colorado Department of Transportation, August.